A time delay ultrasonic imaging system

Thesis

A TIME DELAY ULTRASONIC IMAGING SYSTEM

Thesis submitted by

COLIN J S DAVIES B.A.

for the degree of

Doctor of Philosophy

Faculty of Technology

The Open University, Milton Keynes

August 1982

Date of submission: 1-8-82

Date of award: 11-10-82

Acknowledgements

The author wishes to thank Dr. D. I. Crecraft for his inspiring and helpful supervision. Thanks are due to the people who have assisted by making apparatus, in particular P. Wilson, P. Garner, R. Hermann, C. Bluck and the staff of the University's mechanical workshop. Thanks are also due to British Rail for the use of their laboratory at Derby and to Dr. K. G. Hall for his assistance with British Rail's schlieren apparatus. The author acknowledges the financial support and facilities provided by the Open University. Finally, thanks to my wife Anne for years of encouragement and for typing the first draft and to the typist Diane Holl.

Abstract

The design and construction of a time delay ultrasonic imaging system is described. After describing previous and existing methods of ultrasonic imaging, the probable advantages of relative simplicity in comparison with phased arrays, avoidance of side lobes, improved resolution and the disadvantages of ambiguity and distortion of the time delay system are discussed. Polyvinylidene fluoride (PVF_2) is used as a transducer material because its high damping enables one to produce single cycle ultrasonic pulses in water and its flexibility enables it to be formed into a curved surface. The properties of PVF_2 as a transducer are examined both by library search and by practical experiment. Schlieren images are shown of the ultrasonic wave front emanating from PVF_2.

A system for imaging under water is designed that comprises one transmitting and four receiving transducers. These are made from PVF_2 film on a cylindrical nylon backing, and construction methods are given. The system is controlled by a Rockwell AIM 65 desk top computer and the image is shown on a television screen. The design of both hardware and software is discussed, and methods are suggested for later improvement. The imaging system is demonstrated using four receiving transducers, and the improvement that can be achieved using more transducers is shown by simulating eight receivers. It is shown that, while the time delay system suffers from spurious images caused by ambiguities, it is free from the effect of side lobes because of the short pulse used. The design of a sectioned transducer that should reduce the number of ambiguities is outlined. In the system demonstrated, the image repetition period is two minutes, but with improved computation, this could be reduced to ten seconds or less. The problems envisaged in imaging in metal are discussed and methods of overcoming them are suggested.

Table of Contents

List of illustrations

Chapter 1 Previous work on acoustic imaging

1.1 From 1929 to the 1960s

In 1929, Sokolov proposed a method of using ultrasound to produce optical images, and the first demonstration of this appears to have been in 1934. The object to be imaged was immersed in water in the path of a vertical ultrasonic beam and an acoustic lens above the object focussed the ultrasound on to the water surface. The image appeared as a disturbance on the water surface and could be seen when illuminated obliquely. (Blitz 1971). During World War 2 Pohlmann devised a method for inspecting shell cases. The ultrasound from the insonified object was passed through a cell containing a large number of very small aluminium discs. These behaved as Raleigh discs which rotated by amounts depending on the local acoustic pressure and formed a visual image of internal defect when the cell was illuminated. (Blitz 1971). In 1950 Sokolov described his image converter. The incident acoustic beam set up a charge pattern image on a piezoelectric plate and a scanning electron beam converted the charge to an electrical signal. This system was further developed by Smyth Poynton and Sayers during the 1960s. (Blitz 1967).

1.2 A, B and C scan images

Three types of two dimensional image can be displayed, usually on a cathode ray tube.

An A scan is used for flaw detection and thickness gauging and does not form an image in the usual sense of the word as no brightness modulation is used. It is a display of reflecting

targets along the direction of a pulsed ultrasonic beam. The range is proportional to the distance on a conventional oscilloscope trace from the point of triggering to the point where the trace is deflected vertically by the return pulse from the target.

A B scan makes an image in the plane formed by the direction of the beam and a direction at a right angle to it. The oscilloscope display copies the image plane and is brightness modulated in proportion to the return echo strength from each part of the plane. A P.P.I. radar could be said to give a B scan.

A C scan makes an image in the plane formed at right angles to the direction of the beam at a chosen distance along the beam. The display is brightness modulated as in the B scan. The Sokolov image converter produces a C scan and the television picture of the test card could be called a C scan.

Over the last decade many types of ultrasonic imaging systems have been devised. These can be divided into groups, some of which use continuous and others use pulsed ultrasound to insonify the target. Of the systems using continuous ultrasound the most important are:

1.3 Holographic systems

Holography is based on the principle that a diffraction pattern from a 3 dimensional object can be recorded as a 2 dimensional square law intensity pattern and reconstituted to produce a 3 dimensional image of the original object. Great efforts have been made to apply the principles of holography to acoustic

imaging, and many different systems have been tried but little work appears to have been done since 1978. Holography is a two step process of recording the hologram and reconstituting the image, and even if a computer is used the programme takes too long to allow real time images.

The technique of forming a dynamic hologram on a liquid surface and reconstituting it with laser light was developed to overcome this problem, and real time images produced (Brenden 1975)(Aldridge 1972). However, the sensitivity is said to be generally inferior to direct imaging techniques.

There appear to be two inherent problems with holographic acoustic imaging systems. Firstly because the ultrasound used to constitute the hologram has a much longer wavelength than the light which reconstitutes the image, the image will be distorted, principally in depth. The depth will be exaggerated by a factor equal to the ratio of the two wavelengths which is likely to be about 1000.

Depth distortion can be partially corrected by photographic reduction or by computer reconstruction of the image, but holographic acoustic images are essentially two-dimensional C scan type because of this distortion.

The second and more serious problem is that the use of coherent waves in holographic systems gives rise to speckle on the image caused by phase cancellations and reinforcements. After the

image has been optically reconstructed both optical and acoustic speckle appear. A particular form of speckle (know as ringing) interferes with structural details of interest especially around sharp edges. (Aldridge 1972) (Melen et al 1979) (Mahfuz Ahmed 1979).

1.4 Bragg diffraction imaging

This is one of several developments of Pohlmann's cell. Instead of being detected by the rotation of small aluminium Raleigh discs, the spatial distribution of intensity of the acoustic field is detected by the degree of diffraction of a coherent beam of light passing through the cell. Mechanical displacement of particles due to a sound wave gives rise to local density variations in the medium, and as the optical refractive index is related to the density, an ultrasonic beam will set up an optical diffraction grating in an optically transparent medium.

Images suffer from ringing and speckle because of the use of coherent sound and light. (Wade 1975) (Doyle 1977) (Ahmed and Wade 1979).

1.5 Ultrasonovision

This is a name given to imaging by ultrasonic interferometry, and is a development of Sokolov's "disturbed water surface method" previously mentioned. Instead of being focussed onto the water surface, the acoustic field from the object is focussed onto a thin ($\sim$ 6 μm) metallised plastic film under the water. The metallised film forms one of the mirrors of an optical Michelson interferometer, and an interrogating laser beam scans the

reflecting surface in a raster. The local displacement of the metallised film is proportional to the local acoustic field intensity, and this can be measured by the scanning interferometer. The laser light is reflected onto a photodiode and displayed on a cathoderay tube. C scan images of biological objects have been demonstrated by the system. (Havlice and Taenzer 1979). A problem has been that the sensitivity depends on the optical path difference. When it is an integer multiple of $\lambda/2$, the sensitivity is zero. The sensitivity decreases with increasing frequency but is said to be "still quite good at 4 or 5 MHz". (Szilard and Hanstead 1982). Even so, this method has never been taken seriously by practitioners of non-destructive testing.

1.6 Image Converters and Piezoelectric detectors

Sokolov's image converter has been developed for use in ultrasonic cameras, and C scan transmission images of objects have been demonstrated. (Hill 1976) (Brown et al 1976) (Jones 1977).

An ideal C scan image converter would be a highly sensitive two-dimensional piezoelectric array of about 10^5 receiving elements, each with its own connection to an electronic video storage system. The existance of such an ideal system has not yet been reported. Harrold (1969 and 1974) describes a 10 x 10 element array with transducer cells of PZT5 cut into 2 mm squares.

Reports from Stanford Electronics laboratories describe a 16 x 16 element array with transducer cells of lead zirconate titanate or lead metaniobate cut into 2.2 mm. squares. (Plummer et al 1978).

A later report describes an array using PVF_2 film as the piezoelectric transducer. An array of MOSFETs is implanted into a silicon wafer and the 25 um thick PVF_2 piezo film is bonded to the wafer so that it is capacitatively coupled to the gates of the MOSFETs. The resulting structure has been called a POSFET and transducer cell sizes down to 0.1 mm square are said to be attainable. (Swartz and Plummer 1980).

An array of n x n piezoelements can be accessed by multiplexing 2n address lines. (Harrold 1969). (Maginnes et al 1974).

Practical piezoelectric detection systems have been constructed using linear arrays of 200 or so transducer cells which are used to detect one line of the image. The electronic readout can be displayed on a screen or put into a digital store, and either the linear array or the image is then physically translated to scan another line of the image so that a two dimensional (C scan) image can be built up. Frame repetition rates of 15 per second have been reported for the S.R.I. system in which the acoustic image is focussed, a line at a time, across a stationary linear array of 192 piezoelectric elements by a moving acoustic lens system. (Havlice and Taenzer 1979).

It has been pointed out that image converters and piezoelectric detectors do not rely on the use of coherent sound beams, and experiments have shown that a significant reduction in the number of artefacts and a corresponding improvement of image quality results when the sound beam is neither spatially nor temporally

coherent. (Havlice and Tainzer 1979).

Of the systems using pulsed ultrasound the most important are:

1.7 Schlieren imaging

P. D. Hanstead described a method of imaging acoustic discontinuities which he described as "Direct Ultrasonic visualisation of Defects (DUVD)". The system was developed by A. H. Hayman and appears to be a development of Bragg diffraction imaging in which the coherent light and sound sources have been replaced by pulsed sources which are synchronised to give a Schlieren image of the ultrasonic pulse. The system is said to lack sensitivity compared with pulse echo systems. (Hanstead 1973) (Hayman 1977). However, with incoherent light and sound there should not be the speckle problem associated with Bragg diffraction imaging.

1.8 Ultrasonic microscopy

Most systems use pulsed ultrasonic waves with frequencies from 300 MHz to 2 GHz. The object is moved with respect to the transducer and is scanned with a very narrow beam ($\sim$ 1 μm) of ultrasound. The coupling medium is water, and the ultrasound is either transmitted through or reflected off the object. A C scan image is produced and a resolution of better than 1 μm reported. (Penttinen and Luukkala 1977) (Quate et al 1979).

1.9 Pulse echo with mechanical scan

B scan images for medical investigations have been produced by this method for several years. In commercial instruments a

transducer on a supporting arm is placed against the body to be imaged and manually rotated so that the pulsed ultrasonic beam emanating from it is swept through an arc in the patient's body. The position and angle of the transducer is sensed electrically and communicated to the display so that the scan lines of the image correspond to the direction of the ultrasonic beam in the patient, and the brightness at any point depends on the strength of the return echo pulse. The image is built up in a video store and continually displayed as a still picture. The image quality depends on the skill of the operator who must develop a good scanning technique.

The scanning process can be mechanised by arranging for rotating or oscillating transducers to be coupled to the patient by a water bath. A real time image can be obtained, but the bulk and inconvenience of these scanners has restricted their acceptance by the medical community. (Havlice and Taenzer 1979).

1.10 Pulse echo by linear switched array

The linear switched array is also called the "collimated array" and the "stepped array".

Several systems are available, but usually a large number of narrow transducer elements, each about 10 mm long, are laid side by side to form an array about 100 - 150 mm long. A small group of elements is activated at a time, and by disconnecting the last element and connecting the next element of the array the small group of elements is stepped along one element at a time.

There are two reasons for this. Firstly, a group of elements gives better sensitivity than a single element. Secondly, each active part of the transducer array of width D produces an ultrasonic beam of wavelength λ which is in cross section an approximately collimated replica of that active part up to a distance of about $\frac{D^2}{4\lambda}$. Beyond this in the far field the beam diverges at an angle of about $\frac{\lambda}{D}$ radians.

The system operates in the near field and although the depth of the near field is extended in proportion to the square of the number of elements and the far field divergence is reduced in proportion to their number, the lateral resolution is reduced as the number of elements is increased. The use of shorter wavelengths allows a reduction in the number of elements but does not allow greater depth of imaging because of increased attenuation with frequency.

These constraints used to limit collimated arrays to imaging superficial structures at small depths (Melen et al 1979) (Havlice and Taenzer 1979). The latest types of ultrasonic scanner in use in hospitals produce a rectangular B scan image in real time, and although they are said to operate with a switched array they give good lateral resolution and penetrate to sufficient depth to allow the imaging of a foetus. How this is achieved has not yet been made public.

1.11 Pulse echo phased array

Phased arrays use acoustic pulses of a single frequency several cycles long. The simplest arrangement has a linear array of small transducer elements.

Consider such an array of width D, containing transducer elements of width W and spacing d. (see Figure 1.1).

When using sound of wavelength λ, the field of view of the individual transducer elements will be a lobe of effective angular width approximately λ/w radians. (see Figure 1.2).

The angular field of view of the whole array will be restricted to the overlapping of the individual lobes from each element side by side which will approximate to a wider lobe of similar shape. If all the elements are used together the field of view will be restricted to a much narrower lobe of width approximately λ/D radians. (see Figure 1.2).

By properly phasing the signals to and from the individual transducer elements of the array it is possible to arrange for the sound waves to and from any part of the target lying within the wide lobe to be suitably delayed so that they add in phase. Waves from most other parts of the target arrive with differing phases and cancel each other. The effect is that a particular portion of the target can be selected as if there were a steerable beam (in the form of the narrow lobe of angular width λ/D) operating within the wide lobe of the individual elements.

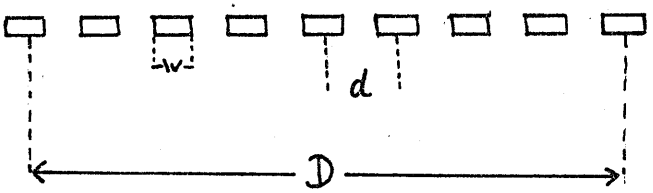

Fig. 1.1 Transducer array

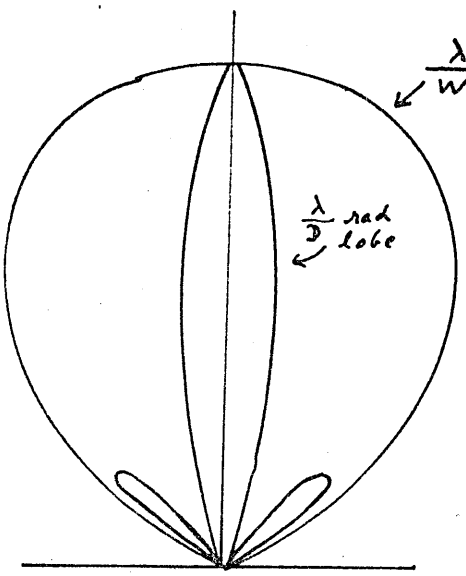

Fig. 1.2 Polar plot of sound intensity. Main beam directly ahead.

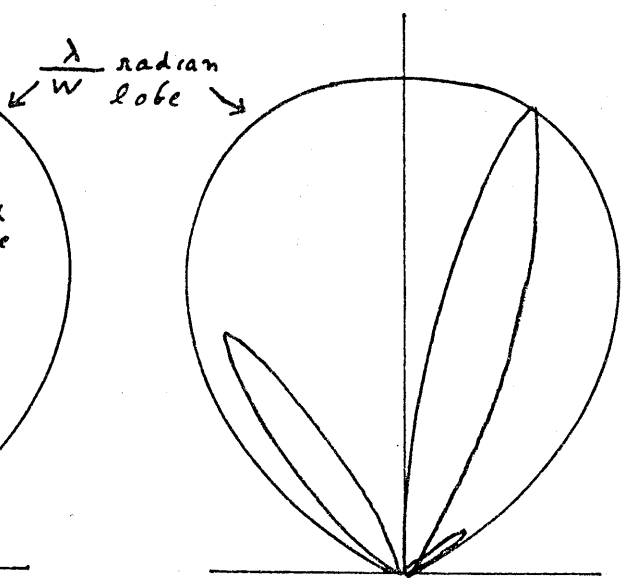

Fig. 1.3 Main beam steered to the right.

A problem that arises is that sound waves to and from those parts of the target that lie at angles of multiples of λ/d radians from the part of the target being investigated will also add in phase. This gives rise to ambiguities.

The situation can be represented by drawing side lobes (often called grating lobes) at angles of λ/d each side of the main steerable beam. (see Figure 1.2).

While the system is looking directly ahead, the constraint of the wide (λ/w) lobe will attenuate the grating lobes. When the main beam is steered to one side it too will become attenuated by the directivity function of the individual elements and the side lobe following it will become less attenuated until at a main beam angle of $\lambda/2d$ the main lobe and side lobe will be of comparable size. (see Figure 1.3) (Beaver et al 1975).

According to Melen et al (1979), one method of resolving the grating lobe problem involves the use of separate insonification and receiving arrays with different grating lobe patterns. If the same array is used for both insonification and reception, the grating lobes will coincide and be enhanced. Another method is to reduce d by filling the array with a large number of small transducer elements. The grating lobes will move away from the main beam and disappear when $d = \lambda/2$.

Phased arrays require more complicated circuitry than other scanning systems. In particular a variable delay circuit is required for beam steering each transmitting element in the transducer and a variable delay (for focus and beam steering) is required for each receiver unit. Increasing the number of transducer elements to reduce the grating lobe problem will greatly increase the complexity of a circuit that is already complicated.

The need to recognise phase makes it necessary for the pulse to be several cycles long. This limits the range resolution obtainable. Although focussing has been used in the near field of an array, in general phased arrays operate in the far field. The ability to focus in the near field may depend on the number of cycles in the burst.

Phased arrays operate in the far field of the array. In general the near field pattern of a phased array does not form a beam, and application of a phase taper to the array only distorts the near field pattern into a multiplicity of humps. Application of a symmetrical linear or Gaussian amplitude taper to the array can produce a rather wide beam in the near field. This beam can be steered by applying a linear phase taper but it becomes distorted and humped in the process. (Kay and Bishop 1964).

1.12 Sonoscan

While the present research was under way, Hanstead (1979) was independently developing a real time ultrasonic imaging technique called Sonoscan. As there are great similarities between Sonoscan and the system about to be described in chapter two and onwards, Sonoscan will be described in outline here and referred to again in chapter ten.

Referring to figure 1.4, suppose a diverging beam transducer acting as both transmitter and receiver of pulses to be placed sequentially at positions such as A, B and C. D1 and D2 are point reflectors. By converting the observed echo times to ranges, it would be possible to draw arcs on the diagram as shown. The positions of the two reflecting points then become defined unambiguously by noting those places where (in this example) three arcs intersect.

A computerised version of the above procedure, with many more transducer positions than in the example given, is the principle of Sonoscan.

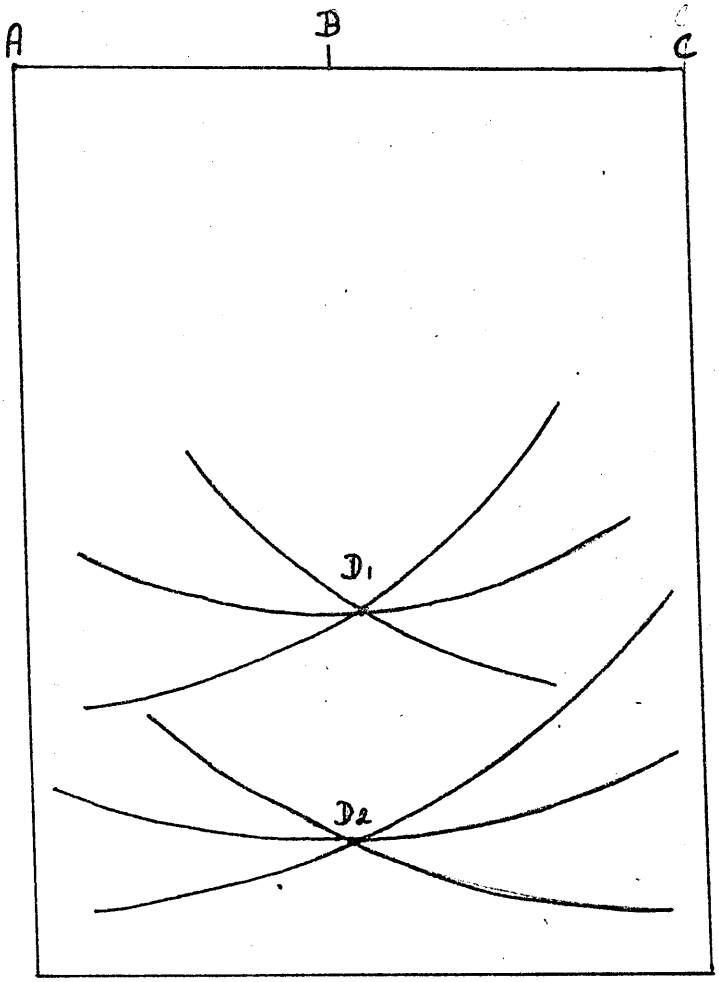

Figure 1.4 Geometrical illustration of Sonoscan principle.

Chapter 2 A time delay acoustic imaging system

2.1 Introduction

A method of imaging was suggested in which time delays instead of phase delays could be used to scan a target with an ultrasonic beam. The advantages would be:

i. The system does not need to be phase sensitive which should reduce circuit complexity.

ii. It is expected that the calculation of a time delay would be easier than a phase delay.

iii. Because there is no need to correlate phase, the ultrasonic pulse lengths can be much shorter than those used in phased array systems. This will improve range resolution.

iv. Ideally a pulse of one cycle can be used. As well as giving a range resolution equal to its half wave length, there will be no interference effects and hence no side lobes to create ambiguities.

v. The device could operate in the near field of the array.

2.2 Explanation of the time delay imaging system

Figure 2.1 shows the system layout. Assume that the system has one insonifying transducer and n receivers.

For a given target point there will be n path lengths, each consisting of the distance from the transmitter to the target

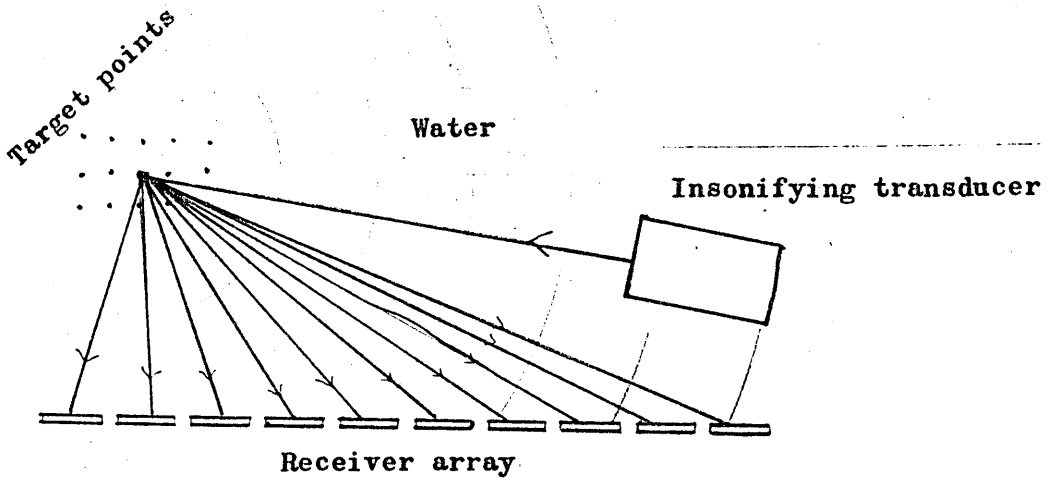

Figure 2.1 A time delay acoustic imaging system layout.

point plus the distance from the target point to each receiver 1 to n.

i. The system calculates path lengths 1 to n.

ii. It sets up time delays corresponding to these path lengths.

iii. It fires a short pulse at the target, and after the delay appropriate to each receiver 1 to n:

iv. It samples the output of receivers 1 to n for a period that is short compared with the ultrasonic wave period:

(a) taking samples of the received pulse over several repetitions should improve the signal to noise ratio

(b) sampling, at these selected delay times, is equivalent to cross-correlating the received wave with the expected wave which would be received from a point source, at the selected point, on the assumption that such a wave would suffer no difference in attenuation between the longer path lengths and the shorter ones. That is, if the expected wave is assumed to suffer relative delays (phase shifts) due to the path-length differences, but not relative attenuation due to the path-length differences, then the amplitudes of the signals received by the array elements will all be equal, but the phases of those signals will differ. Correlation with such a signal involves multiplying each of its element amplitudes, which are equal, with each of the corresponding element amplitudes of the

actual received signal. Because the expected signal is assumed to have equal amplitudes, these can be taken as unity. So correlation against the received signal simply involves multiplying it by one at the selected delay times, that is, sampling the received signal.

(c) The assumption that the expected wave would produce equal amplitudes on all array elements is probably a gross approximation to make in the near-field case. In the far field, the assumption is probably valid.

(d) Suppose the target is metal, immersed in water. Then the majority of the path length difference would probably occur in the water. We could then probably ignore attenuation caused by absorption, and simply account for spherical spreading, in the water, from the selected point source. On this basis, the expected wave would be expected to suffer relative attenuation related to path length, from target point to receiving array, by the law (power) proportional to $1/(\text{path length})^2$, or (received voltage amplitude) proportional to 1/(path length). So, as a more accurate alternative to iv:

v. (Alternative to iv) Sample the element outputs using the delays set up in ii.

Multiply each sample by a weighting factor proportional to 1/(path length).

This will obviously take more calculating time.

vi. In either case iv or v, the strength of the signal received from the selected target point is interpreted in terms of its relative strength compared with that of a fictitious point source, at the same point in the target, radiating at such an intensity as to cause the reception of the "expected" wave described above.
For case iv: Add all the n samples, and divide this sum by n, the sum which would be obtained if all the samples were of maximum possible amplitude.
For case v: Add all the weighted samples, and divide this sum by the sum of the squares of all the weighting factors.

vii. The corresponding point in the c.r.t. image is then illuminated at an intensity proportional to the 'relative strength' signal found in vi.

viii. The system is then ready to investigate the next target point, in response to either manual control or automatic scanning voltages, either of which must specify the next target point in terms of range and bearing (or range and distance off main axis).

Chapter 3 Requirements, theoretical limitations in performance and problems envisaged with the time delay system

3.1 Requirements

The system requires:

i. Transducers that will generate very short ultrasonic pulses, (preferably of only one cycle) in the MHz range. See Chapter 4.

ii. A method of calculating the distances from transducers to target points and providing this information to the coordinating system in iv. The requirements are outlined below and detailed in Chapters 5 and 7.

iii. A method of sampling the electric outputs of the receiving transducers over periods in the order of 10 - 100 ns, calculating a factor to correct for attenuation and beam spreading and multiplying the sample values by this factor, adding the corrected samples from all the receivers and displaying the result as a brightened spot on a raster. See Chapter 5.

iv. A system for coordinating i - iii above and scanning the target. See Chapter 5 and below.

Calculation of distances

In the most general case there is a transmitting transducer at (x_T, y_T, z_T), a receiving transducer at (x_r, y_r, z_r) and a target point at (x_t, y_t, z_t). (See Figure 3.1).

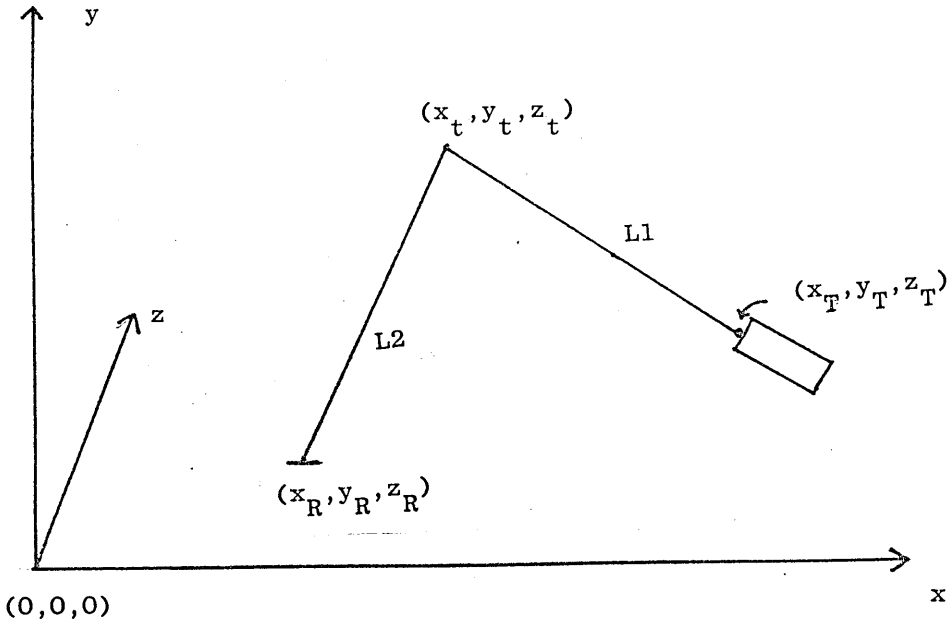

Fig. 3.1 Coordinates of transmitting and receiving transducers and target point.

$$L_1 + L_2 = \{(x_T - x_t)^2 + (y_T - y_t)^2 + (z_T - z_t)^2\}^{\frac{1}{2}} +$$

$$\{(x_r - x_t)^2 + (y_r - y_t)^2 + (z_r - z_t)^2\}^{\frac{1}{2}}$$

The distance $L_1 + L_2$ will be called the path length.

For each target point (x_r, y_r, z_r) the system must calculate one value of L_1 and r values of L_2 (where r is the number of receivers). Each target point requires r path lengths to be calculated.

Three ways of doing this are:

i. By hard wired circuitry. This would be fast in relation to the time taken to travel to the target and back and is probably the best method in a final product. However it would be very inflexible and inconvenient for developing a system.

ii. By computer. This would be comparatively slow, but very flexible and probably the best method for developing a system.

iii. By accessing a look up table in which the lengths have previously been stored. This would be faster than ii and more flexible than i but would require several Mega bytes of rapidly accessible memory. For a system imaging at a range of 150 mm the path lengths will be up to about 400 mm. A pulse duration of 50 ns would permit a resolution of 0.1 mm in water, hence the path length must be known to 1 part in 4000. This requires a

12 bit binary number of $1\frac{1}{2}$ bytes of memory to be stored for each receiver and each target point. A system with 20 receivers and a display raster of 400 x 400 resolvable points (representing a square image plane 4 cm side) would need about 5 Mega bytes of memory.

3.2 Scanning

C scanning is achieved by incrementing x_r and z_r while holding y_r constant. For B scanning x_r and y_r are incremented and z_r held constant.

The target points cannot be incremented until the coordinating system has obtained new values for the path lengths and also not until a sufficient number of pulses have been sampled for adequate signal averaging. The scanning rate will be limited by the greater of these two factors, the former being dependent on the method used to obtain the data and the latter on the greatest path length, the velocity of sound and the system noise.

3.3 A B scan time delay system

Further theoretical aspects of the time delay system will be considered using a simplified two dimensional model in which a B scan is made in the (x,y) plane and all the transducers are on the line y = 0.

Figure 3.2 shows part of such a system. The transducers are in a linear array and the first four are shown. The left hand transducer transmits short ultrasonic pulses to the target and the others receive the echoes.

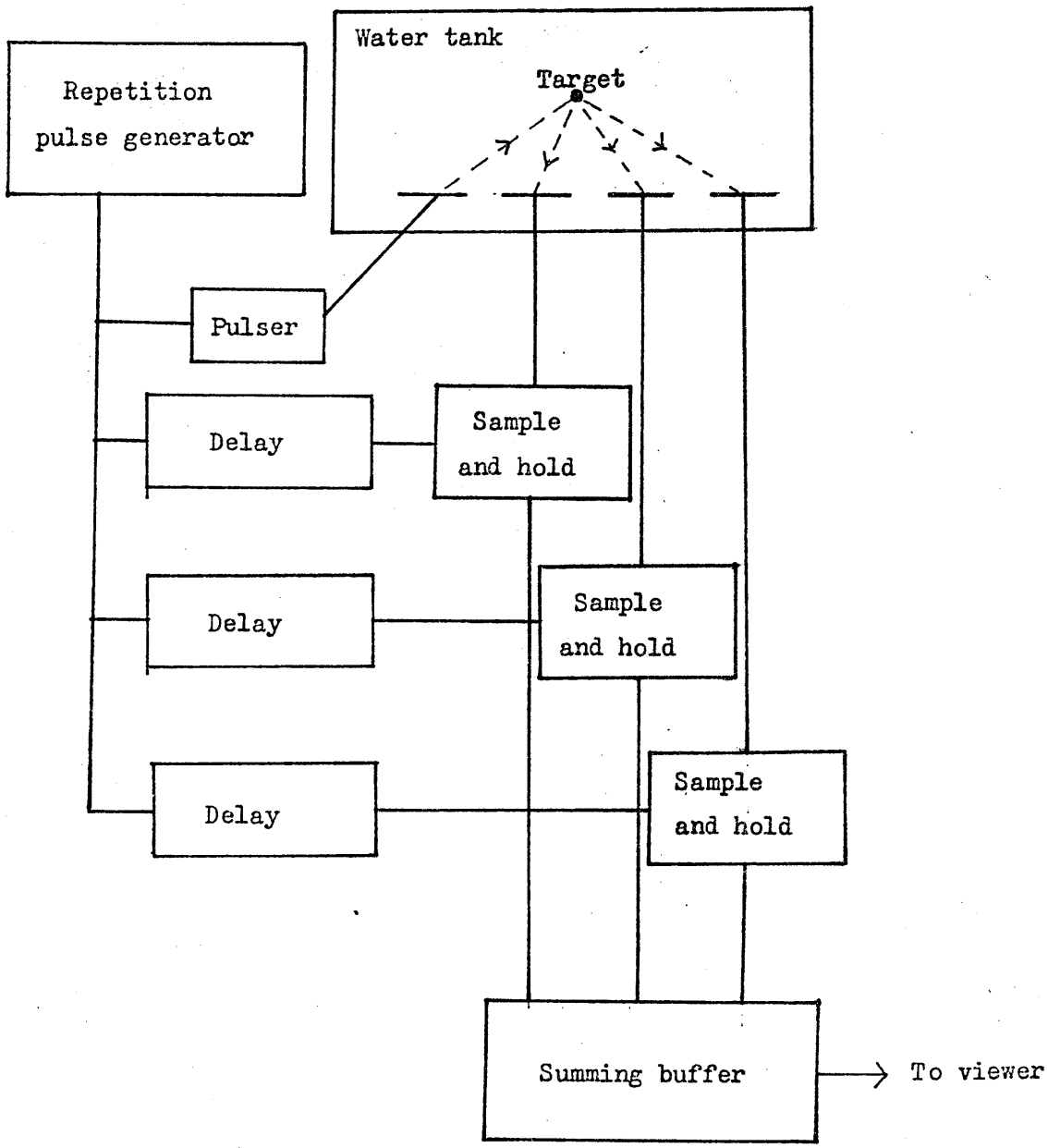

Figure 3.2 B scan time delay imaging system

A signal from the repetition pulse generator causes the pulser to fire and opens the gate in the sample and hold circuits after delays which are appropriate to the target point being investigated. Any echoes picked up by the receiving transducers will be sampled at the correct times and passed to the summing buffer.

3.4 Resolution of the time delay B scan

The degree of resolution that such a system could give depends on:

i. The pulse duration.

ii. The velocity of sound.

iii. The position of the target point.

iv. The distance between the transmitting and receiving transducers.

Consider the particular situation shown in Figure 3.3. All distances are in millimetres in a B scan plane. A transmitter is at point (0,0) and a receiver at (50,0). The target is a rectangular block 50 x 100 mm, with corners at (0,80), (0,130), (100,80), (100,130). The transducers and target are in water. For a point (a,b) in the target, the round trip distance will be $(a^2 + b^2)^{\frac{1}{2}} + ((50 - a)^2 + b^2)^{\frac{1}{2}}$. Call this the "path length".

Assume:

i. The sound velocity in the water and in the target is 1.5 mm/μs

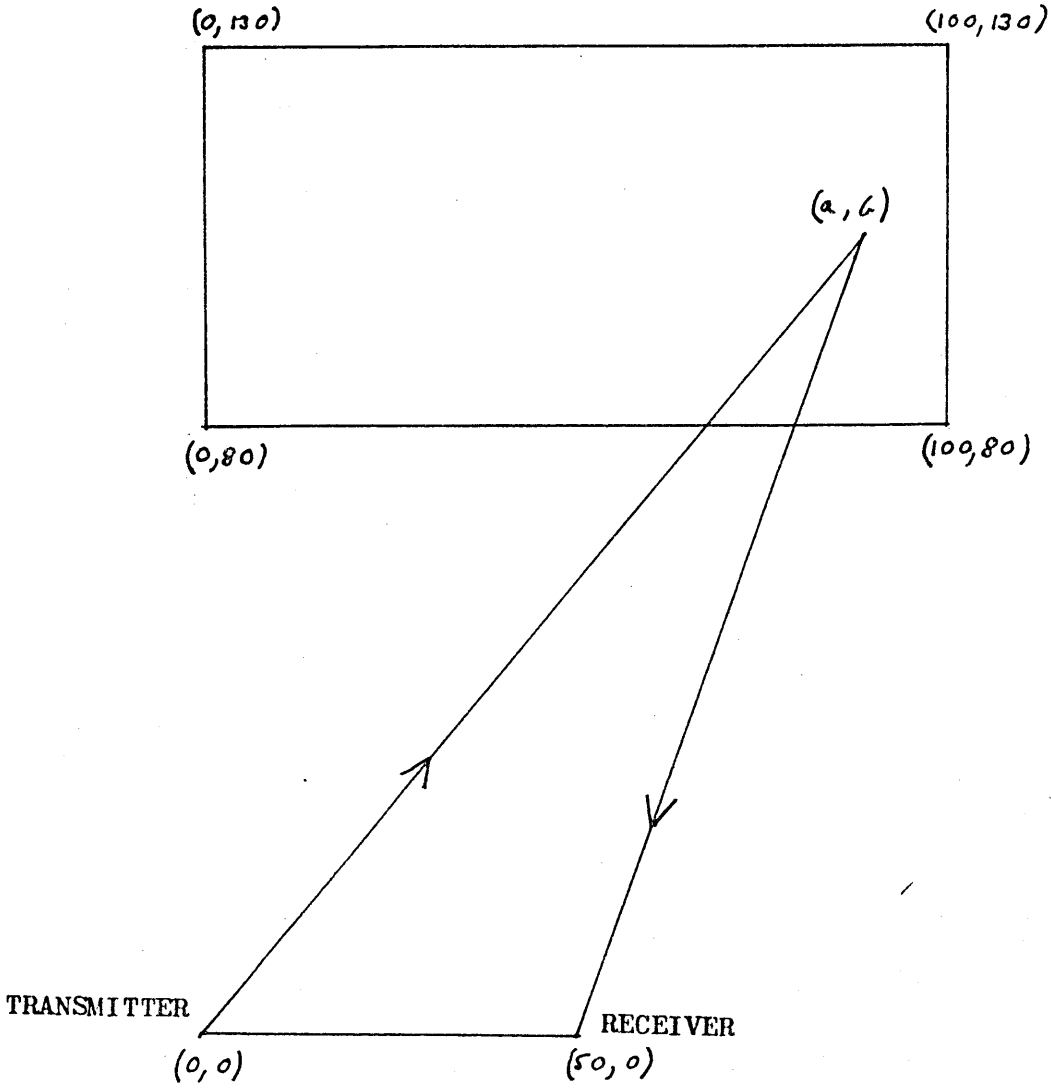

Fig. 3.3 System layout for determining target resolution in figs. 3.4 and 3.5.

ii. The system can resolve a 20 ns time difference. This is equivalent to a difference in distance of 0.03 mm in the journey from transmitter to target point to receiver.

In general the path lengths for a pair of neighbouring points, P and Q, will differ, and by dividing this difference by 0.03 mm the number of resolvable points between P and Q is obtained, and by further dividing by the distance in mm between P and Q the average number of points per millimetre along that line is obtained.

A computer was programmed to calculate the lateral resolution (at 5 mm intervals) and the range resolution (at 10 mm intervals) in terms of resolvable points per mm attainable in different areas of the target.

The results are shown on Figure 3.4 for range and figure 3.5 for lateral resolution.

The range resolution improves slightly with increasing range, tending to a limit of $66\frac{2}{3}$, or double the path length resolution. The range resolution is greatest along x = 25, and falls off by some 10 - 15% along the x = 100 line.

The lateral resolution varies considerably. In general it is lowest when the range resolution is highest and vice-versa. It is very poor indeed along x = 25, that is halfway between the transmitter and receiver. It improves off axis and at lower ranges.

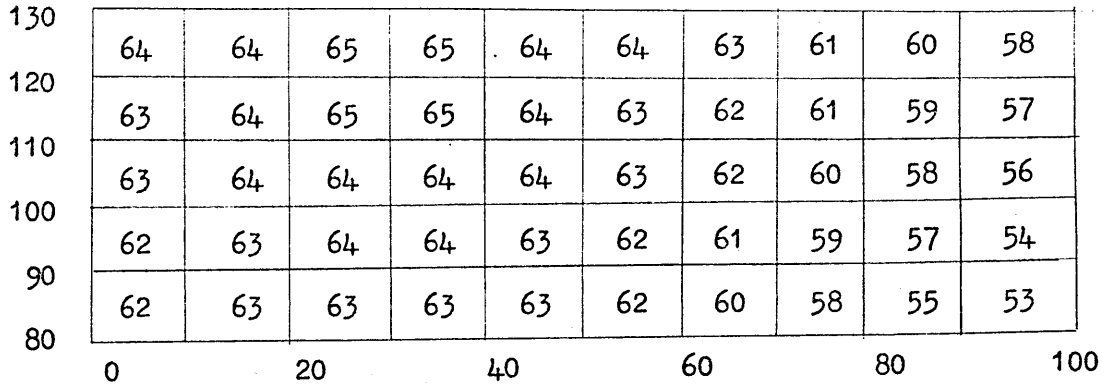

Fig. 3.4 Vertical or range resolution obtainable in 50 x 100mm. target shown in figure 3.3.
Resolvable points per millimetre.

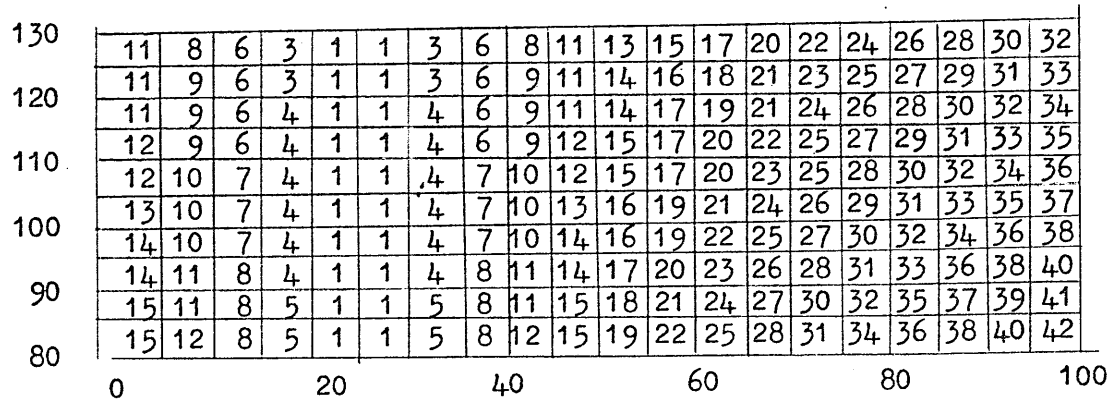

Fig. 3.5 Lateral resolution obtainable in 50 x 100 mm. target shown in figure 3.3.
Resolvable points per millimetre.

Other receivers would have their regions of good and poor resolution in different parts of the target.

The conclusion is that it would be best to have the target off axis to the array. The lateral resolution would be greatly improved while the range resolution would not be unacceptably reduced.

3.5 Ambiguity

Figure 3.6 shows part of an array with transmitter T, receivers R, R', R" etc and target points P and Q.

The reflection from P will be sampled by receiver R when R's gate pulse is delayed by a time equivalent to the path length TP + PR. This path length occurs for all the points on the ellipse with foci T and R passing through P, and consequently P will be imaged as an arc of that ellipse. Similarly Q will be imaged as a confocal elliptical arc passing through Q. The samples from receivers R', R" etc. will produce further pairs of confocal elliptical arcs passing through P and Q. One focus will always be at T and the other at R', R" etc.

The brightness of each arc is proportional to the sampled signal voltage. At points where the arcs cross the brightness of each is added as samples of signals from different receivers are added and in particular this happens at the target points which are imaged more brightly than the background. If the screen brightness is turned down sufficiently to suppress the unwanted arcs only the

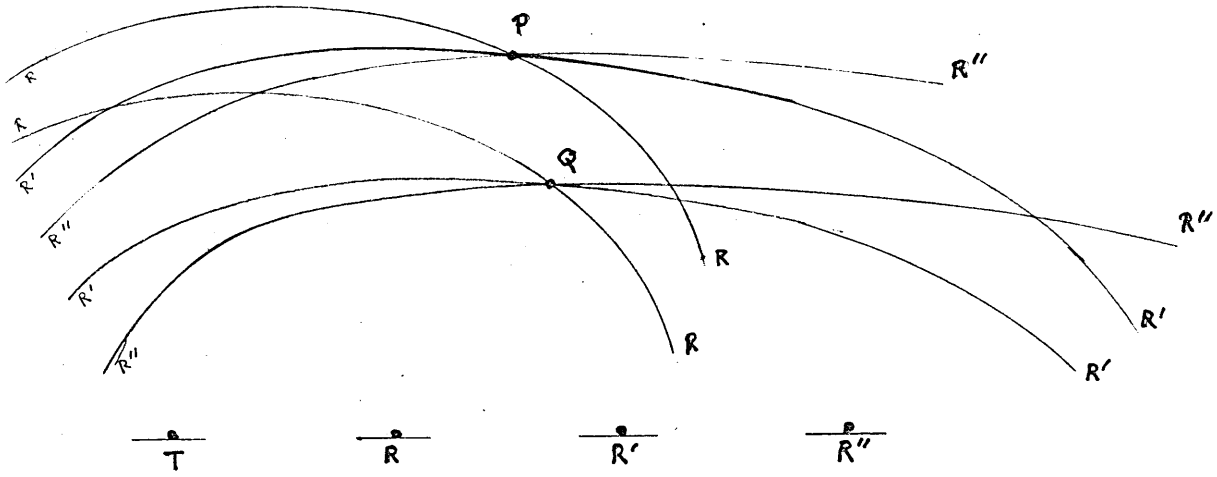

Fig. 3.6 Ambiguities from intersecting ellipses with foci at T and at the three receivers.

brightened image points should show.

Unfortunately the arcs also cross in other places and this will cause ambiguities. Figure 3.7a shows the sort of effect one would get if four target points were imaged using four receivers. The arcs are approximated by parallel straight lines for simplicity. They cross in groups of four on the target points and elsewhere in pairs so that one should be able to suppress these ambiguities by turning down the screen brightness sufficiently to put the crossing pairs into the black. Call ambiguities resulting from these pair crossings "low level ambiguities".

However the arcs do not need to cross to be added in brightness. Addition will happen as soon as the arcs become sufficiently close to each other for the system to be unable to resolve them separately. Two arcs crossing at a small angle could produce a brightness increase in a row of image points as in Figure 3.7b. This could be suppressed by reducing the screen brightness, as it is a low level ambiguity but where three or more arcs come sufficiently close they will form brighter points of ambiguity as in Figure 3.7c. Call these situations "high level ambiguities". The brightness of the wanted image above absolute black will increase with the number of receivers and it is hoped that with a large number of receivers the brightness of the wanted image will be much greater than the brightness of the background of crossing arcs.

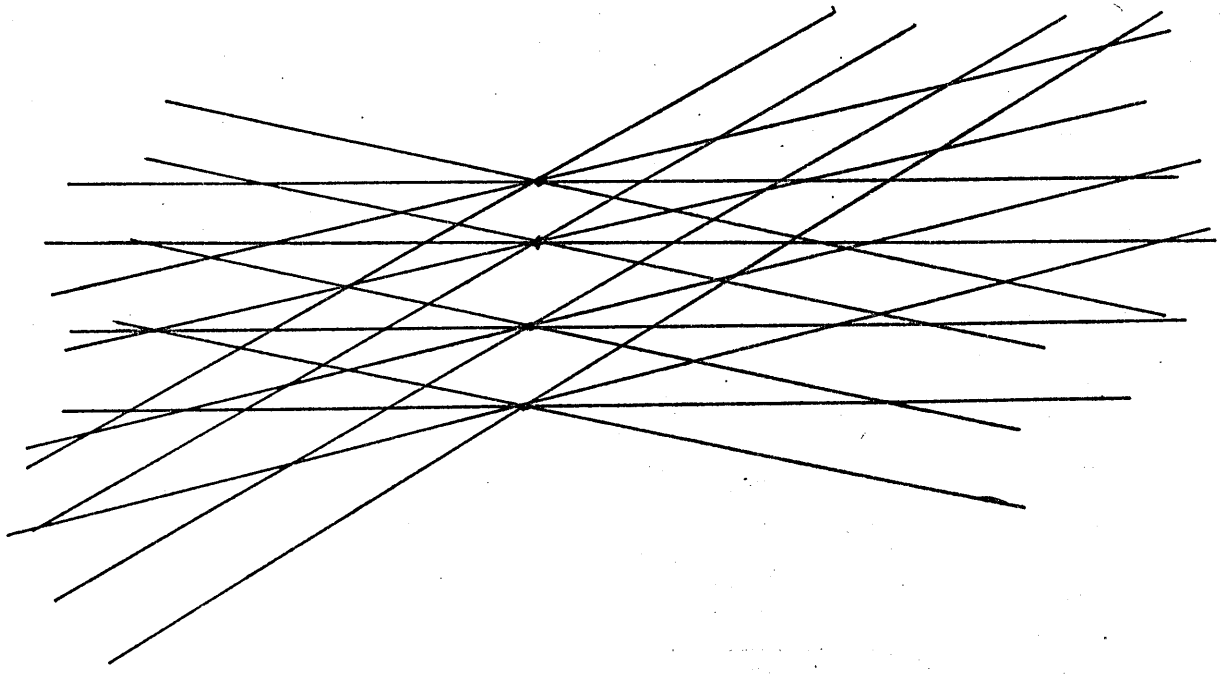

Fig. 3.7a Ambiguities resulting from intersecting lines passing through the target points.

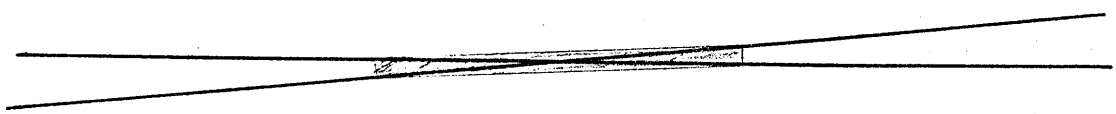

3.7b Low level ambiguity. The shaded area is brightened.

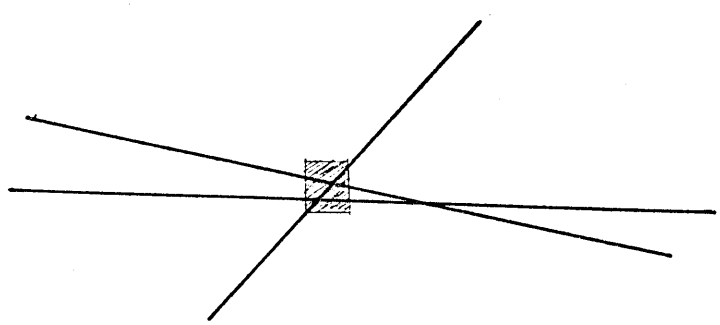

3.7c High level ambiguity. The shaded area is brightened.

To verify this a computer simulation was considered, but it was decided to leave this until after a working imaging system had been built and studied. Meanwhile an exercise on paper indicated:

i. For a system with r receivers imaging n target points there will be nr arcs and $\frac{(n^2 - n)(r^2 - r)}{2}$ unwanted crossings of one arc with another (low level ambiguities).

ii. In a practical situation up to 20% of these crossings will take place off the screen, but the total number of low level ambiguities will be of this order.

iii. An improvement in system resolution would reduce the number of high level ambiguities by reducing the number of cases where three or more arcs could come sufficiently close to add brightnesses.

iv. The number and position of the high level ambiguities depends very critically on the relative positions of the target points to one another in terms of the array coordinates. If the target is rotated through even a very small angle the points at which three or more arcs approach sufficiently to produce high level ambiguities will be completely changed.

3.6 Image distortion caused by change of sound velocity

In the case of a metal target in water, the ultrasonic pulse will be refracted at the water/metal boundary and will travel at a higher velocity once it is inside the target.

Figure 3.8 represents a 50 x 200 mm steel bar immersed in water at a range of 200 mm from the transducer array. A pulse of ultrasound from T to R via P will have to travel by the route marked. This assumes that the velocity of sound in steel is four times that in water and that the beam will be refracted according to Snell's law at the water/metal boundary.

The point P will be imaged as if it were on an ellipse with path length $TI_1 + RI_2 + \frac{1}{4}(I_1P + PI_2)$.

In general this will not be the same as the straight line distance TP + PR, and the image will be distorted.

Suppose a transducer in water at (0,0) sends a sound pulse to a target at (x,y) in metal via a point (a,b) on the water metal boundary. (Figure 3.9).

If the velocity of sound in the metal is μ times its velocity in water, and the metal face is parallel to the x axis at distance b then:

$$\mu = \frac{\sin i}{\sin r} = \frac{\sqrt{a^2 + b^2}}{\dfrac{x - a}{\sqrt{(x - a)^2 + (y - b)^2}}}$$

This gives an iteration formula for a, which converges well in most cases.

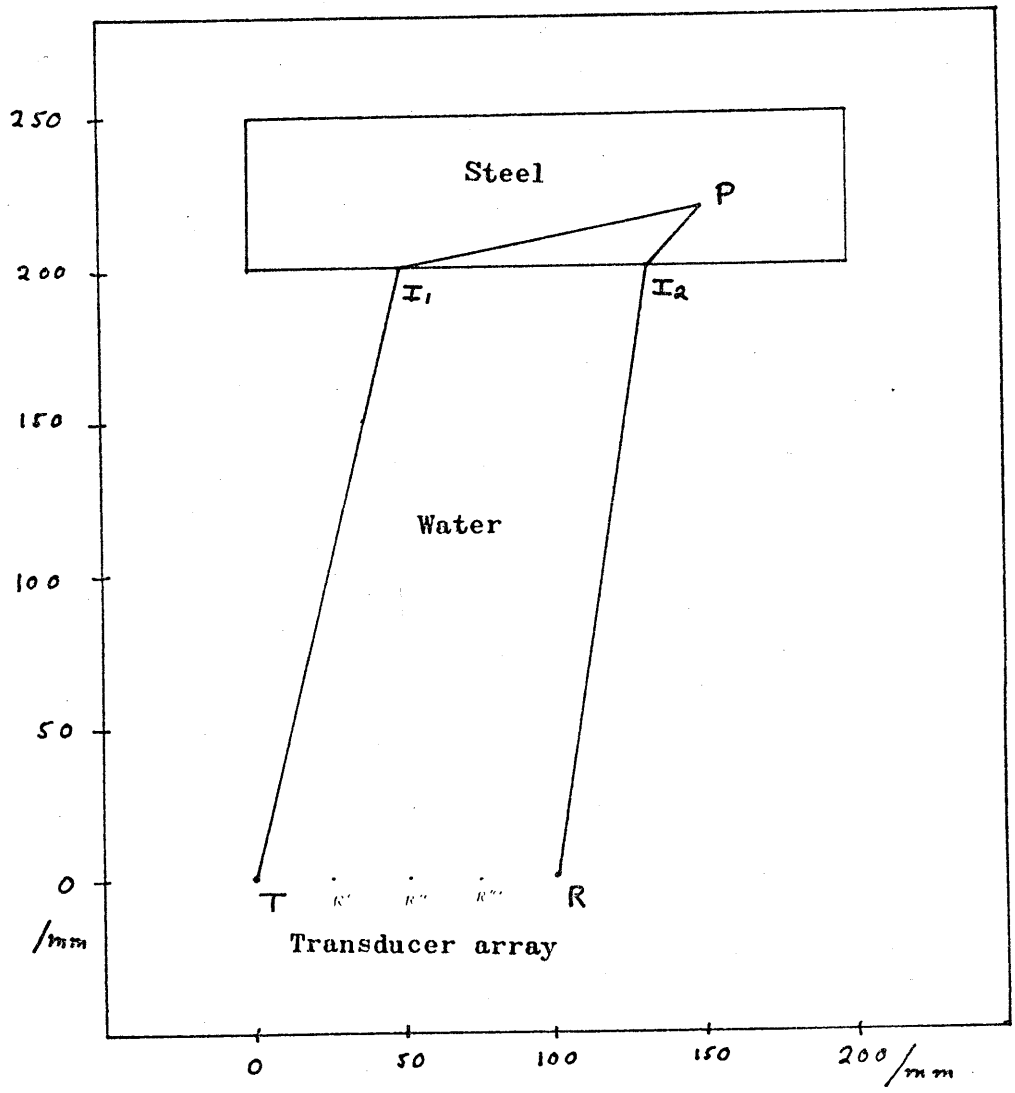

Fig. 3.8 Path of ultrasound through water and steel to and from a target point in the steel.

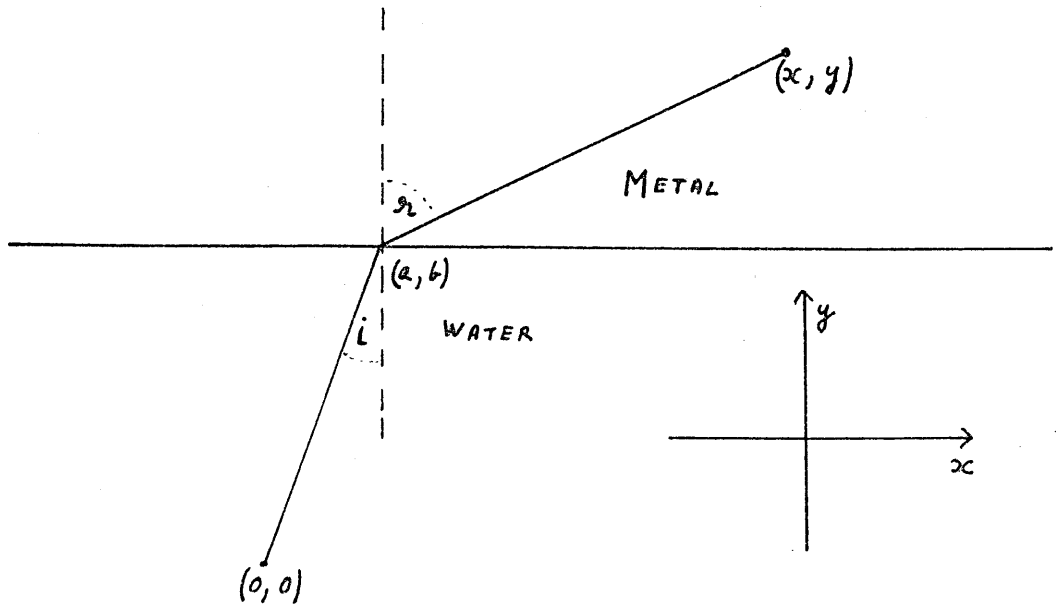

Fig. 3.9 Refraction of sound at a water-metal boundary.

$$a = \sqrt{\frac{\mu^2 b^2}{1 - \mu^2 + \frac{(y - b)^2}{(x - a)^2}}}$$

Knowing a, one can calculate the path length from transducer to target.

An exercise was conducted to investigate the degree of image distortion that could be expected if the target is metal in water.

A model using separate transmitting and receiving transducers (thus producing a system of intersecting ellipses) was considered to be unnecessarily complicated for this exercise. Instead it was assumed that two common mode transmit/receiver transducers (giving a system of intersecting circles) were situated at (100,0) and (300,0) in water and that the target was a 100 mm thick steel bar at 200 mm range.

Figure 3.10 shows the layout looking from above. The common mode transducers are marked TR_1 and TR_2.

A computer program was written to calculate the coordinates of the image of a point (x,y) in the target.

i. The path lengths from TR_1 and TR_2 to the water metal boundary and then to a point (x,y) were calculated.

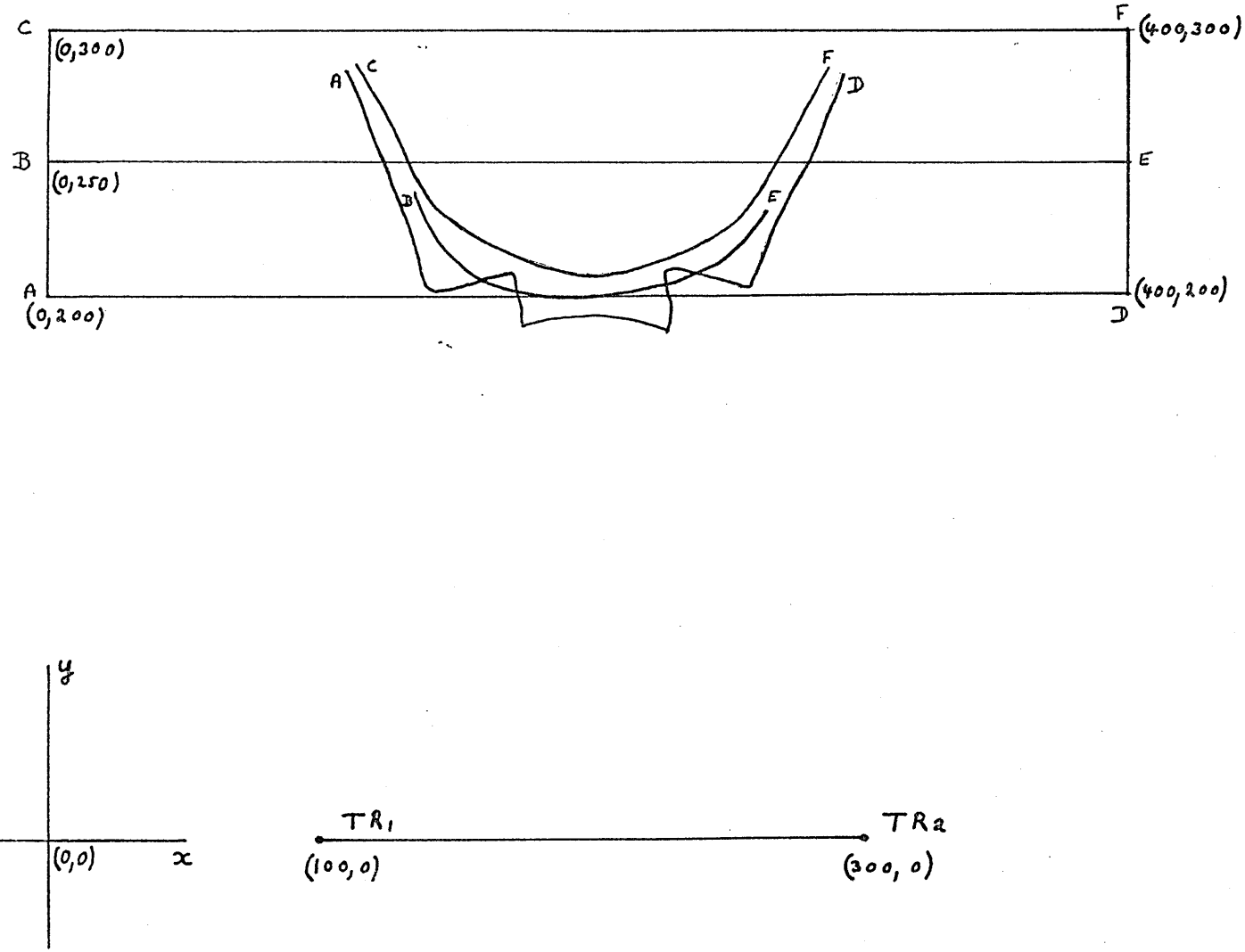

Fig. 3.10 Distortion of imaged object due to sound velocity differences.

ii. The second part of the path length was divided by four and added to the first part. This gave a figure proportional to the time of flight of the pulse from TR_1 and TR_2 to (x,y) and hence the distance as if it had travelled entirely in water.

iii. These distances were taken as radii of a pair of circles centred at TR_1 and TR_2, and their point of intersection (for $y > 0$) calculated. This was taken as the imaged coordinate of (x,y). The image to be expected from a rectangular target is crescent shaped, and is drawn superimposed on the real target in Figure 3.10. This particular image shape results from the transducer spacing and target range chosen for this exercise. More than two transducers would be needed for a practical system and calculations show that circles or ellipses centred on more than two receiving tranducers and resulting from a given target point would not normally intersect at the same point and could not form an image.

If the distortion by a particular imaging system can be modelled mathematically then it should be possible to reconstruct the undistorted image by computer. In the time delay system discussed here, each pair of receivers will introduce a different distortion pattern, hence a system using n receivers will have $\frac{n!}{2(n-2)!}$ different distortion patterns. This would require a great deal of computation to reconstruct the image.

The conclusion is that the inside of metal objects would best be imaged by applying the transducer array directly to the object and not via a water bath.

Chapter 4 Polyvinylidene fluoride as a transducer for ultrasound

4.1 Introduction

A paper by Bui et al (1976) indicated that short ultrasonic pulses could be generated from "Poled PVF_2 film" and transmitted into water.

As this could well be the answer to the problem of finding a transducer capable of providing short pulses for the imaging system, it was decided to investigate the properties of PVF_2 film.

The available literature was studied, and, since this research started, a great deal more has been published.

The thermoplastic polyvinylidene fluoride is also called PVF_2 and PVDF.

It has been sold for many years by the Pennwalt Corporation under the name "Kynar" which is described as "a high performance thermoplastic characterised by toughness and corrosion resistance", and is used for packaging, electrical insulation and anti-corrosion pipe linings. (Pennwalt).

The Kureha Chemical Company manufactured it for use as the dielectric in capacitors.

In 1969, Kawai demonstrated that it had piezo-electric properties, (Kawai 1969) and by the mid 1970s the Kureha Chemical Company was manufacturing a piezo-electric form of the plastic under the name

Kureha KF Piezo Film.

Vinylidene fluoride is an obsolescent name for 1,1 difluoroethene.

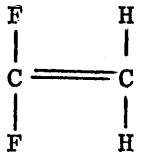

This compound polymerises when one part of the double bond joins onto the carbon of the next molecule.

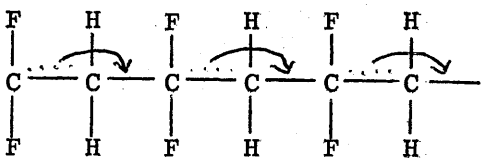

and forms a polymer (polyvinylidene fluoride) consisting of about

90% - CH_2 - CF_2 - CH_2 - CF_2

and about 10% - CH_2 - CF_2 - CF_2 - CH_2

- CF_2 - CH_2 - CH_2 - CF_2

PVF_2 exists in at least three crystal forms known (a little confusingly) as

α or Phase II

β or Phase I

γ or Phase III

The Phase II or α form (Figure 4.1a) appears mainly in melt cast PVF_2. Its crystal structure is approximately as above with the fluorine and hydrogen atoms alternating on both sides of the carbon chain which is not planar as drawn for clarity, but a helix when viewed lengthwise. The C - F structures are highly polar but, in a unit cell, the dipoles cancel each other. The Phase II crystal is

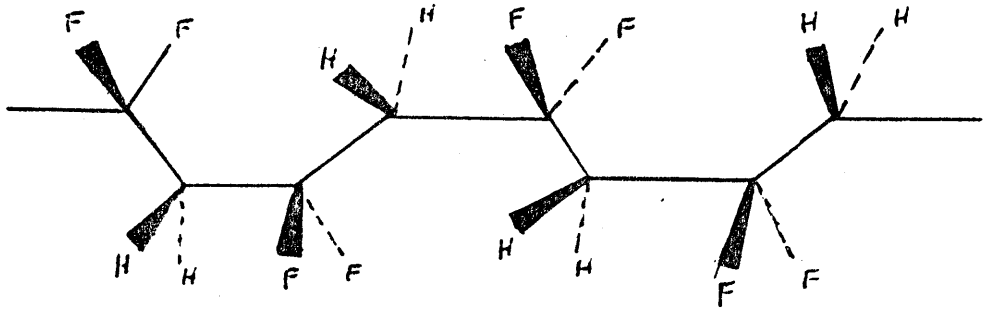

Fig. 4.1a Phase II PVF_2

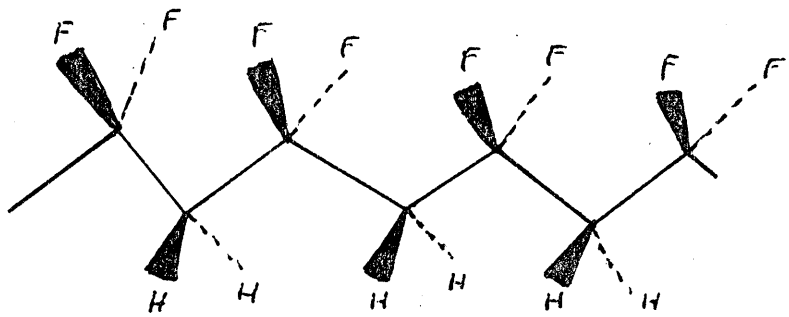

Fig. 4.1b Phase I PVF_2

thus non polar and non piezoelectric. Under a poling field of between 100 and 200 MVm^{-1} phase II is converted to phase II_p. This has a dipole moment of 4.3×10^{-30} Cm (Sessler 1981) and is piezoelectric. At poling fields above $4 \times 10^{8} V^{-1}$ a considerable amount of phase I (β) is produced (Newman 1979).

The Phase I or β form appears in oriented PVF_2 made by stretching or rolling the melt cast α form. It has an (almost) planar chain of carbon atoms in a zig-zag with all the fluorine atoms on one side and all the hydrogen atoms on the other (Figure 4.1b). The dipole moment is now perpendicular to the chain axis and a single crystal of Phase I is thus polar and piezoelectric. The component of the dipole moment parallel to the direction fluorine group - hydrogen group, is 7×10^{-30} Cm. (Sessler 1981).

The Phase III or α form is produced by special heat treatment. It appears to have a planar zig-zag form and is similar to Phase I, but there is some controversy over this. (Bachmann et al 1979).

In addition most PVF_2 film contains 50% non-crystalline molecules.

PVF_2 film is made piezoelectric by poling it with a high voltage. The greatest effect is obtained by stretching the polymer sheet uniaxially, evaporating a conducting layer of metal on each face, then applying a strong electric field between the faces while the film is held at a temperature of about $100^{o}C$ for an hour or two and then allowing it to cool with the polarising field still applied.

However, Sussner and Dransfeld (1978) have pointed out that PVF_2 films can be poled at room temperature and consider that stretching prior to poling is not a necessary condition for the occurrence of the piezoelectric effect.

4.2 Causes of Piezoelectricity in PVF_2

The literature from 1976 to 1982 indicates three main causes of the piezoelectricity in PVF_2.

i. The Phase I (β) type molecules are rotated by the strong poling field at high temperatures so that their dipoles line up in the same direction and are locked in place when the plastic cools. Scheinbeim (1979) has shown that the piezoelectric effect increases linearly with the phase I (β) content. (Murayama 1976, Tamura 1977, Scheinbeim 1979, Woodward 1977).

ii. The high temperature and the poling field partially convert the phase II (α) to phase I (β) and to phase II_p, a new phase with identical unit cell dimensions to normal phase II but with a different molecular packing (Burkard and Pfister 1974, Ohigashi 1976, Newman 1979). Phase II_p should have about 60% of the piezoelectric effect of the phase I (β), and published values for the d constants tend to confirm this. (Ohigashi 1976).

iii. Positive charges are injected into the surface of the PVF_2 film by the positive poling electrode. (Murayama 1976).

Sussner and Dransfeld (1978) have demonstrated that the piezoeletric effect occurs only in the PVF_2 immediately in contact with the positive poling electrode and that the film is polarised inhomogeneously in such a way that the piezoelectric constant varies across the thickness of the sample. Latour (1980) has cut poled PVF_2 into thinner slices and by investigating the piezoelectricity in each slice gives a tentative confirmation to these results when applied to phase I (β). Sussner and Dransfeld maintain that the piezoelectricity in PVF_2 originates from the physical processes at the metal-polymer contact and not from a dipole alignment in any of the crystal phases, and the volume fractions of the phases I and II have little bearing on the piezoelectric effect.

Figure 4.2 is a graph, published by Fukada and Furukawa (1981), showing the distribution of electric field through the thickness of the film when polarising voltages are applied. The field is concentrated near the positive electrode.

However, Sessler (1981) observes that uniform polarisation can be obtained with fields in excess of 170 MVm^{-1}. Bacon (1982) reports that the g constant of some poled biaxially stretched PVF_2 used for a hydrophone is uniform throughout the thickness. He does not give the poling details.

4.3 Determination of piezoelectric constants in PVF_2

The piezoelectric properties of materials are conventionally shown in the form of a matrix. (Blitz 1967, Gooberman 1968). The convention adopted by Murayama (1976) and Fukada (1981) for the

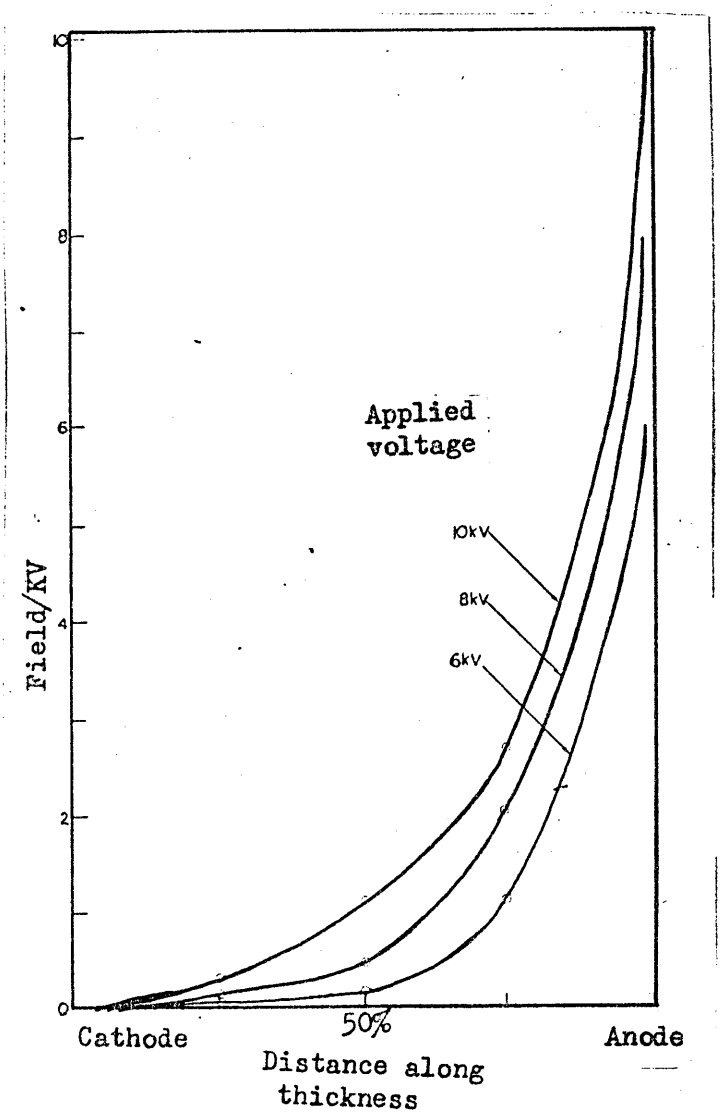

Fig. 4.2 Distribution of electric field through thickness of film (Fukada and Furukawa 1981).

piezoelectric matrix for PVF_2 is used here.

The Z axis is taken perpendicular to the plane of the film and parallel to the polarising electric field.

The X axis is taken in the direction of orientation or stretching, or if the film is unstretched, it is usually taken along the long axis of the roll of film.

The Y axis is perpendicular to the X and Z axes.

Subscripts 1, 2, 3 refer to the directions X, Y, Z and 4 refers to a shear in the 1-2 plane etc. For example, d_{32} means the piezoelectric strain constant measured in the Y direction when the electric field is applied along the Z direction.

PVF_2 film poled without stretching has the matrix;

$$d_{ij} = \begin{matrix} 0 & 0 & 0 & 0 & d_{15} & 0 \\ 0 & 0 & 0 & d_{15} & 0 & 0 \\ d_{31} & d_{31} & d_{33} & 0 & 0 & 0 \end{matrix}$$

This is intended to show that 13 of the 18 values are zero, and that d_{15} has the same value as d_{24}, and that d_{31} has the same value as d_{32}.

If the film is poled after uniaxial stretching the matrix is;

$$d_{ij} = \begin{matrix} 0 & 0 & 0 & 0 & d_{15} & 0 \\ 0 & 0 & 0 & d_{24} & 0 & 0 \\ d_{31} & d_{32} & d_{33} & 0 & 0 & 0 \end{matrix}$$

Values of piezoelectric constants for PVF_2 have been published in the literature, and it is evident that their values depend on the method of stretching and poling the film and on the conditions under which the measurements are made.

Table 4.1 gives details of d constants published by six authors. For the purpose of assessing the transduction capabilities of PVF_2 the d_{33} constant is the most important. Unfortunately, it is the most difficult to measure. Burkard and Pfister (1974) seem to have been the first to measure d_{33} and showed that it is negative. (meaning that the film becomes thinner when a positive voltage is applied to the face that was positive during poling). The measurement was made at 0.3 Kelvin and is included for historical interest.

Ohigashi (1975) poled uniaxially and biaxially stretched PVF_2 under various voltages and determined the d constants over a range of temperatures from about $-200^{o}C$ to $+100^{o}C$. The five values in Table 4.1 are the ones he published for room temperatures ($22^{o}C$ and $25^{o}C$).

Kepler and Anderson (1978) used two different methods to find d_{33}. All the authors except Ohigashi found d_{31} and d_{32} by measuring the charge that appeared on the surface when the foil was strained.

Table 4.1

Author	PVF_2 film	Poling	d_{31} x $10^{-12}CN^{-1}$	d_{32} x $10^{-12}CN^{-1}$	d_{33} x $10^{-12}CN^{-1}$	Remarks
Burkard and Pfister 1974	25μm thick Unoriented	$3.5 \times 10^7 Vm^{-1}$ 100°C 2 - 3 hours	About 0.03	About 0.03	About - 0.3	Measurements made at 0.3 Kelvin
Kureha Chemical Co. 1975	Uniaxially stretched 9μm thick "Kureha# 9KF Piezo-film"	No details	23	2.3	Not given	
Murayama et al 1976	Uniaxially stretched	No details	Typical 20 Maximum 50	Typically $\frac{1}{10}$ of d_{31}	Not given	
Ohigashi 1975	Uniaxially stretched 80μm thick	$11 \times 10^7 Vm^{-1}$ 115°C. 2 hours	27.9	4.8	- 17.4	Measured at 25°C by piezoelectric resonance method
		$7.8 \times 10^7 Vm^{-1}$ 120°C. 2 hours	Not given	Not given	- 14	Measured at 22°C by piezoelectric resonance method
Kepler and Anderson 1978	Uniaxially stretched Kureha # 30 KF Piezo-film 30μm thick	No details	21.4	2.3	- 31.5	d_{33} by direct measurement. Room temperature.
					- 33.3	d_{33} by hydrostatic measurement. Room temperature.
Ohigashi 1975	50μm thick Biaxially stretched	$4.8 \times 10^7 Vm^{-1}$	Not given	Not given	- 7.5	Measured at 22°C by piezoelectric resonance method
Kepler and Anderson 1978	25μm thick capacitor grade. Biaxially stretched	$6 \times 10^7 Vm^{-1}$ 100°C. $\frac{1}{2}$ hour	4.34	4.36	- 12.4	d_{33} by direct measurement. Room temperature.
					- 13.5	d_{33} by hydrostatic measurement. Room temperature.
Woodward 1977	25 μ m thick Biaxially stretched	$4 \times 10^7 Vm^{-1}$ 100°C 20 minutes.	Not given	Not given	(-) 35	

Ohigashi measured the resonant frequency of the foil in length and thickness modes and then calculated d_{31}, d_{32} and e_{33} by assuming that at resonance the foil would behave as a conventional piezoelectric transducer with equivalent circuit as in Figure 4.3a and applying the formulae appropriate to this. (Blitz 1967, 3.19, 3.24, 3.31). (He then calculated d_{33} from the approximate formula $d_{33} \simeq e_{33}/c^{D}_{33}$).

Kepler and Anderson found d_{33} firstly by measuring the change in thickness of the foil caused by applying a sinusoidal voltage in the order of 20 V at 10 Hz, and secondly by measuring the charge produced against hydrostatic pressure when the foil was immersed in an inert pressurised liquid. The d_{33} value was calculated from the formula:

d hydrostatic = $d_{31} + d_{32} + d_{33}$

Woodward (1977) found d_{33} by measuring the change in thickness of the film when up to 300 volts DC was applied.

4.4 Discussion of results of different authors

Kepler and Anderson's results differ by less than 10% but are about double those obtained by Ohigashi. Woodward's result for d_{33} (Biaxial) is over double those of Kepler and Anderson.

It is suggested that Ohigashi's results are too low for one or more of the following reasons:-

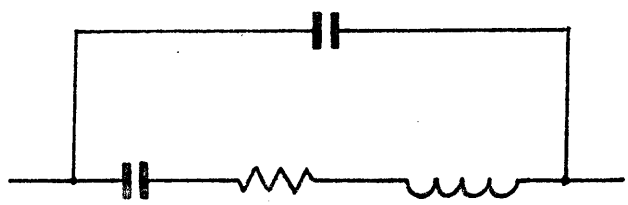

Figure 4.3a Equivalent circuit of piezoelectric transducer.

i. Ohigashi used 80 and 50 μm thick film and Kepler and Anderson used 30 and 25 μm. If the dielectric constant varies through the thickness of the film with the greatest effect near the positive surface when poled, then the overall value of d_{33} would depend on the film thickness. For the same poling field, a poled 50 μm thick PVF_2 film would show about the same piezoelectric effect as would a double layer of 25 μm film with only one layer poled. A thicker film would have a smaller value of d_{33}.

ii. As well as obtaining the d constants, Ohigashi used the resonant frequency of the film to calculate the acoustic Q and the sound velocity through the film (V_3). His calculations were based on the assumption that a freely suspended piezofilm of thickness t resonates at a frequency corresponding to a wavelength $\lambda = 2t$. However, Sussner and Dransfeld (1978) have reported that as a result of the inhomogeneity of the piezoelectric properties, freely suspended PVF_2 film shows its strongest resonance at twice this frequency, that is when $\lambda = t$. This suggests that the resonant frequencies obtained by Ohigashi may have been too high, and this would give him a high value for V_3 and low values for Q and d_{33}. It is therefore interesting to note that Ohigashi's value for V_3 is 2560 ms^{-1} against the more usually quoted value of 1960 ms^{-1} (Woodward 1977) and that Bui et al (1977) report that they "consistently obtained larger values of Q than those obtained by Ohigashi (14 as compared with 9)".

iii. There is some evidence that the elastic modulus of PVF_2 increases with frequency, and an increase of "perhaps a factor of

two is expected when going from 10 Hz to 100 MHz" (Sessler 1981). For a given value of the piezoelectric constant e, d will vary inversely with the elastic modulus and if this increases with frequency, d will decrease. Ohigashi's measurements were made at frequencies around 10 MHz and Kepler and Anderson's at around 10 Hz.

From a comparison of the poling conditions one would expect Woodward's result for d_{33} to be about two thirds of that from Kepler and Anderson. At 35 pCN^{-1} for biaxially stretched film it is in fact nearly three times as great and this cannot be explained from the available information.

From the results of Ohigashi, and Kepler and Anderson, it appears that d_{33} for uniaxially stretched film is about double that for biaxially stretched. This is to be expected if the former contains mainly the phase I (β) and the latter the phase II (α), as Sessler (1981) reports that for equal poling fields phase I (β) material shows about 7/4 the d_{31} and d_{33} values of the phase II (α).

The implication is that one should use uniaxially stretched film for an underwater transducer.

Sound velocity and acoustic impedance

Author	velocity/ms^{-1}	impedance/Mrayl
Woodward 1977	1960	3.5
Bui et al 1977	2040	3.6
Ohigashi 1976		
Uniaxial	2300	4.1
Biaxial	2560	4.6
Alquie et al 1976	2600	4.7

Table 4.2

"rayl" is the S.I. unit of specific acoustic impedance or characteristic impedance, having the dimensions of newton second metre^{-3} or kilogramme second^{-1} metre^{-2} (International Dictionaries of Science and Technology: Sound. Edited by R. W. D. Stephens. Crosby Lockwood and Staples London 1975). It will be used with this meaning throughout this thesis.

Table 4.2 summarises the values for sound velocity and acoustic impedance of PVF_2 film in the "3" direction. A density of 1780 kgm^{-3} is assumed in all cases. Woodward, and Bui et al, appear to have measured the acoustic impedance and divided by the density to obtain the velocity. Ohigashi and Alquie et al both used a vibration method to find the velocity which has been multiplied by the density to give the acoustic impedance.

While conducting tests on the frequency response of transducers to be used in the imaging system (section 6.6), the value of 3.7 M rayl was obtained. The method is detailed in section 6.6.

Relative permittivity

The relative permittivity of PVF_2 is generally taken to be about 13 by all authors. Ohigashi gives 13.2 at 25°C, 16.1 at 41°C and 3.6 at -106°C.

The capacitance of various samples of Kureha KF piezofilm was measured with a 1 KHz capacitance bridge, and indicated that the relative permittivity at room temperature for 30 μm film was 12.2 ± 1.8 and for 9 μm film was 14.4 ± 2.0. (The tolerances result from manufacturer's thickness tolerances).

Most analyses of the electrodynamics of piezoelectric transducers make the assumption that the change in relative permittivity due to stress T and strain S and the change in elastic modulus due to electric field E and displacement D are relatively small and can be ignored (Gooberman 1968, Blitz 1967). With the superscript denoting the quantity held constant during measurement, $\varepsilon^S = (1-k^2)\varepsilon^T$ and $S^D = (1-k^2)S^E$. The piezoelectric constant k for PVF_2 is reported to be about 0.1 to 0.2 and the error resulting from assuming $\varepsilon^S = \varepsilon^T$ and $S^D = S^E$ is therefore between 1% and 4%. This is much less than the uncertainty of the piezo constant values and can be ignored for PVF_2.

In this case, the five piezoelectric constants (d,e,g,h,k) are approximately related to each other and to the absolute permittivity ε and to the elastic modulus S of the foil by the formulae:

$e \simeq ds \simeq h\varepsilon \simeq gs\varepsilon$

$dh \simeq eg \simeq k^2$

This approximate relation can be shown conveniently as a commutative diagram. (Figure 4.3b).

Table 4.3

Piezoelectric constants of PVF_2 foil obtained by various authors compared with other piezoelectric materials.

Material	d_{33} 10^{-12} CN^{-1}	k_{33}	h_{33} 10^{9} NC^{-1}
Uniaxial PVF_2			
(Ohigashi) Poling 110 MVm^{-1}	-17.4	0.205	-2.42
(Ohigashi) Poling 78 MVm	-14	0.185	-2.44
(Kepler and Anderson) (average)	-32.4		-1.23
Biaxial PVF_2			
(Ohigashi)	- 7.5	0.122	-1.98
(Kepler and Anderson) (average)	-13.0		-1.14
Woodward	-35		-0.43
Quartz (x cut)	2.3	0.095	3.92
Ba Ti O_3	190	0.50	1.32
PZT - 4	289	0.70	1.70
PZT - 5	593	0.752	0.95

Table 4.3 summarises values of d_{33} and k_{33} given by various authors for PVF_2 film and Woodward's values for other materials. Only Ohigashi has determined values of k_{33} for PVF_2, and the other authors quote his values. All the values for h_{33} have been calculated

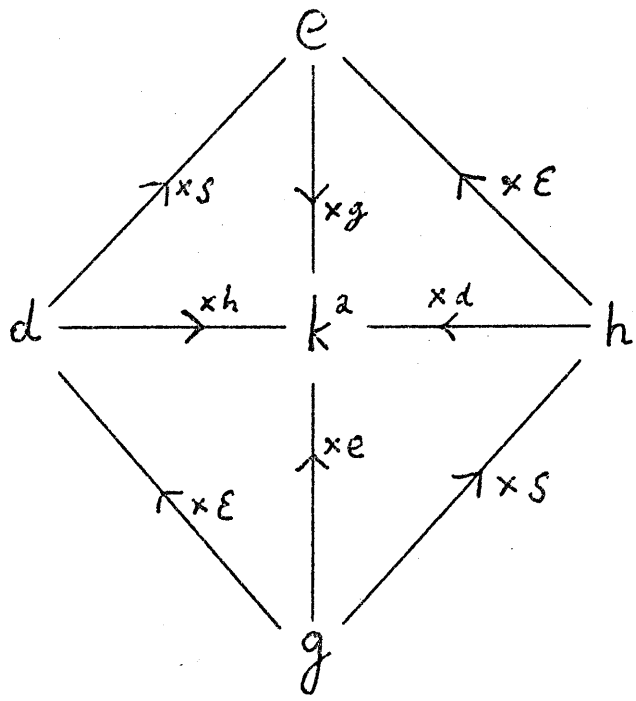

Fig. 4.3b Commutative diagram showing approximate relations between piezoelectric constants.

from the relation $h \simeq k^2/d$.

It is interesting to note that while d values vary by two or three orders of magnitude, the h values are all of the same order.

Ohigashi (1976) shows that for PVF_2 film, e_{33} and k_{33} remain almost constant with temperature from -170 to + 70°C, while s decreases and d_{33} increases. (One would expect a polymer to become more compliant when warmed, and Figure 4.3B shows why d_{33} increases as a result).

Ohigashi does not mention g or h, but with e_{33} and k_{33} constant with temperature then g_{33} must also be constant. h_{33} must decrease with temperature and ε must increase. A graph of the increase of ε_{33} with temperature has recently been published by Sessler (1981).

It has been confirmed that ε_{33} decreases with frequency, falling from 14 at 0 Hz to about 6 at 10 MHz and 4 at 100 MHz (Leung and Young 1979). If the elastic modulus increases with frequency as suggested earlier, g would remain constant with frequency, although d and h would not. Bacon (1982) considers that a reasonable working assumption is that g does not vary with frequency.

4.5 Comparison of PVF_2 with ceramic transducer materials

Woodward (1977), assessing the suitability of PVF_2 as an underwater transducer material, argues that it cannot be as good as PZT or barium titanate as a projector because its d_{33} value is so much lower, and that it cannot be as good a receiver either, because its

relative permittivity is so much lower although its g_{33} value is higher.

Table 4.4 shows some of Woodward's values.

Material	d_{33} $10^{-12}CN^{-1}$	g_{33} $10^{-3}Vm^{-1}Pa^{-1}$	ε_R	ρC $10^6 rayl$
PZT - 4	289	26.1	1300	34.5
PZT - 5	593	19.7	3400	34.2
$BaTiO_3$	190	12.6	1700	25.0
PVF_2	35	330	12	3.5

Table 4.4

His argument seems to be based on three rules of thumb that can often be found in transducer manufacturer's data sheets:

1. In a motor situation a large deformation is required for a small applied voltage, hence a high d value is needed.
2. In a generator situation a large voltage is required for a small force applied, hence a high g value is needed.
3. The capacity of the transducer is proportional to the relative permittivity of the piezo material. A large capacity is required in a receiver to reduce signal loss due to the shunt capacitance of the connecting cable, hence a high ε_R value is needed.

In fact, d and g are based on electric field strength not voltage, and both field strength and capacitance are inversely proportional to the thickness of the dielectric. These rules should be quite satisfactory when comparing transducers of similar thickness and similar values of acoustic impedance but should not be used to compare PVF_2 film with ceramic transducers where these parameters differ by an order of magnitude or more.

Redwood (1963) quotes the formula:

$$F = \frac{-Z_l \, h \, C_o \, V}{Z_c + Z_l}$$

for the amplitude of the wave of force radiating from the front face of a transducer (impedance Z_c) into a load (impedance Z_l) upon the instantaneous application of a voltage V. F is the total force (stress x area), C_o is the electrical capacitance of the transducer and h is the piezoelectric constant for the stress developed per unit applied charge density.

It is instructive to apply this formula to compare the outputs of the ceramic transducer described in Redwood's paper with a 25 μm thick PVF_2 foil transducer of the same area when both transmit into water.

The specification of Redwood's transducer, (probably barium titanate) is: Zc = 25 M rayl, h = 1.5 GNC^{-1}, C_o = 1 nF,

diameter = 1 cm.

A circular 25 μm PVF_2 transducer 1 cm in diameter would have a capacitance of 360 pF (assuming R = 13). Taking the extreme values of Z_c and h_{33} for PVF_2 from tables 4.2 and 4.3 and applying Redwood's formula for an input of 100 volts and a water load (Z_1 = 1.5 M rayl),

For Redwood's transducer F = -8.5 N

For 25 μm PVF_2 (Zc = 3.5 M rayl, h_{33} = -2.44 GNC^{-1})

F = 26.4 N

For 25 μm PVF_2 (Zc = 4.7 M rayl, h_{33} = -0.43 GNC^{-1})

F = 3.7 N

These results suggest that PVF_2 film should be about as good as a barium titanate plate transducer when used under water.

Experimental work on PVF_2 foil

4.6 Aluminium coated PVF_2

A quantity of "Kureha KF Piezo film" was obtained, in sheets 100 mm square and in thicknesses of 9 μm and 30 μm. It had been uniaxially stretched and poled by the manufacturer and had conducting surfaces of aluminium. One side of each sheet was marked with an ink line which indicated the direction of stretch and marked the surface that was positive during polarisation.

In order to try the film as a piezoelectric transducer for use under water, squares of about 10 mm side were cut from the 30 μm thick film and glued to the flat surfaces of some rectangular brass bars using Araldite AV/HV100. It was expected that the glue layer would

be thin enough to allow the rear surface of the foil to be capacitatively coupled to the brass bar which was earthed. A connection was made to the front faces of the piezofilm, and the bar was submerged in water. By driving one piece of film with the 300 volt negative voltage spike from a Lehfeldt flaw detector and displaying the output from another film on an oscilloscope, it was quickly established that the foil would transmit and receive ultrasonic pulses through water.

The aluminium coating on the foil was unsatisfactory and as a result the transducers ceased to work after a few minutes.

There are four main problems with the aluminium coatings.

i. The highly electropositive aluminium is in direct contact with the water which acts as an electrolyte. If there is a D.C. path from the coating to another less electropositive metal under the water the coating will start to dissolve, and the foil surface will become covered with gas bubbles which impede the ultrasound and generate low frequency random noise as they form and break off.

ii. The electrical conductivity of the surface coating varies greatly from one place to another. The manufacturer's specification states that the surface coating of a piece of foil 10 mm wide and 60 mm long will have a resistance of between 3 and 30 ohms when measured lengthwise.

In fact any strips of this size that were checked had a resistance of 5 ohms or less but the resistance of strips 60 mm long and 1 mm

wide varied between 110 and 250 ohms and 0.5 mm wide strips varied between 250 and 450 ohms.

iii. It is difficult to make a reliable electrical connection to the aluminium surface. Silver loaded epoxy resin does not make a good contact because the silver evidently reacts chemically with the aluminium and forms a poorly conducting barrier. Under water the aluminium coating quickly dissolves in the neighbourhood of the silver epoxy resin through electrolytic action.

Attempts were made to attach wires to the aluminium coating of the foil using an ultrasonic welder. They were unsuccessful because the PVF_2 under the coating does not form a rigid base, and the vibration energy of the welder was absorbed by the polymer before it could weld the aluminium. The only reliable way of getting a good electrical connection is to fold a piece of aluminium foil into a little pad at least four layers thick, and clamp this on to the piezofilm surface using an aluminium plate held down with aluminium screws and connected with aluminium wires. This forms a good contact over a large area and minimises electrolytic problems.

iv. The aluminium coating is not sufficiently firmly attached to the PVF_2. This and the uncertain surface resistance preclude its serious use as a transmitting transducer. Provided that the whole of the aluminium coating and the connecting clamp are under water, the foil will usually function for a limited period as a transmitter of ultrasonic pulses when driven by high voltage pulses. After a few minutes or a few days, parts of the foil will cease to radiate

ultrasound because electrical discontinuities appear in the coating. Out of water (with an air loading), the coating lasts only a few seconds.

It is interesting to use a binocular microscope to watch the surface of a piece of foil when it is connected to the output of the flaw detector. After switching on, little fragments of the aluminium surface start to fly off, and, and at 100 x magnification, give a very spectacular display like a miniature snowstorm. The disturbance always starts near the electrical connection to the coating but can erupt at isolated areas of the foil. The display ceases when the electrical connection becomes isolated after 10 or 20 seconds.

4.7 Gold coated PVF_2

A conducting surface of an inert metal like gold should overcome problems (i) and (iii), and while the evaporation of gold under a vacuum was the obvious technique to use, the University had no facilities to do this. Instead, a conducting gold layer was deposited onto the polymer by sputtering.

Method

38 mm x 21 mm rectangular pieces of "KP Piezofoil" were soaked in a solution of potassium hydroxide to remove the aluminium, then washed in dilute nitric acid followed by distilled water.

The sputtering process generates sufficient heat to melt the polymer unless it is backed by a block of metal to act as a heat sink, and the small size of the sputtering chamber limits this block

to a maximum of 38 x 21 x 4 mm thick. Brass blocks were used and the PVF_2 was glued to one face using Araldite AV/HV100. During the sputtering process, the polymer crinkles and melts at the edges, but with practice, one can deposit sufficient gold without melting too much polymer.

After sputtering, the areas of damaged polymer can be cut away with a scalpel and a connection made to the gold surface with silver loaded epoxy resin. The brass backing forms the other electrode.

It is interesting to note that although the film almost melts while being sputtered, the piezoelectric properties are not destroyed. They are probably reduced as the manufacturer's data shows that at $90^{o}C$ d_{31} will fall from 20 to 14 pCN^{-1} in one day. Repoling after sputtering should restore the full piezoelectric property but this has not been tried as the transducers work sufficiently well as they are.

Transducers made this way have worked satisfactorily as transmitters and receivers of short ultrasonic pulses for over three years. They have withstood drive pulses of up to - 600 volts in and out of water as well as rough handling.

The electrolytic problem is minor. Under water the gold electrode becomes slightly positive and account must be taken of this when connecting an amplifier. The gold does not dissolve or form a layer of bubbles, but may become covered with a layer of calcium carbonate. This can be removed with dilute acid, but it has no apparent effect on the performance of the transducer and does not

seem to generate noise.

It is very easy to make a good electrical connection to the gold with silver loaded epoxy resin, and after three years' use, the gold surface shows no sign of coming off. Figure 4.4 shows one of the brass backed transducers on a piece of pin board. Figure 4.5 shows the typical Chad shaped pulses that these brass backed foil transducers produce from a reflecting thick metal target when used in pulse echo common mode under water. They were driven by a Panametrics pulser 5052PR which gives a pulse of - 300 volts with a rise time of less than 25 ns.

The major disadvantage of these transducers is that they produce a succession of short pulses as a result of reverberation in the backing. Ideally the backing should absorb all the sound that passes into it from the foil, but it has also to be a good conductor of heat and only 4 mm thick. Brass was the most absorbant metal available. Figures 4.6 and 4.7 shows that the main pulse reflected from a thick metal target is followed by a succession of inverted pulses of the same shape at 2 μ sec intervals from the back of the brass backing.

4.8 PVF_2 as a transducer over an angle

The imaging system requires transducers that will transmit and receive ultrasonic pulses over a plane angle for a B scan and a solid angle for a C scan.

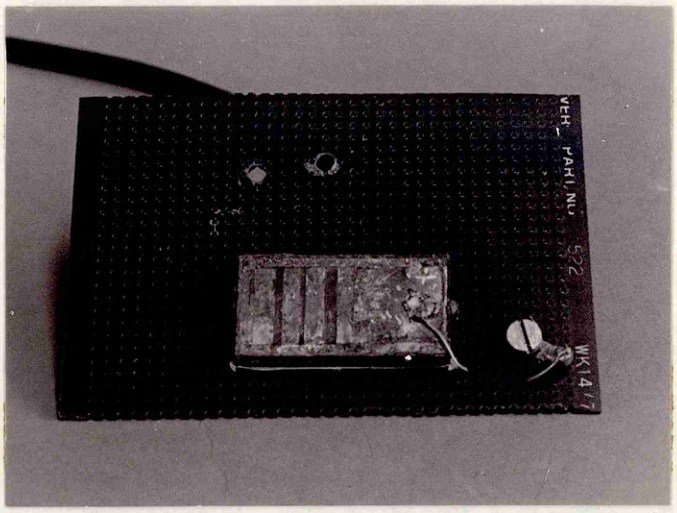

Fig. 4.4 Gold coated PVF_2 on brass backing.

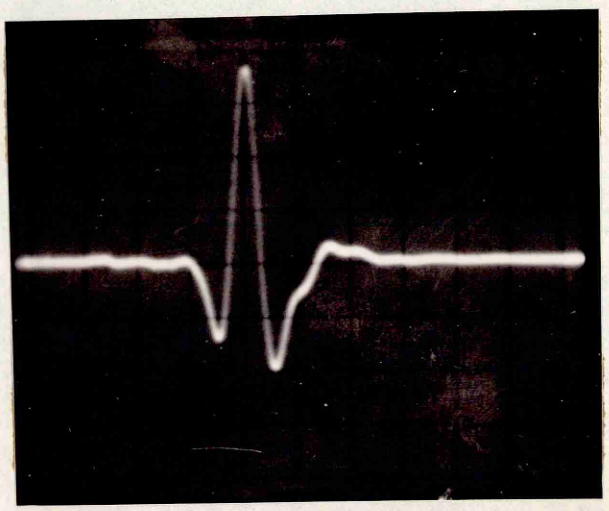

30 μm foil

100 ns per division

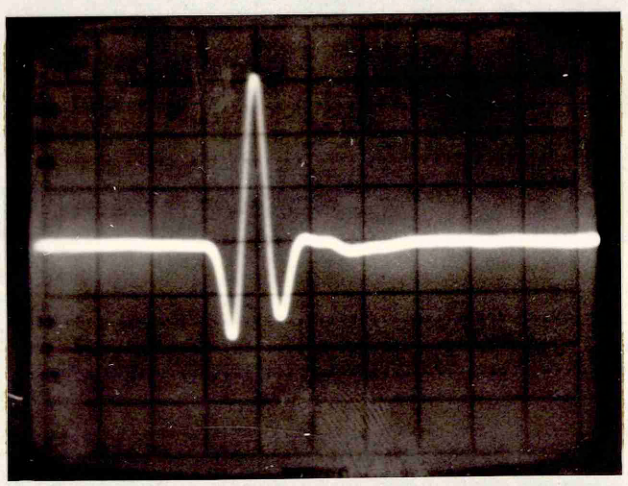

9 μm foil

100 ns per division

Fig. 4.5 Common mode response of brass backed PVF_2 transducers.

Fig. 4.6 Common mode response of 30 μm thick PVF_2 brass backed transducer.
500 ns per division.

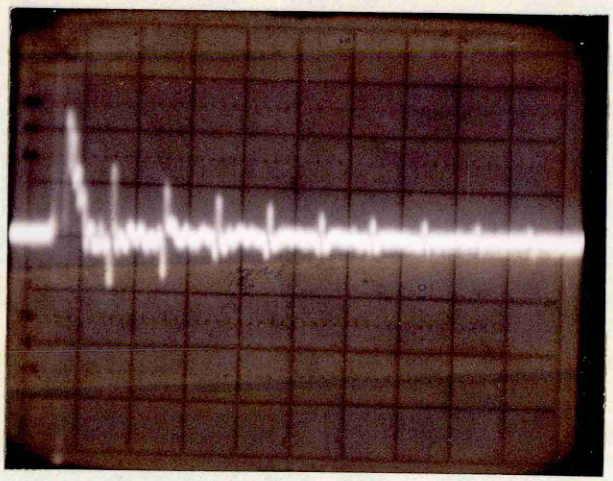

Fig. 4.7 As above.
2 μs per division.

Transmitting and receiving over a plane angle was achieved by wrapping PVF_2 foil around a cylinder. Cylinders of brass, perspex and nylon with diameters from 19 mm to 51 mm were tried as backings for strips of aluminium coated PVF_2 film, and it was shown that these would act as receivers of ultrasound from all directions in the plane normal to the foil surface. A strip 10 mm wide had a response within $\pm$ 0.5 dB at all points around the cylinder, but a strip 1 mm wide or less had a lower response that varied by $\pm$ 3 dB or more. This was put down to variations in the conductivity of the coating. (See Section 4.6).

For transmitting, gold coated foil had to be used, in most cases. Brass and (to a lesser extent) perspex were found to be unsatisfactory for use as cylindrical backings because reflections inside the cylinder were picked up by the PVF_2 as a series of small pulses after the first arrival. Nylon cylinders did not give this problem and nylon has been used as a backing for all subsequent PVF_2 transducers. Nylon has an acoustic impedance of about 3 M rayl, and Araldite AY103/HY991 about 2.4 M rayl. The impedance of the film is about 4 M rayl (section 4.4, Table 4.2), so that PVF_2 nylon and araldite are a good acoustic match.

The obvious approach to transmitting and receiving over a solid angle was to use PVF_2 film moulded into a spherical surface. It was apparent that flat sheets of PVF_2 could not easily be formed into a dome shape without using a mould at a high temperature, after which the foil would probably need repoling. Aparatus to do any of this was not available.

An experimental three dimensional surface was made by clamping each end of a 50 x 100 mm rectangular piece of 30 μm aluminium coated PVF_2 foil between pairs of wooden blocks (Figure 4.8). The block pairs were pulled apart by a spring and one pair of blocks rotated slightly in relation to the other along the spring axis so that the foil was strained into a three dimensional surface (Figure 4.9). Such a surface is usually called "A hyperbolic parabaloid". When this was immersed in the water tank it could be used to transmit and receive ultrasonic pulses from both sides over a solid angle of at least 74^{o} laterally and 24^{o} vertically at roughly constant amplitude. The path length of a pulse originating from such a surface would be difficult to calculate.

A further method of making a transducer with a response over a solid angle is to use a very narrow strip of PVF_2 film wrapped around a cylinder.

A heavily damped commercial ultrasonic probe which produces short pulses (Figure 4.10) was used to insonify strips of aluminium coated foil wrapped around a perspex cylinder under water. Polar plots were made of the response along the long axis at points around the circumference (Figure 4.11).

The response of the narrow foils varied by up to 4 dB from one place to another, and the individual polar plots were very lopsided. On average the response of a 0.75 mm wide strip fell by 3 dB at about 22^{o} off axis and that of a 0.5 mm strip by about 27^{o}. Figure 4.12 shows the average lateral response of a 0.5 mm wide strip

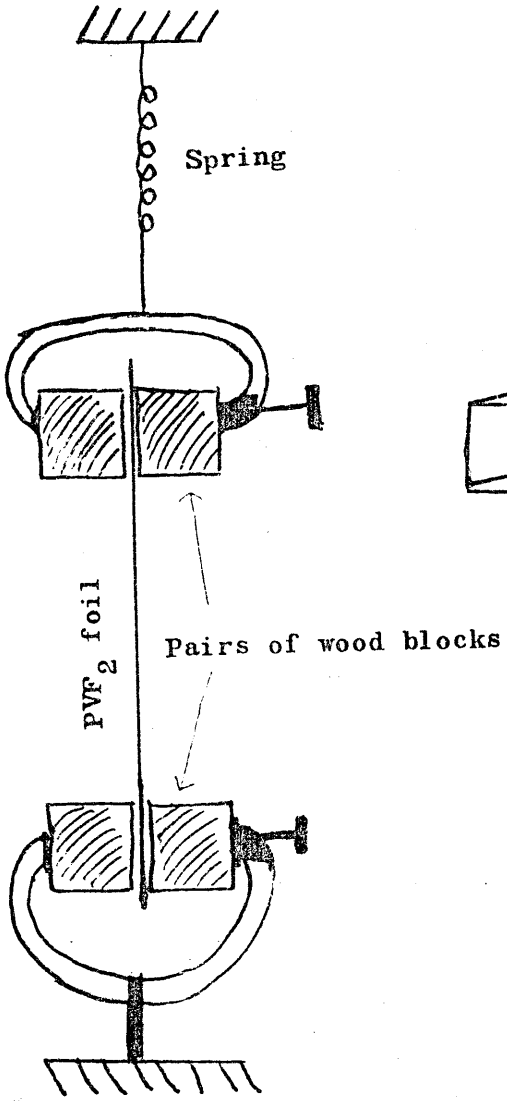

Fig. 4.8 PVF_2 film clamped between wood blocks and tensioned.

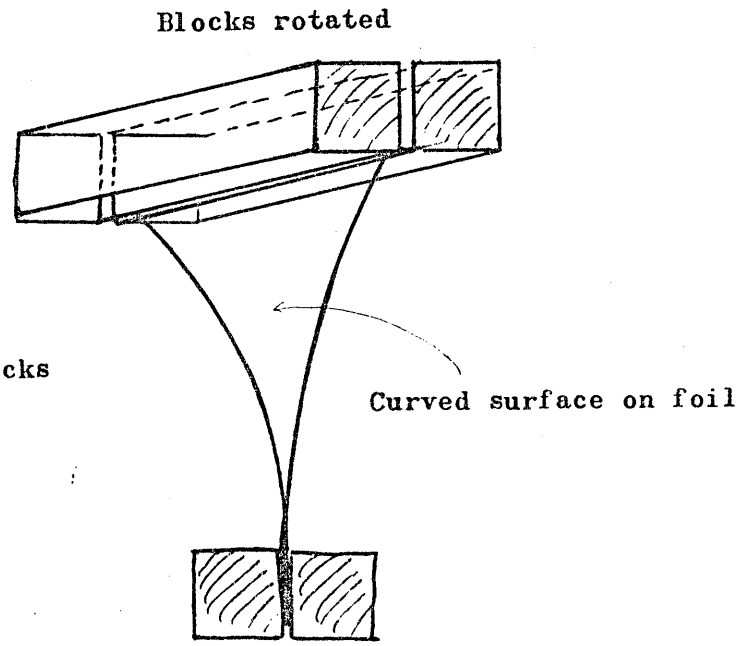

Fig. 4.9 Blocks turned to form 3 dimensional curved surface on PVF_2 film.

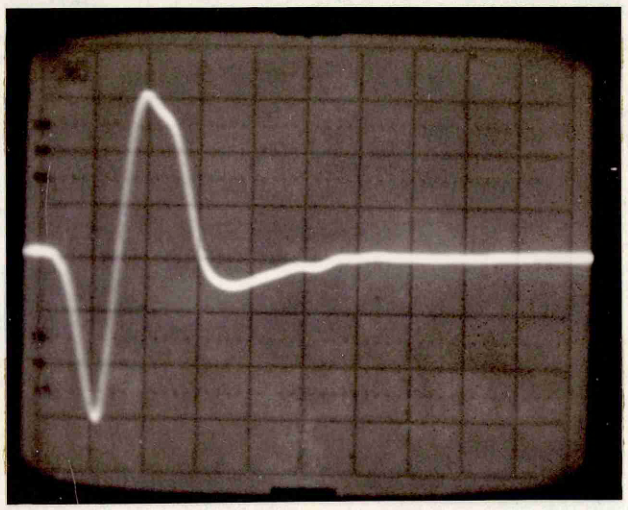

Fig. 4.10 Response of heavily damped commercially made ultrasonic probe.
100 ns per division.

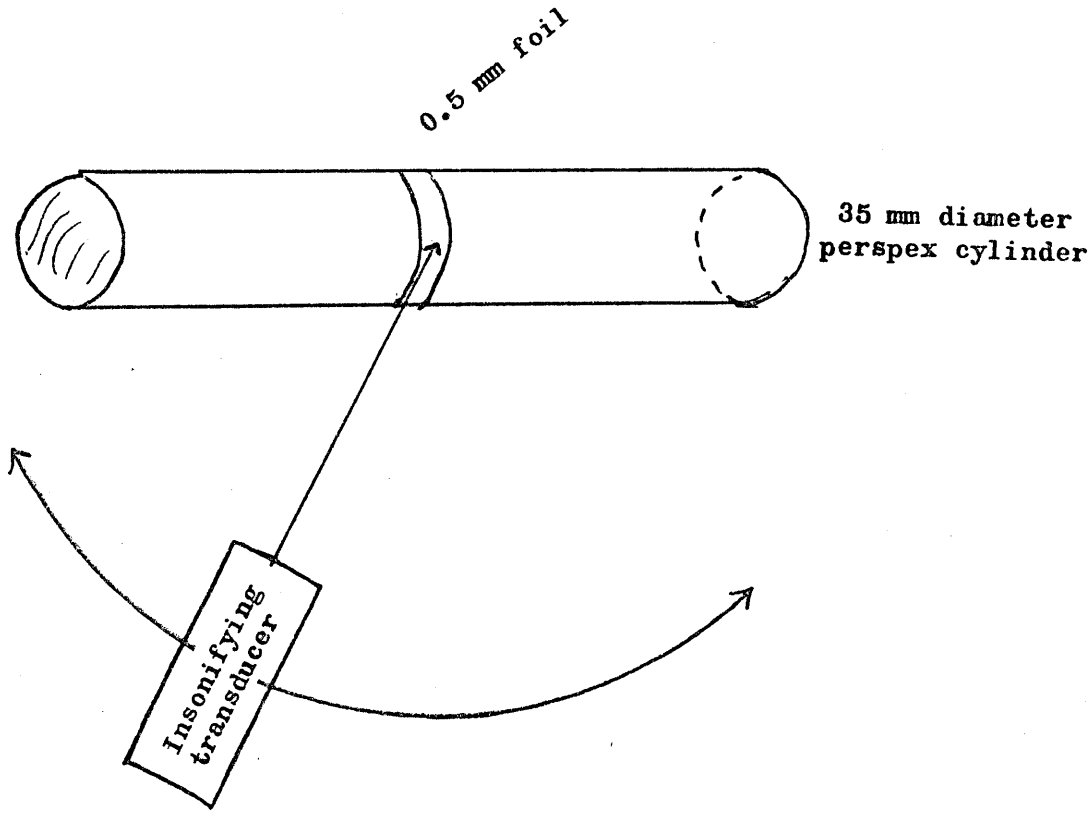

Fig. 4.11 Method of measuring off axis response of narrow strip of PVF_2 film wrapped around a cylinder.

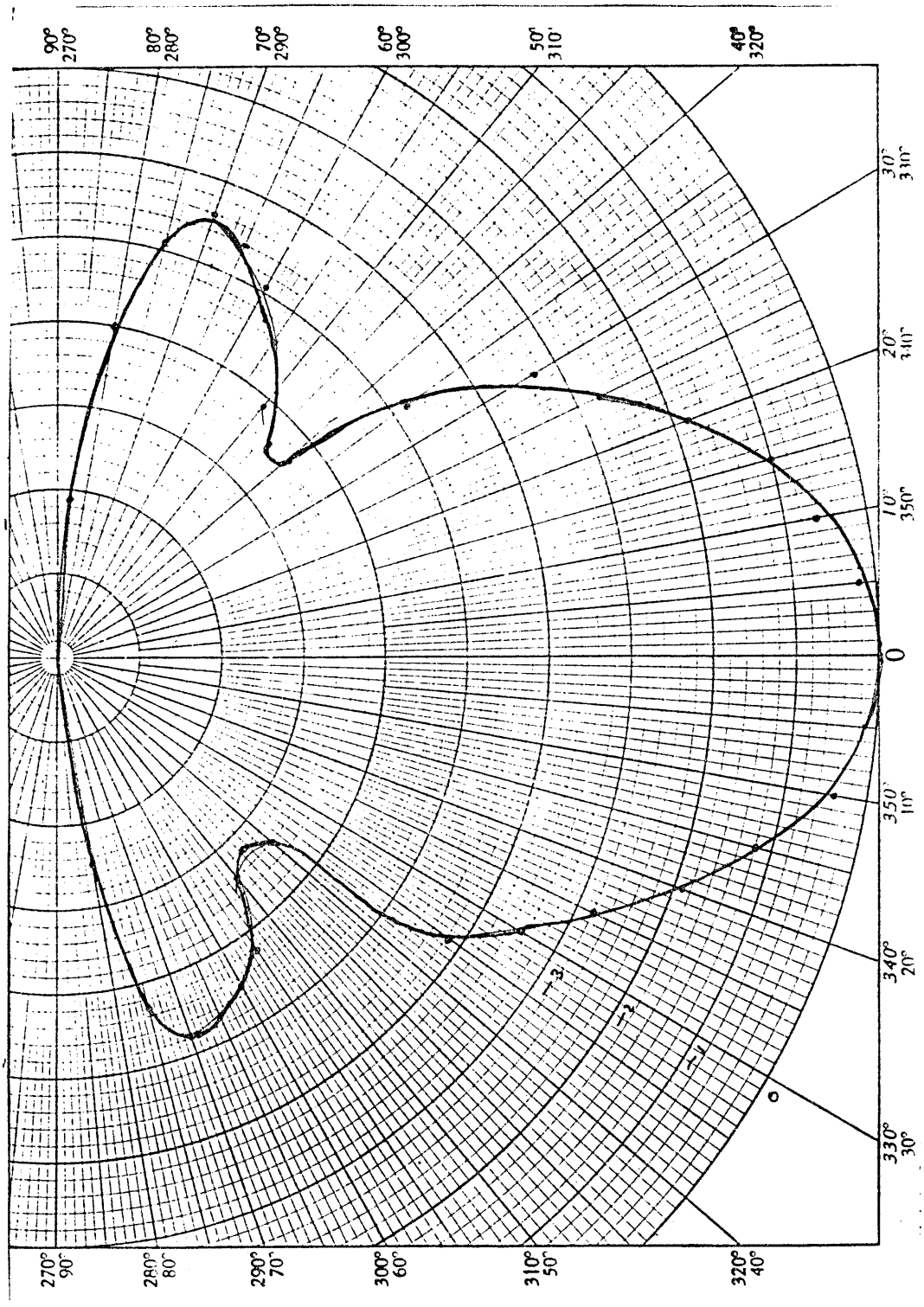

Fig. 4.12 Polar plot of response of 0.5 mm wide PVF_2 foil on 35 mm. diameter perspex cylinder taken along the cylinder axis. Eaoh large division represents 1dB.

on a 35 mm diameter perspex cylinder.

It was concluded that narrow strip transducers could be used as receivers over a solid angle if the surface conductivity could be made more uniform. (Gold coated foil was not available at this stage).

A spherical shell film transducer seems the best solution for solid angles, and Micheron and Lemonon (1978) have since reported the development of moulded and poled PVF_2 transducer domes for use as directional loudspeakers.

It was decided to discontinue this line of research and to concentrate on the design and construction of a two dimensional imaging system.

4.9 Gold and chromium coated PVF_2

At this stage of this research, the manufacturer of "KF Piezofilm" ceased supply. It was necessary to find another source of film, but it soon became clear that it was not generally available. Two pieces of gold coated piezofilm were kindly donated by a company that wishes to remain anonymous.

The film was described as being 25 μm thick, biaxially stretched, PVF_2 which had been coated first with a 50 nm layer of chromium and then with a 200 nm layer of gold. The metal coatings had been put on by a two stage evaporation process in a vacuum of about

10^{-3} Pa and the film had then been poled by applying a high voltage between the coatings for about 20 minutes at about 100°C and the voltage was maintained as the temperature was then reduced to ambient.

The chromium acted as a key for the gold, and the double coating was said to be able to withstand "the Sellotape test". (If Sellotape is pressed on to the foil and peeled off, the coating remains on the foil). Foil that passes this test is expected to be satisfactory as a transmitting transducer and the coating will not come off in use.

The two pieces of film were roughly circular, about 100 mm in diameter. Transducers were made from these by cutting out rectangular strips with a scalpel and etching unwanted areas of metal from the surface. The gold coated film had to be used very sparingly as so little was available. It had to be used for transmitting transducers but the development work on the receivers was done with KF aluminium coated foil (of which there was plenty remaining). Gold coated foil was only used for receivers when the final design was clear.

4.10 Manufacture of cylindrical transducers with PVF_2 film

i. Etching the coating on the PVF_2 film:

Masking the areas of foil not to be etched is difficult, and the technique needs perfecting. The problem is that the foil is very floppy and has to be coated on both sides.

Application of photo resist to one side makes the foil try to curl up, and gravity then ensures that the coating will be uneven. The

photo resist contracts as it dries causing the as-yet uncoated side to become slightly convex. Photo resist applied to this side drains to and over the edges, rewetting the first side.

The gold areas to be retained are protected by hardening the photo resist over them with ultraviolet light. A pair of photographic masks, one for each side of the foil, is used to block off the ultraviolet light from those parts to be etched.

Figure 4.13 shows an example of the masks for a foil transducer with three separate active elements and a common earth. Great care has to be taken to ensure that the photo resist covers well everywhere and that it is properly irradiated with ultraviolet light. The iodine in the gold etch goes under the mask with great ease, and there were a number of accidents as a result. Ultraviolet treatment is best done in the reprographic department: the ultraviolet lamps used for printed circuits can make the foil very hot.

Etching solutions: Gold. Dissolve 15 gm potassium iodide and 25 gm iodine in 250 ml water. Use at room temperature.

Chromium. Dissolve 12.5 gm ceric sulphate in 250 ml. water, add 18.5 ml nitric acid. Use at room temperature.

Etching the exposed gold and then the chromium each takes about one minute. The photo resist mask can then be removed with trichloroethelene.

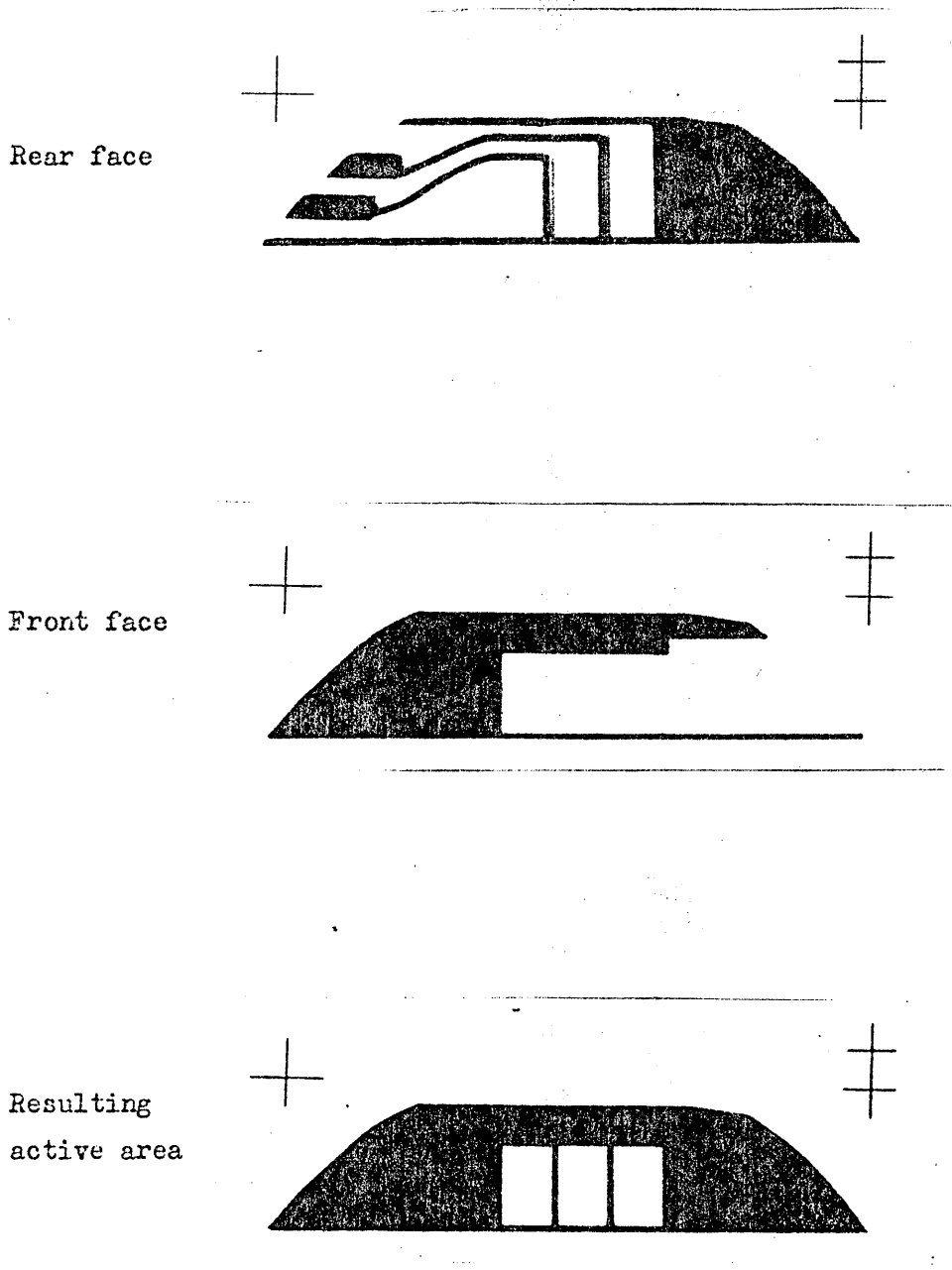

Fig. 4.13 Photographic mask for transducer with 3 sections.
Gold is removed from the black areas but remains in the clear areas.

ii. Glueing PVF_2 to nylon

The etched PVF_2 foil is glued to the nylon using Araldite AY103/HY991, an epoxy resin with very low viscosity. This allows the foil to be pressed smoothly on to the backing with a minimum of thickness of adhesive. Setting takes several hours and there is time to make adjustments and squeeze out air bubbles. Connections are made to the gold coating using RS Silver-Loaded Epoxy Resin, and the connections covered with Araldite AV138/HV998, an epoxy resin with a very high viscosity.

A problem with nylon is that it absorbs water slightly, and this seems to affect the adhesion of the Araldite AV138/HV998. In a test, a 32 mm diameter x 100 mm long nylon cylinder of mass 91 gm, submerged in water, absorbed 0.22 gm water in 24 hours (and about 1 gm after 2 months). For this reason, the transducers must not be kept under water for long periods without further protection.

Figure 4.15 shows the loop impulse responses of a 16 mm radius cylindrical and a flat nylon backed PVF_2 transducer with a thick metal bar 36 x 36 x 166 mm as reflector. The drive pulse is shown in Figure 4.14. Figure 4.16 shows the impulse response of a 25 mm radius cylindrical transducer when driven by the Panasonics pulser with rise time 10 ns to 50 volts peak. Figure 4.17 shows the reflections from the front and back walls of an aluminium bar when insonified under water by the flat nylon backed PVF_2 transducer.

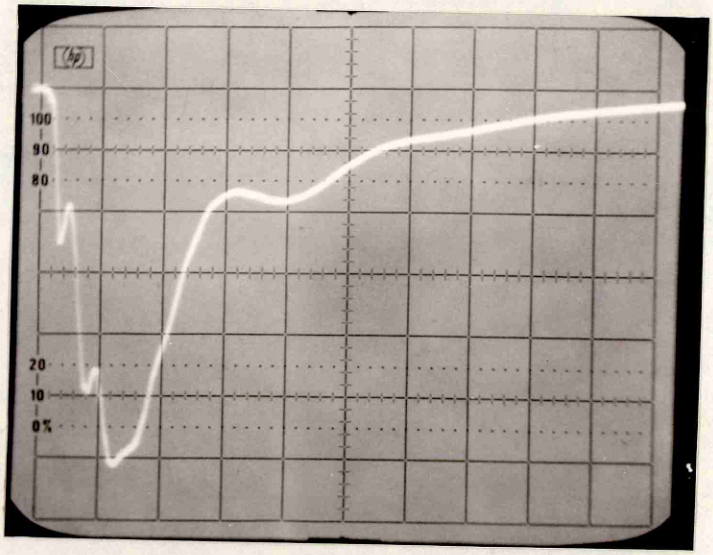

Fig. 4.14 Drive pulse to transducers
50 ns per division horizontally
20 volts per division vertically

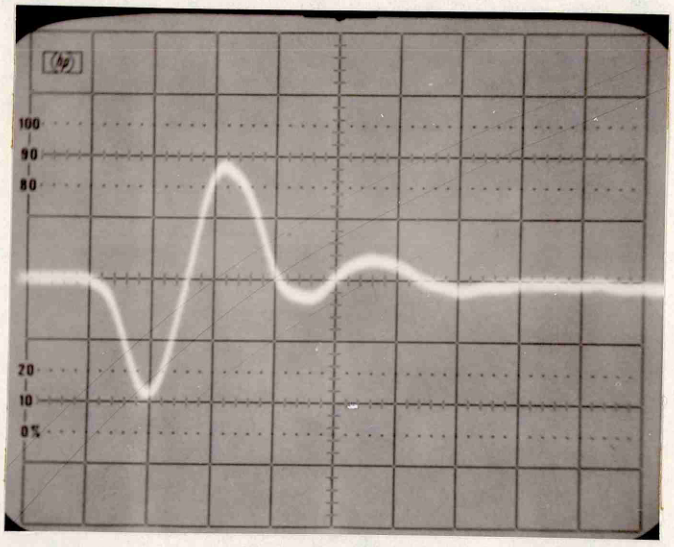

Cylindrical backing
16 mm radius

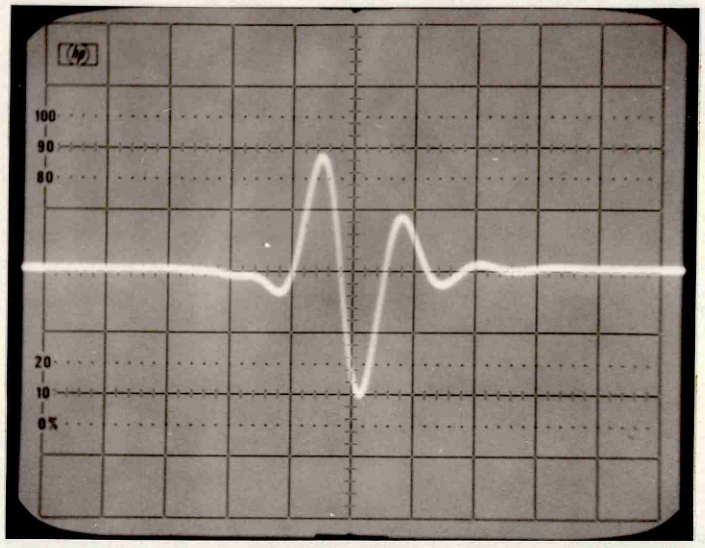

Flat backing

Fig. 4.15 Common mode impulse responses of nylon backed transducers driven by pulse in figure 4.14. 50 ns per division.

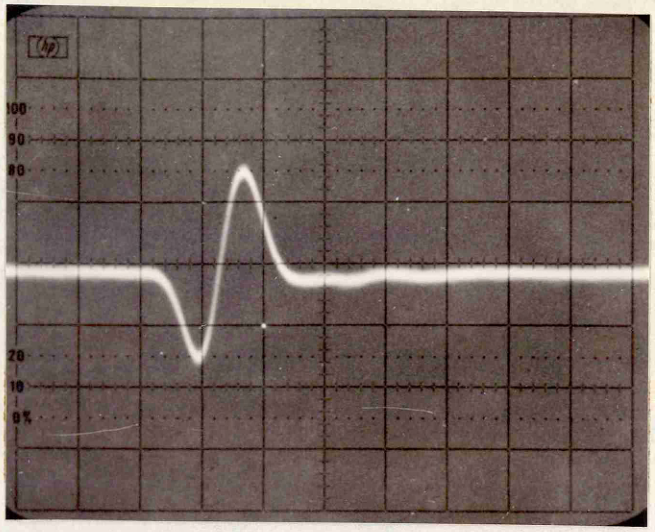

Fig. 4.16 Impulse response of 25 mm radius cylindrical PVF_2 transducer

50 ns per division.

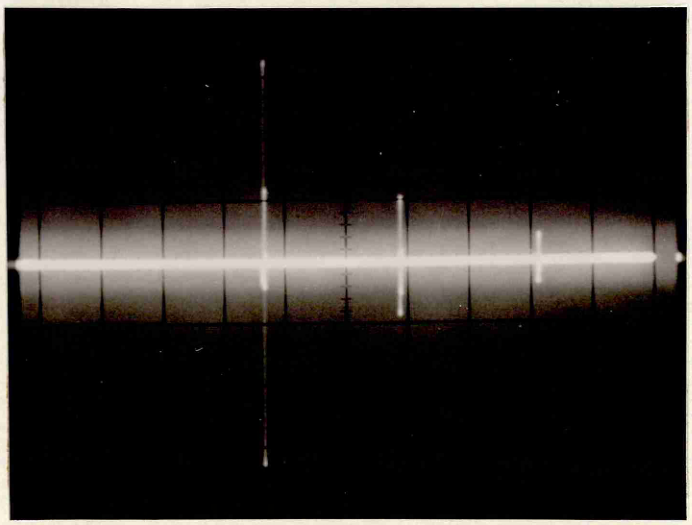

Fig. 4.17 Echoes from front and back walls of aluminium bar. 5 μ s per division.

Two queries that arose about these PVF_2 transducers were:

i. In view of the evidence that the foil is unhomogeneously polarised, is the performance of the transducer affected by which way up the foil is?

Four identical foils were glued to nylon cylinders, three one way up and one the other way up. This one turned out to be neither more nor less sensitive than the average of the other three, but further tests with a separate receiver showed that its output was inverted.

ii. Will the performance of the foil be improved if a d.c. polarising voltage is applied to it during transduction?
The answer is "yes, but the effect is very small". Application of -450 volts d.c. to a foil acting as a receiver gave an improvement of about 0.4 dB in the electrical output. Application of +450 volts d.c. reduced the output by perhaps 0.1 dB. The effect probably depends on which way round the foil has been polarised, but this is unknown with the gold coated foil.

4.11 Visualisation of ultrasonic waves from PVF_2 transducers

British Railways Board kindly allowed their stroboscopic Schlieren system at the Railway Technical Centre, Derby, to be used to visualise and photograph waves of ultrasound produced by the PVF_2 transducers. Figure 4.18 shows a succession of pictures of the wave produced by a 20 mm strip of PVF_2 on a 25 mm radius nylon cylinder. It spreads out with a beam angle of 45^{o} and is reflected

1.

5.

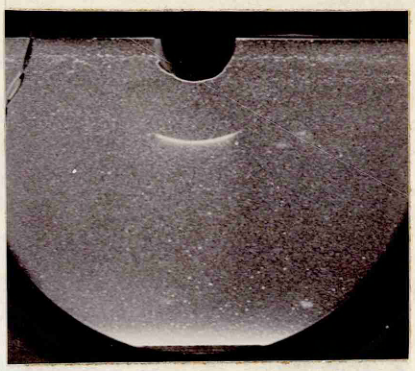

2.

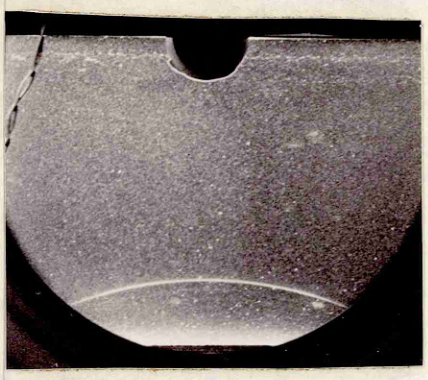

6.

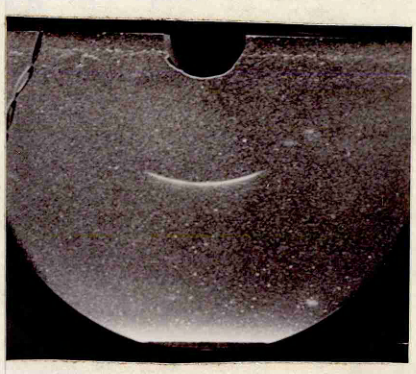

3.

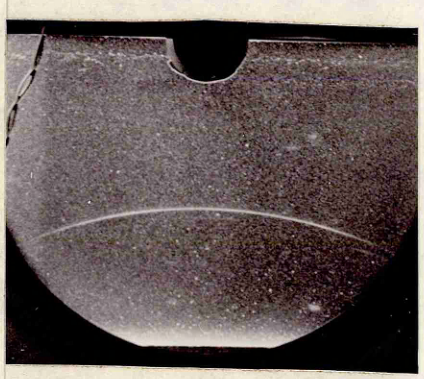

7.

4.

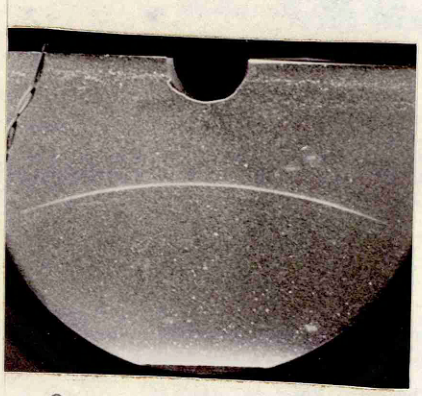

8.

Fig. 4.18 Schlieren images of an ultrasonic pulse transmitted by a 25 mm radius cylindrical PVF_2 transducer, spreading out and being reflected from the bottom of the water tank. The water in the tank is approximately 200 mm deep.

from the bottom of the tank. Figure 4.19 shows the pulses from a 16 mm radius cylindrical transducer. Figure 4.20 shows the wave produced by a plane film transducer with the active area of film 24 mm x 9 mm. The longer side of the film faces the camera so the wave front is 24 mm wide. It is particularly interesting to note that no edge wave can be seen, and that the pulse has the same width long after being reflected from the bottom of the water tank. Compare this with a 20 mm diameter ceramic transducer whose wave front is shown in Figure 4.21. The edge waves are clearly visible and the lightly damped response is evident.

We have shown (Crecraft et al 1982) that if edge waves are produced by PVF_2 transducers, then they must be at least 72 dB below the direct wave in strength. For a ceramic transducer the edge waves are only about 43 to 50 dB below the direct wave.

It was necessary to drive the PVF_2 foil with a pulse of 700 volts or more to produce a wave of sufficient intensity to be visualised. This eventually ruptured the gold coating which ceased to conduct electricity. Figure 4.22 shows one of the damaged transducers. Figure 4.23 and 4.24 shows close up details of the breaks in the conducting surface. In Figure 4.24, the break is in the conducting leads, but in Figures 4.22 and 4.23, the break runs diagonally across the active surface of the transducer. (The dark area T-shaped strip is merely the unwanted result of an accident during etching).

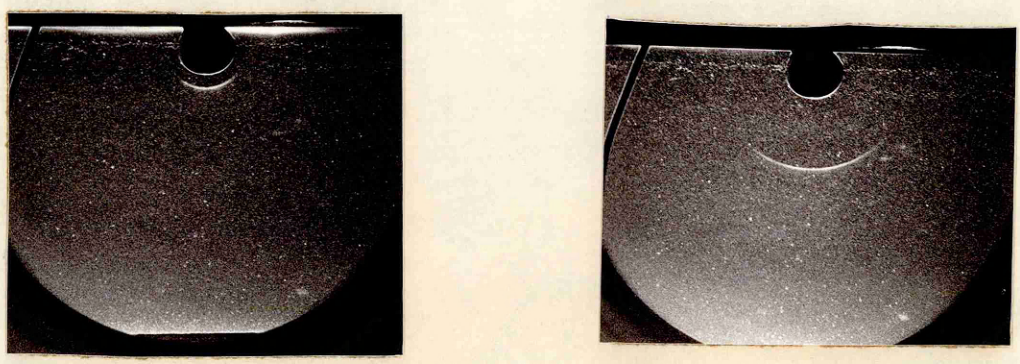

1. 2.

Fig. 4.19 Schlieren images of an ultrasonic pulse transmitted by a 16 mm radius cylindrical PVF_2 transducer.

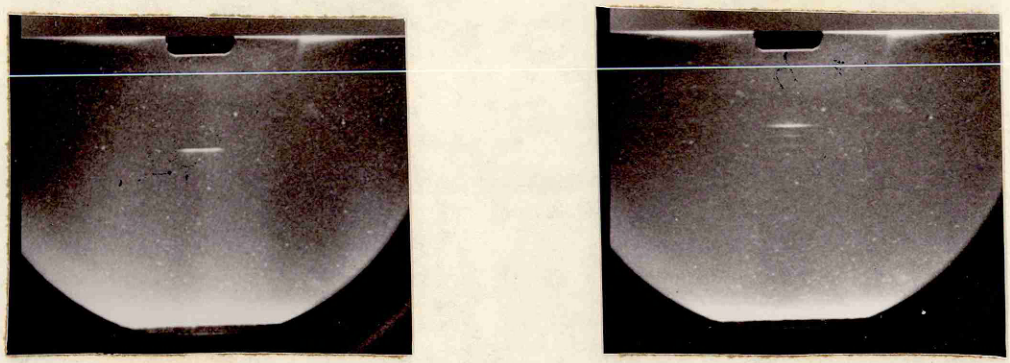

1. 2.

Fig. 4.20 Schlieren images of ultrasonic pulse transmitted by a flat PVF_2 transducer, and reflected from the bottom of the water tank.

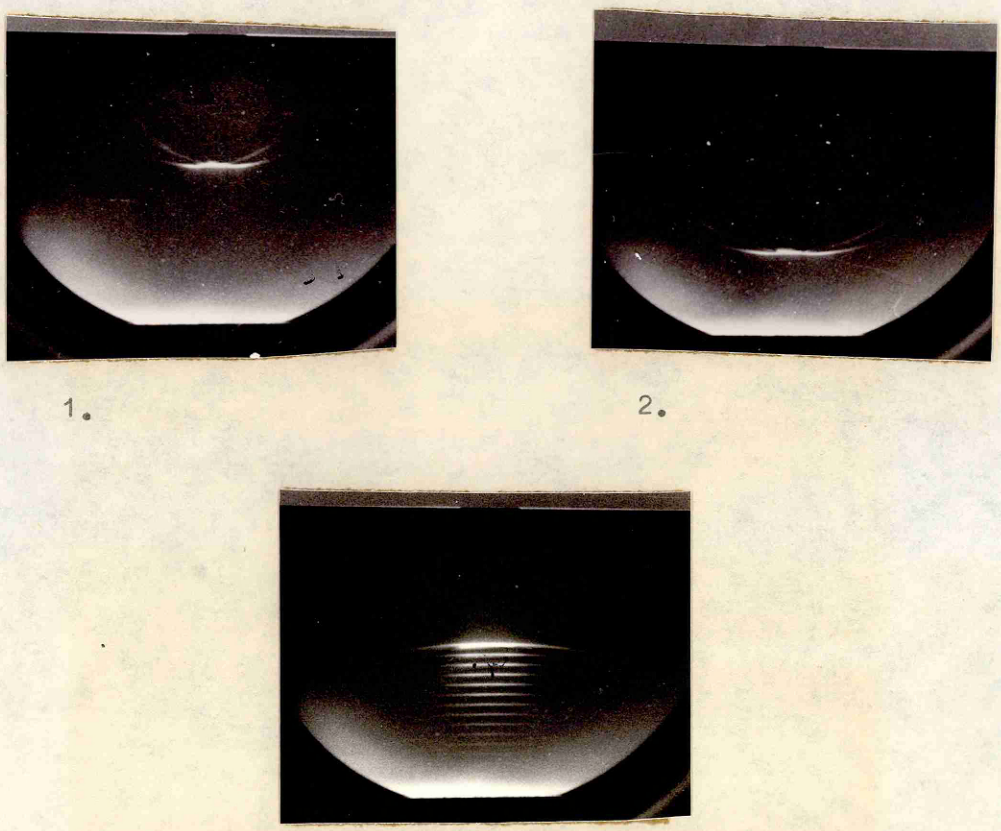

1. 2.

3.

Fig. 4.21 Schlieren images of ultrasonic pulse transmitted by a flat ceramic transducer, and reflected from the bottom of the water tank.

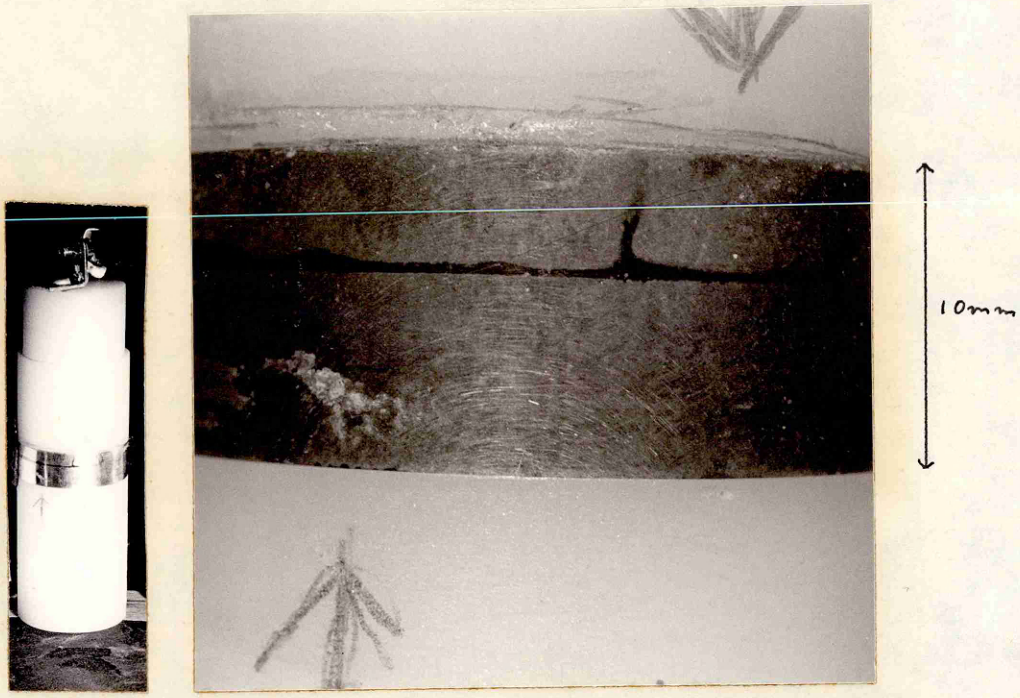

Fig. 4.22 Transducer damaged by high drive voltage. Discontinuity in gold coating on diagonal between arrows. (Large dark horizontal mark is an etching fault.)

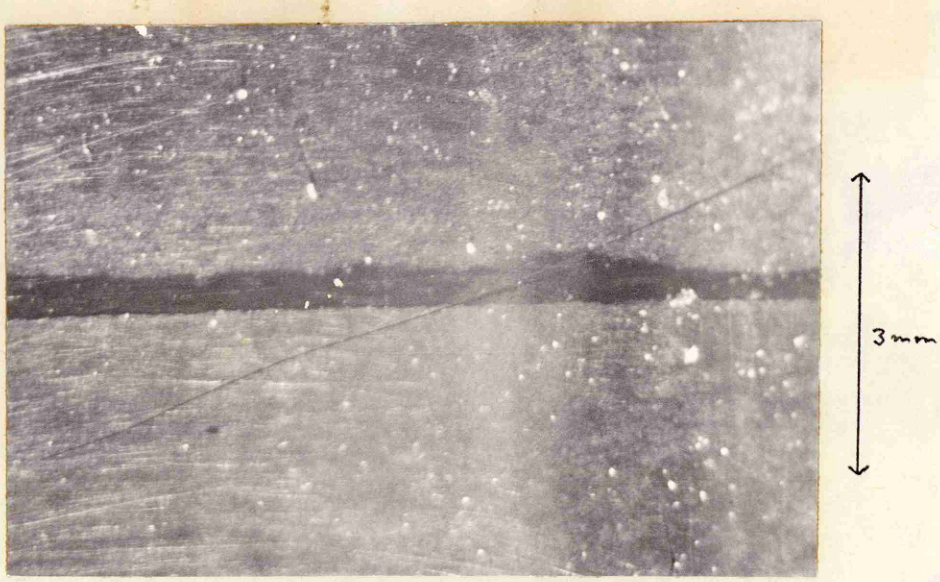

Fig. 4.23 Close up of damage to transducer. Diagonal line is a discontinuity in the gold coating on the active area of the PVF_2 foil.

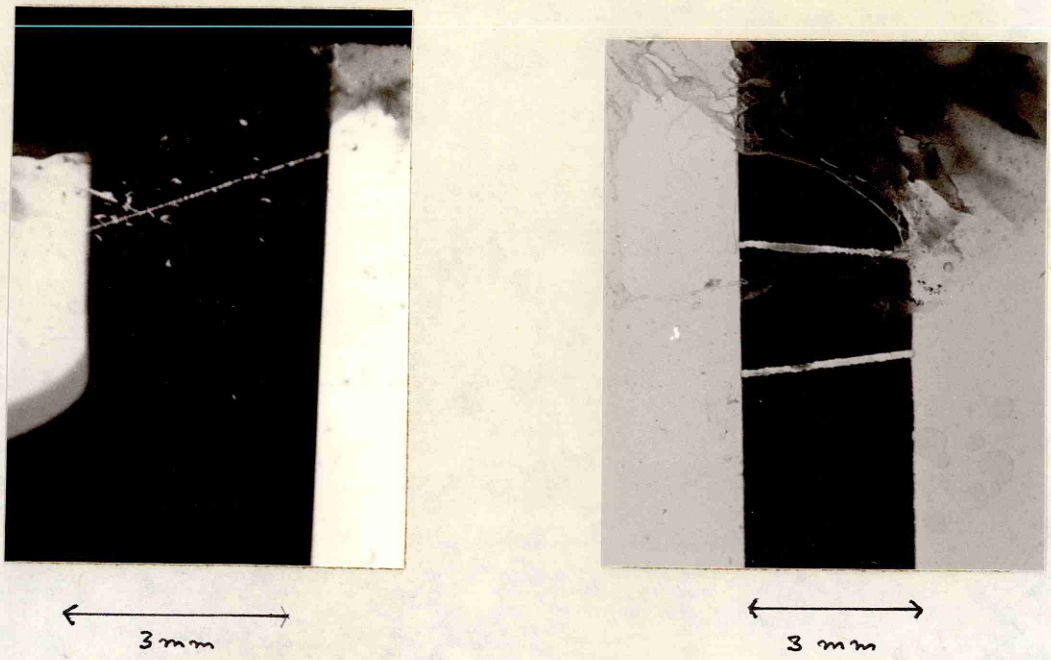

Fig. 4.24 Typical discontinuities in gold coating forming conducting leads on PVF_2 foil caused by high drive voltage.

Further experience showed that even the comparatively low voltage drive pulse of about 300 V from the Panasonic 5052 PR pulser could rupture the gold surface of the foil if the connecting conducting leads were too narrow. Figure 4.13 shows the mask for an experimental transducer used as a transmitter in three sections. First one section, then another ceased to work as the connecting lines ruptured over a period of three days.

4.12 Pulse shape

The PVF_2 foil gives an ultrasonic pulse that is generally of the shape shown in Figures 4.4, 4.5, 4.15, 4.16. The exact shape of the received pulse depends on whether the backing is flat or curved, brass or nylon, the shape of the drive pulse and the impedance of the receiving circuit.

Redwood (1963) gives a method of predicting the shape of a short pulse of ultrasound as transmitted and received by a transducer. Briefly, Redwood's method is as follows:

C is the transducer capacitance

h is the piezoelectric constant (force per unit charge)

V is the applied voltage

t is the time taken for a sound wave to cross the thickness of the transducer, the transit time

Z_1, Z_c, Z_2 are respectively the acoustic impedances of the load, the transducer and the backing.

On application of a voltage V to the transducer, a force

$F = \frac{-Z_1}{Z_c + Z_1} hCV$ will appear at the front face.

After times t, 2t, 3t, 4t, etc, the pulse generated at the back face and then the internally reflected pulses will arrive at the front face. These will have magnitude F times a series of multiplication factors that depend on Z_1, Z_c and Z_2 and are calculated as follows:

firstly, the reflection coefficients $r_o = \frac{Z_c - Z_1}{Z_c + Z_1}$

and $r_x = \frac{Z_c - Z_2}{Z_c + Z_2}$ are calculated.

then the multiplication factors are:

$-1,\ 1 + r_x,\ -r_x(1 + r_o),\ r_o r_x(1 + r_x),\ -r_o r_x^2(1 + r_o)$

at times 0, t, 2t, 3t and 4t.

For PVF_2 on a nylon backing transmitting to water, $Z_1 = 1.5$, $Z_c = 3.5$ and $Z_2 = 3.1$ M rayl.

Hence $r_o = 0.4$ and $r_x = 0.06$.

For PVF_2 on a brass backing transmitting to water, $Z_1 = 1.5$, $Z_c = 3.5$ and $Z_2 = 40$ M rayl.

Hence $r_o = 0.4$ and $r_x = -0.84$.

This gives the multiplying factors for the nylon backing

-1, 1.06, -0.08, 0.03, -0.002

and for the brass backing

-1, 1.16, 1.18, -0.05, -0.40.

Figure 4.25 shows the method applied to a 25 μm thick PVF_2 film on a nylon backing. The transit time is taken as 15 ns.

Solid curve 1 is the drive pulse shown in Figure 4.26. This is drawn below the axis to represent multiplication by -1. Dashed

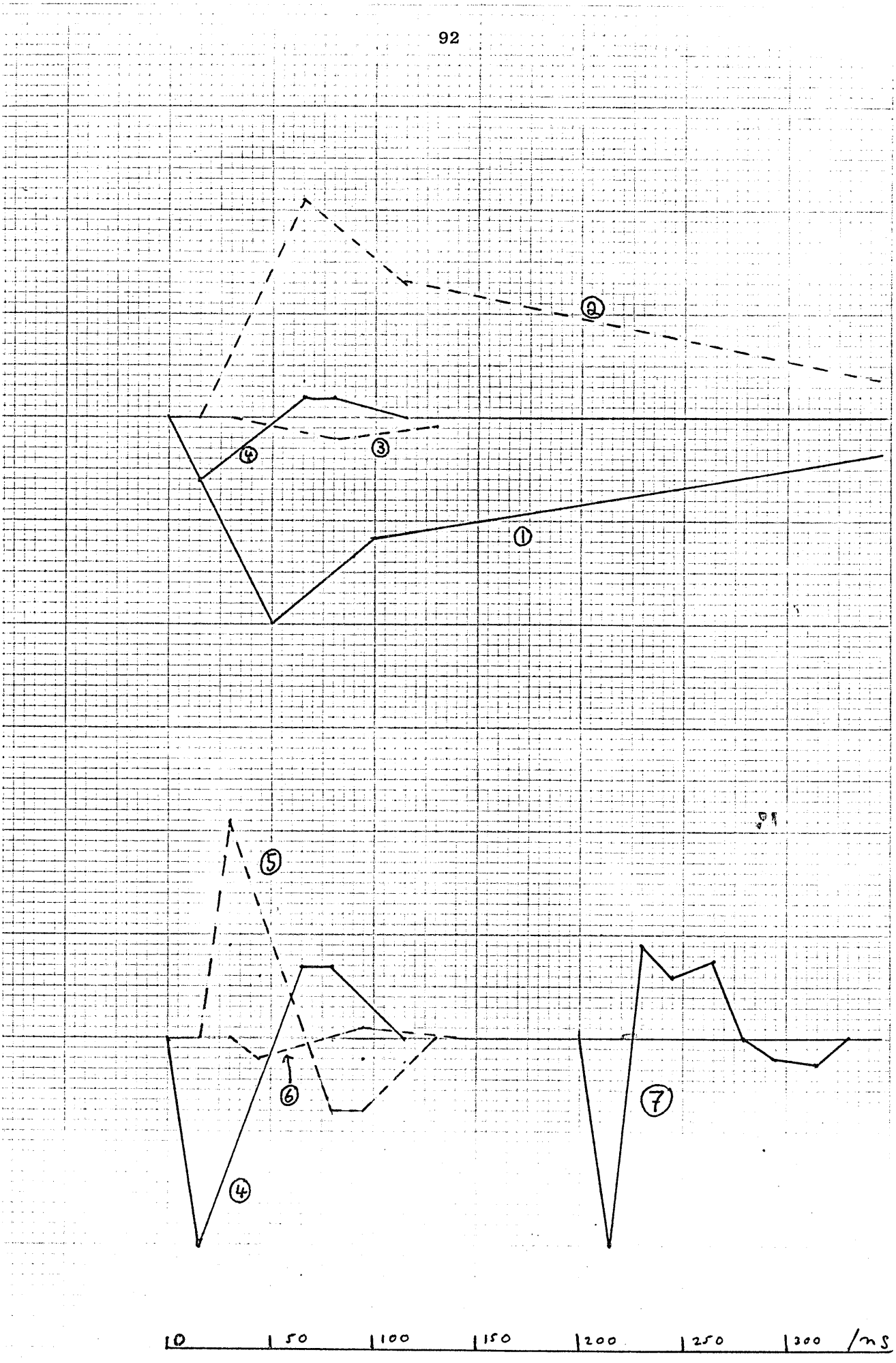

Fig. 4.25 Construction of predicted waveform for PVF_2 on nylon backing. 15 ns transit time.

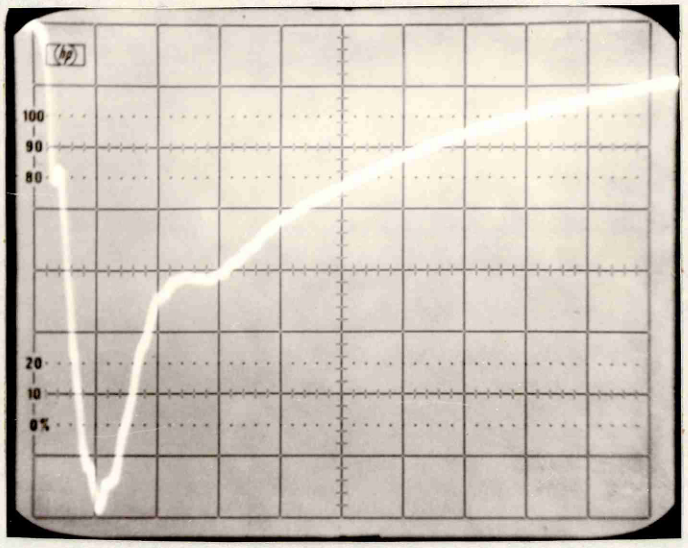

Fig. 4.26 Drive pulse to 25 μm PVF_2 foil.
50 ns per division.

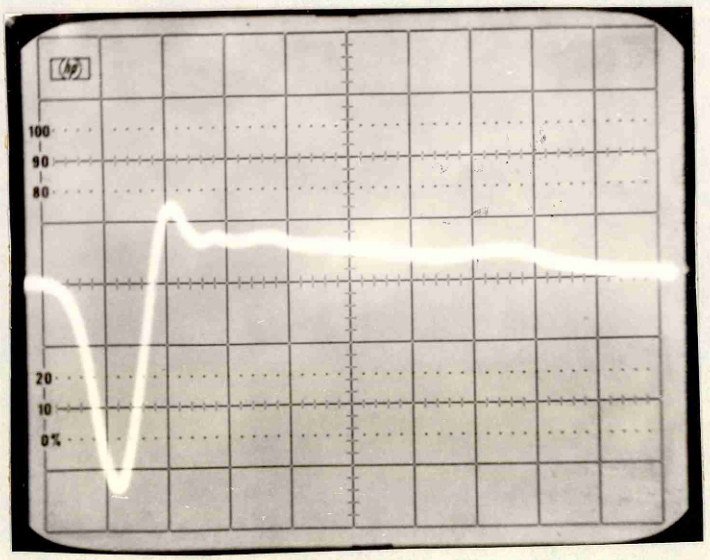

Fig. 4.27 Waveform received from 25 μm PVF_2 driven by pulse in fig. 4.26.
50 ns per division.

curve 2 is the drive pulse times $1 + r_x$ delayed 15 ns, and dashed curve 3 is times $- r_x(1 + r_o)$ delayed 30 ns. Further terms are negligible and are omitted. Curves 1, 2 and 3 add up to solid curve 4 which represents the pulse transmitted into the water. The method works again for the transducer when it acts as a receiver of the pulse in the water, (providing that it is feeding an open circuit).

Curve 4 is shown again (lower) at double the vertical scale. Dashed curves 5 and 6 show the multiplying factors and curve 7 is the output from the transducer. Unfortunately the electrical pulse predicted by Redwood's method bears no resemblance in timing or shape to the pulse that is actually received. Compare Figures 4.25 and 4.27. The predicted pulse has zero crossings at 25, 80 and 155 ns while the received pulse has one zero crossing at 90 and returns to zero at about 550 ns. The prediction for a brass backed transducer (Figure 4.28) is also incorrect although the shape is a better match. Compare it with Figure 4.29. Three possible reasons for the incorrect prediction are:

i. Redwood's formula is an approximation in as much as it does not take the mechanical time constant of the transducer into account. Redwood shows that the overall effect on pulse shape resulting from correcting for the time constant is small, being mainly confined to a slight change in the amplitudes of the peaks. The time positions of peaks and zero crossings are negligibly affected.

ii. The foil when acting as a receiver is not feeding into an open circuit. In fact, the foil is feeding into the pulser damping

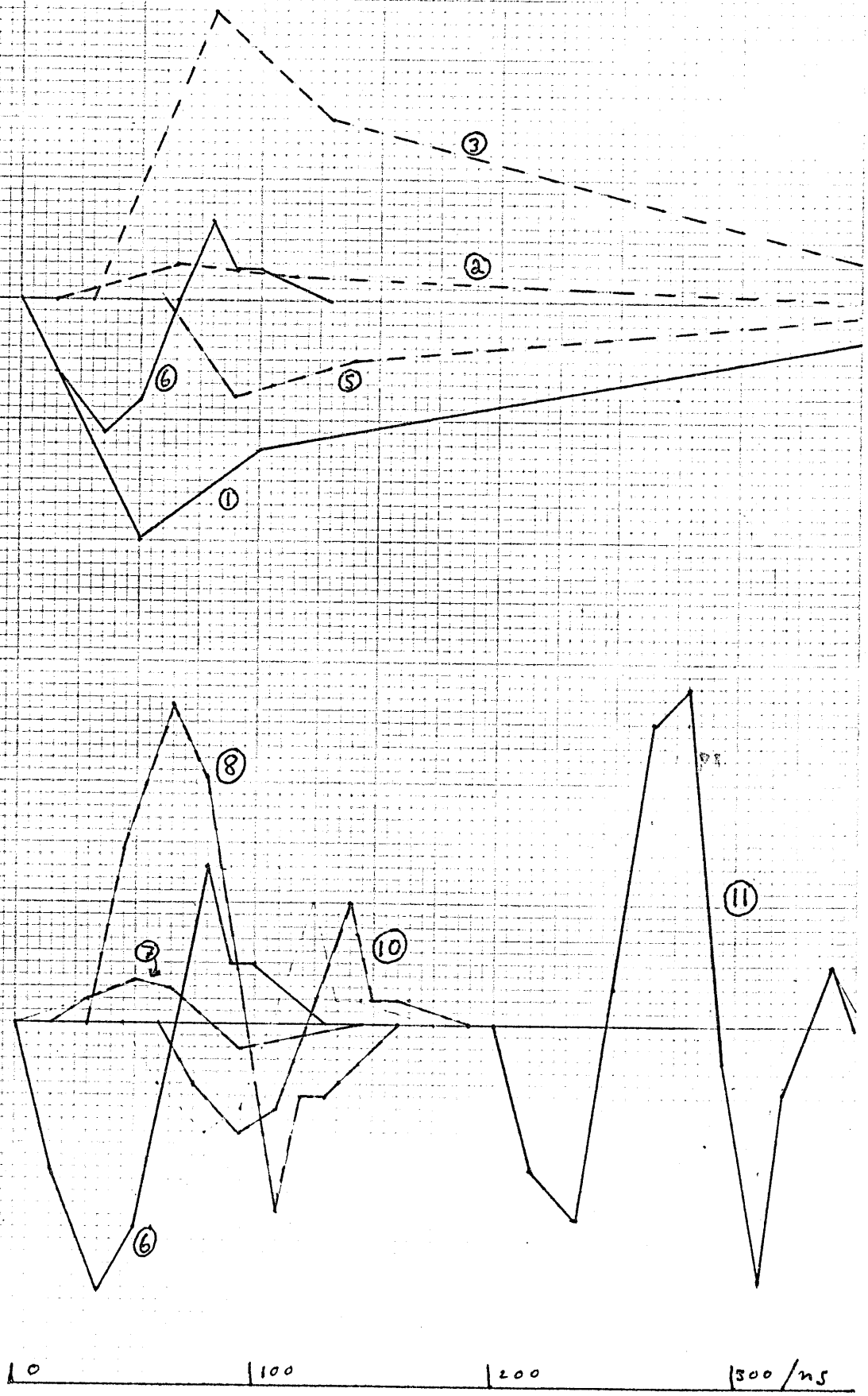

Fig. 4.28 Construction of predicted waveform for PVF_2 on brass backing. 15 ns transit time.

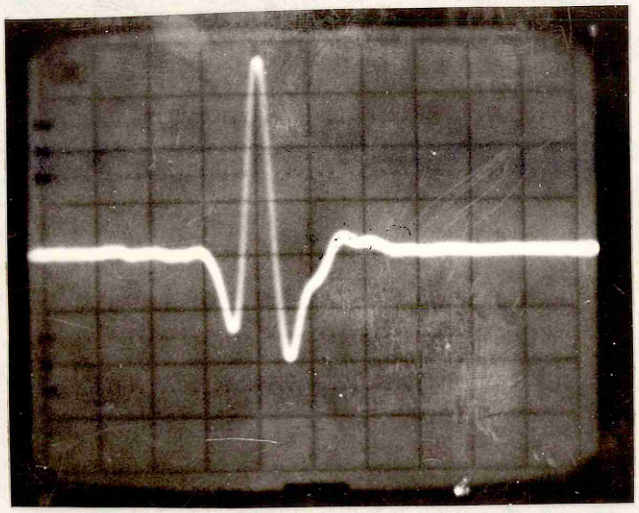

Fig. 4.29 Common mode response of 30 μ m thick PVF_2 on brass backing. 100 ns per division

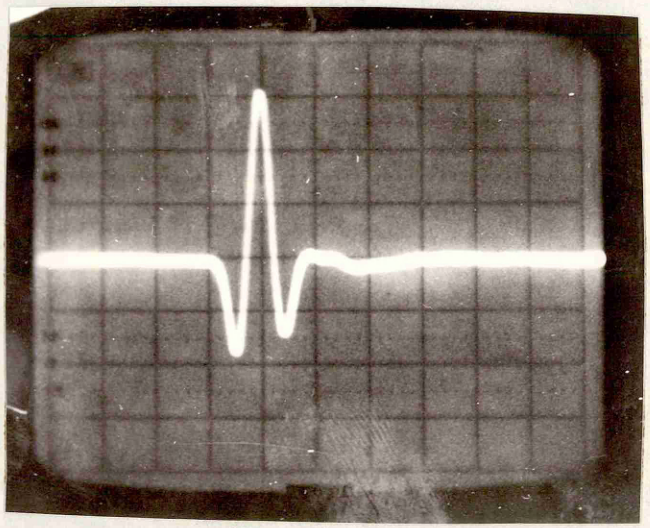

Fig. 4.32 Common mode response of 9 μ m thick PVF_2 on brass backing. 100 ns per division.

resistance, which for these pictures was set at "minimum damping" and would be about 1000 ohms. For open circuit conditions to apply, the time constant of the transducer capacitance and the load resistance must be large compared with the signal duration. The capacitance of the transducers is about 2 nF and the time constant is therefore about 2 μs. This is some ten or twenty times the duration of the greater part of the drive pulse and it seems unlikely that this is the cause of such a big error in the prediction of the pulse shape.

iii. The adhesive, not the nylon or the brass should be regarded as the backing. The adhesive Araldite AY103/HY991 was found to have a sound velocity of 2300 $\pm$ 20 ms^{-1}, a density of 1060 $\pm$ 100 kgm^{-3} and hence an acoustic impedance of 2.44 $\pm$ 0.2 M rayl. r_x for Araldite is therefore 0.19, and the multiplying factors are -1, 1.19, -0,27, 0,09 and -0,02.

Figure 4.30 shows the construction of the prediction for a 30 μm PVF_2 foil on an Araldite backing. The lower curves have the vertical scale multiplied by 4. Curve 9 is the prediction, with 5 zero crossings in 100 ns. Again there is no resemblance to the waveform actually received.

The correct prediction for brass backed foil is in fact obtained by putting the transit time at 25 ns. Figure 4.31 shows the construction, and the solid curve 11 is almost identical to the pulse from 30 μm brass backed film shown in Figure 4.29. Figure 4.32 shows the pulse obtained from 9 μm thick foil on brass backing. It is almost

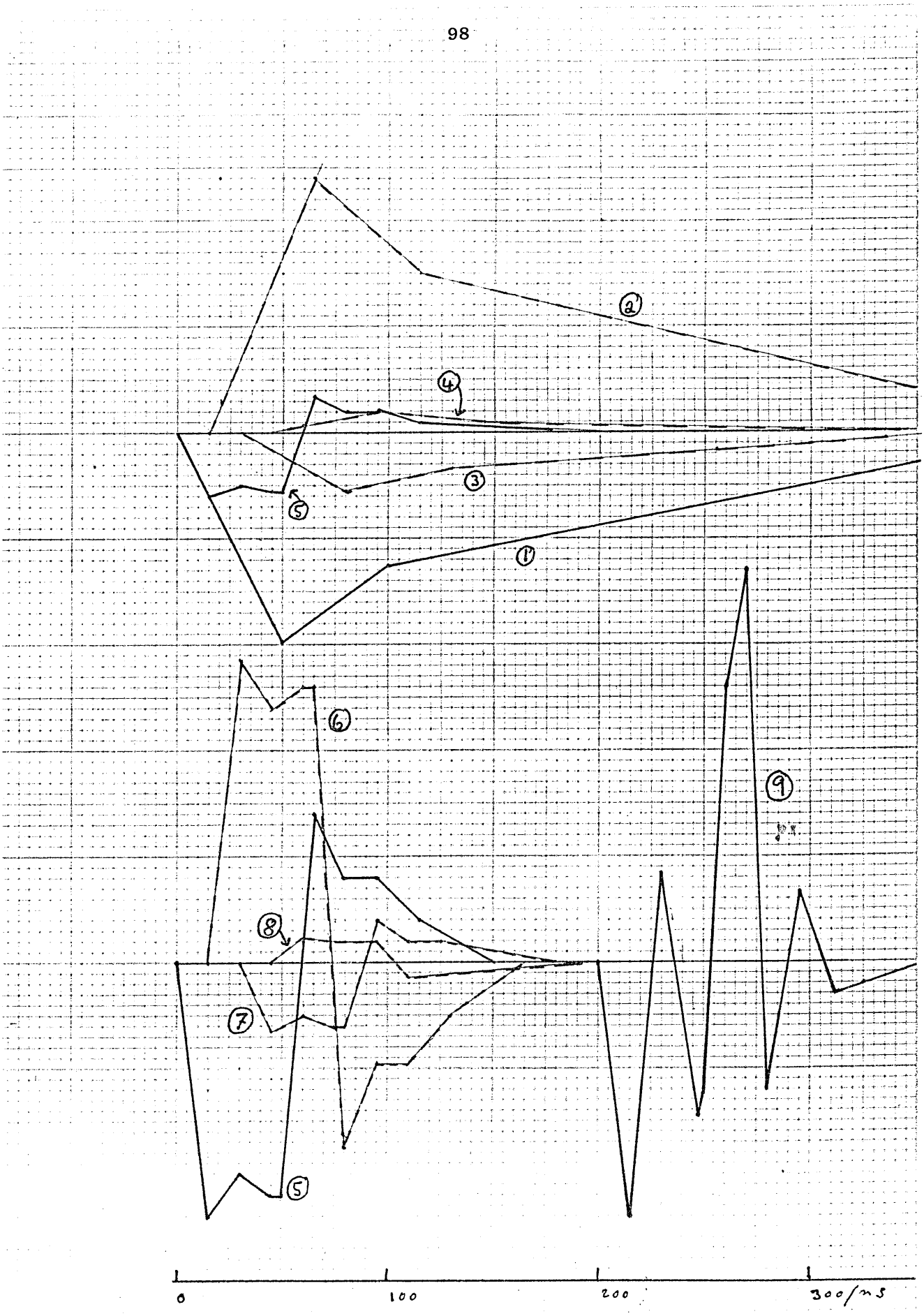

Fig. 4.30 Construction of predicted waveform for PVF_2 on Araldite backing. 15 ns transit time.

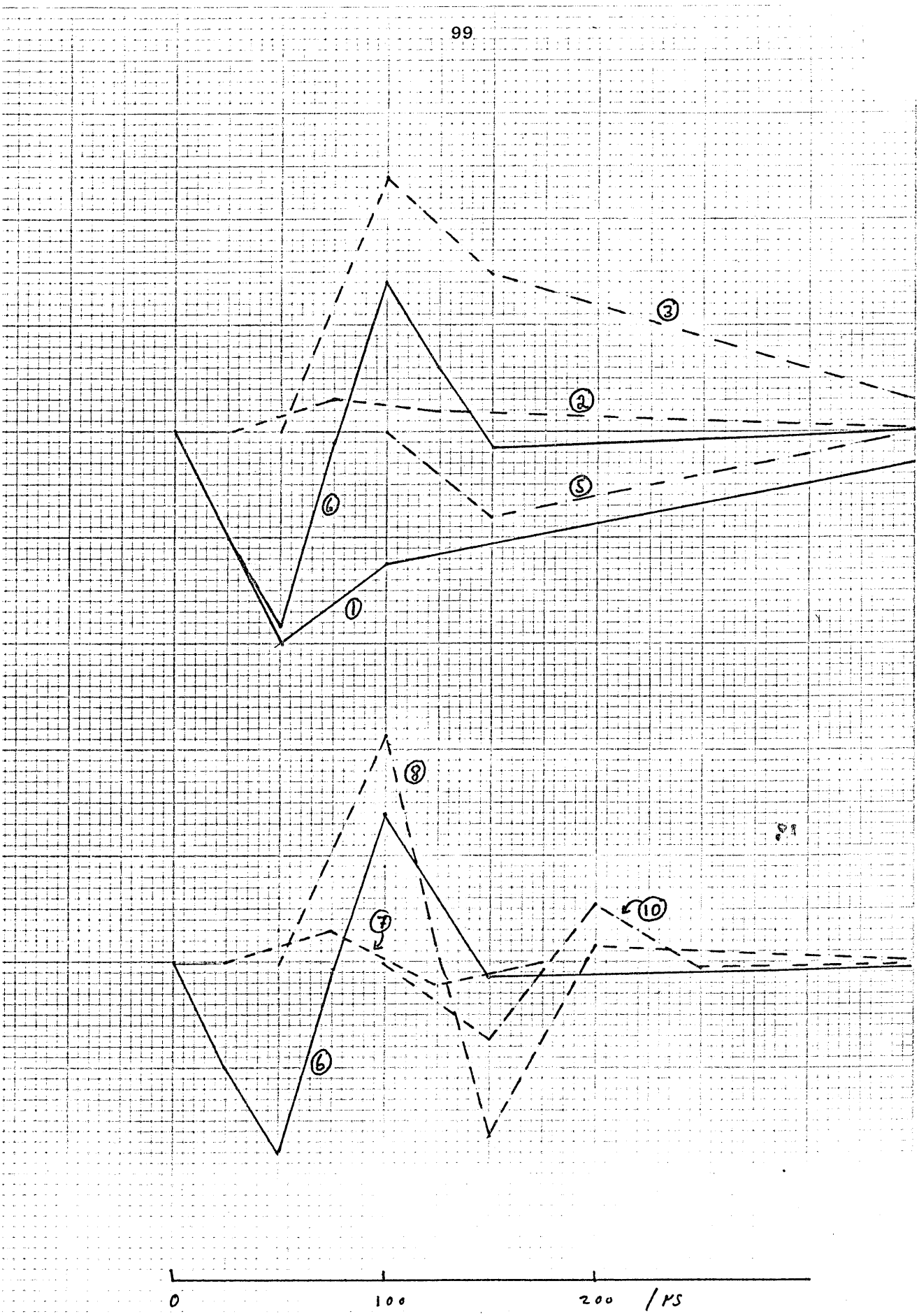

Fig. 4.31A Construction of predicted waveform for PVF_2 on brass backing. 25 ns transit time.

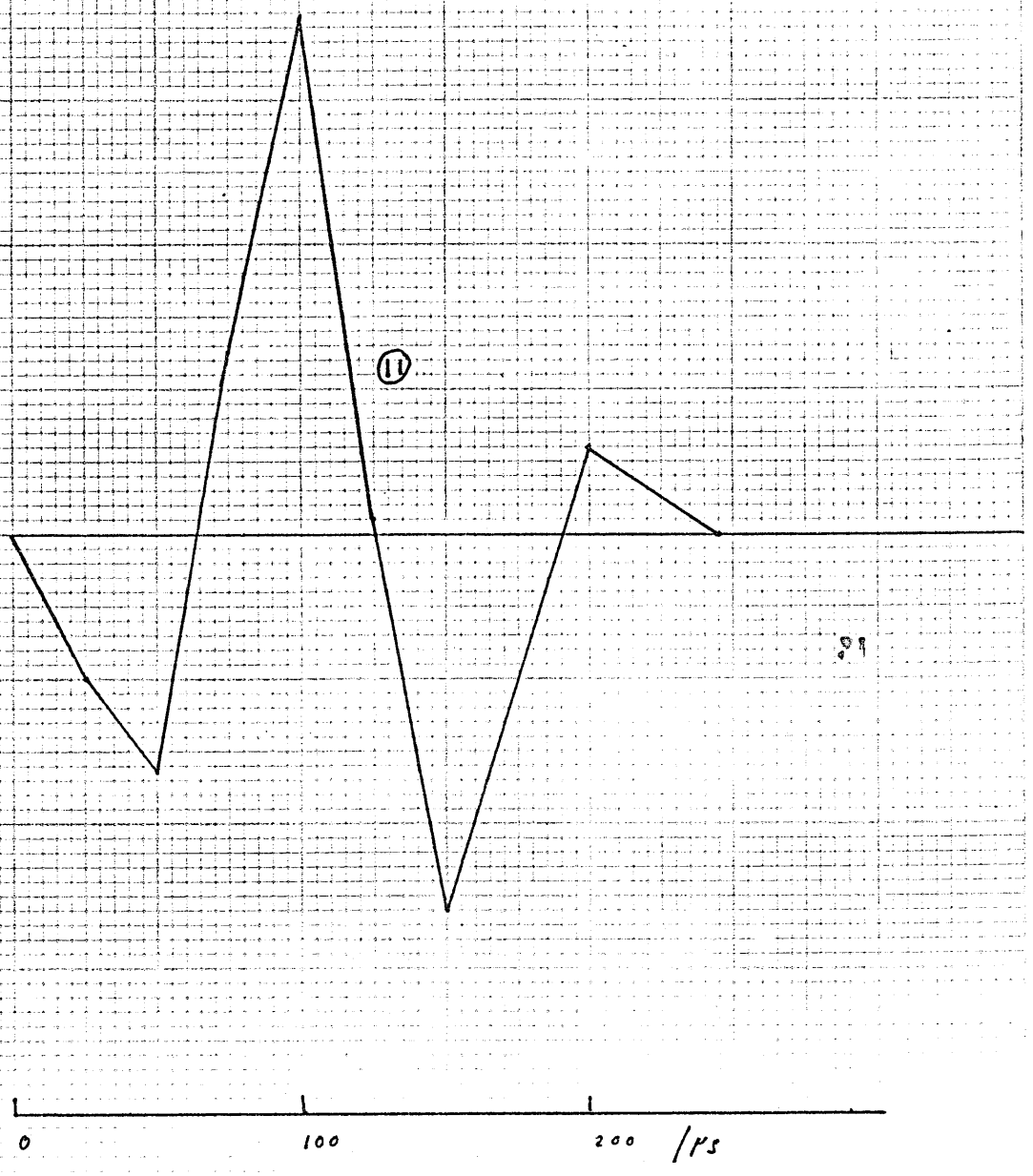

Fig. 4.31B. Construction of predicted waveform for PVF_2 on brass backing. 25 ns transit time.

identical to that from the 30 μm foil. This suggests that the pulse shape produced by these thin films has little to do with the thickness of the film and the transit time, and that to this extent Redwood's method is not applicable.

However a small piece of 580 μm thick copper coated PVF_2 was obtained. Figure 4.33 shows a piece of 10 x 20 mm glued to the end of a brass bar. This was used under water to transmit and receive ultrasound in pulse echo common mode. The drive waveform is shown in Figure 4.34 and the received waveform in Figure 4.35. The transit time for 580 μm should be about 300 ns. Figure 4.36 shows the predicted waveform for 300 ns transit time and Figure 4.37 shows it for 250 ns. The actual waveform received is shown as a dashed curve. In both cases the fit is quite good, and suggests that the correct transit time is about 280 ns. That indicates a sound velocity of 2070 ms^{-1} for PVF_2.

So Redwood's method appears to give the correct result for thick PVF_2 but not for thin. The reason for this is not clear. With a transit time of 15 ns, one would expect a 30 μm film to have a continuous wave resonant frequency of 33 MHz and a 25 μm film of 40 MHz. However, the system having a 30 μm transmitting and a 30 μm receiving transducer in water has a principal resonance of 6.8 MHz (Section 6.4).

The thin film, when used as a pulsed transmitter of ultrasound produces a much longer pulse than theory predicts.

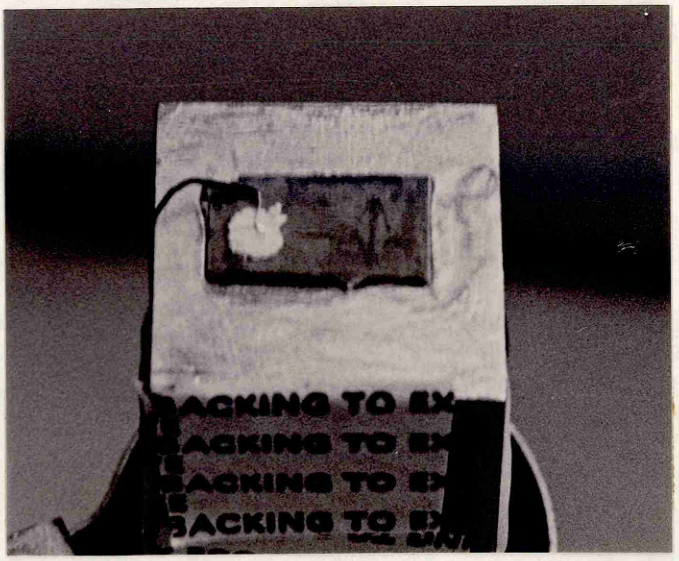

Fig. 4.33 580 μ m PVF_2 glued to brass bar

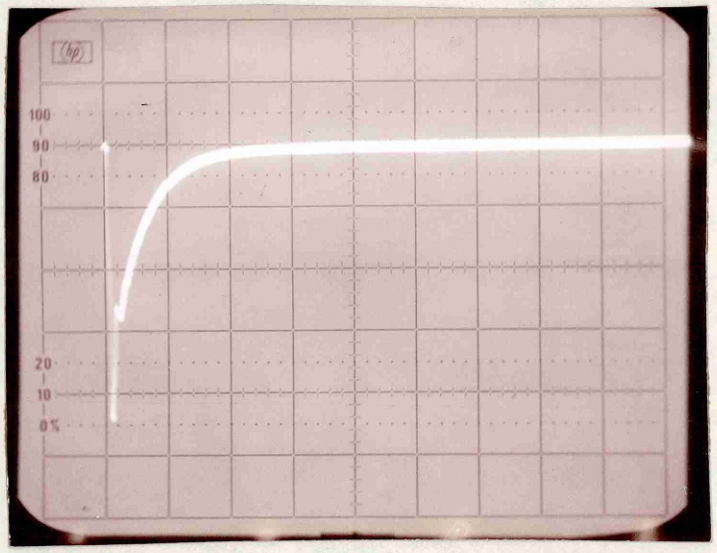

Fig. 4.34 Drive voltage. 50 volts per division vertically. 500 ns per division horizontally.

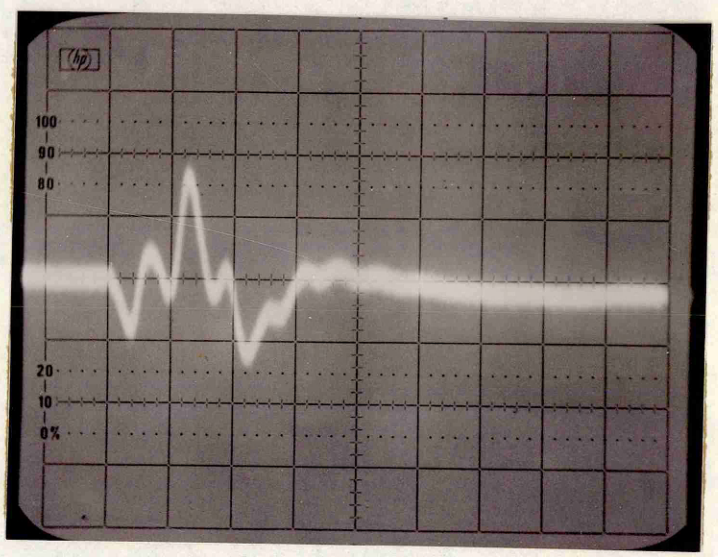

Fig. 4.35 Common mode response of 580 μ m foil driven by pulse in fig. 4.34. 500 ns per division.

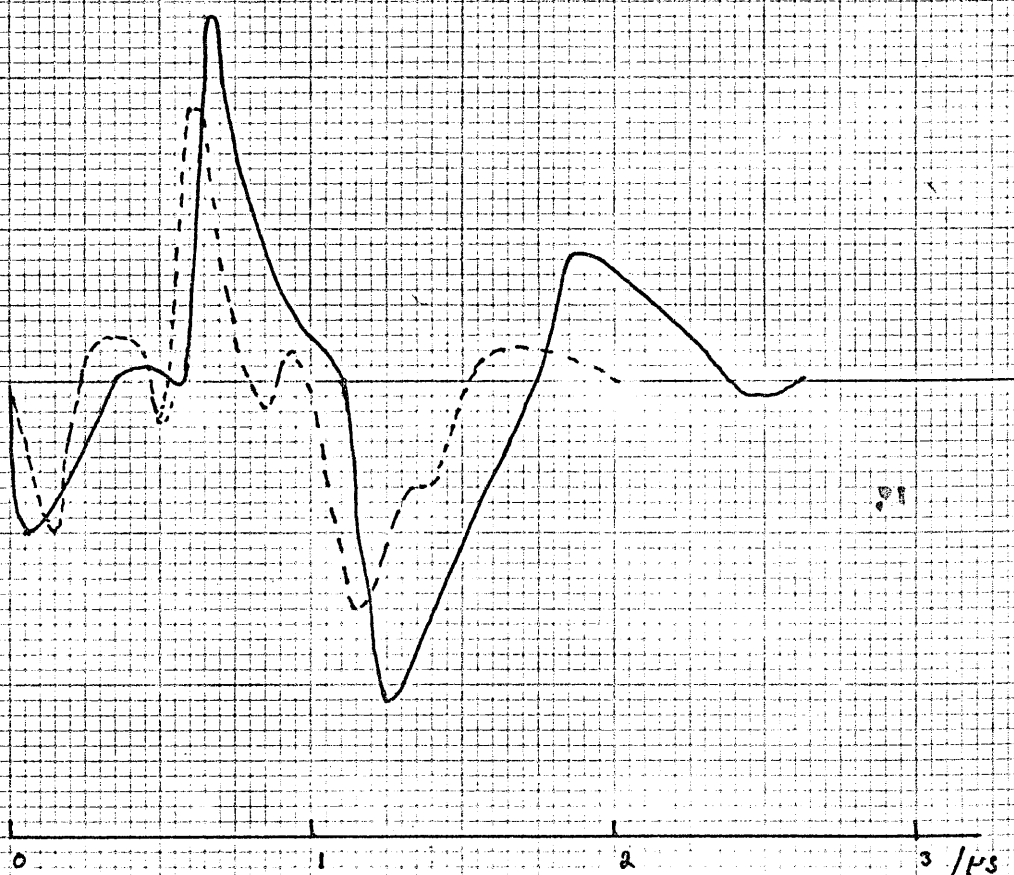

Fig. 4.36 Solid line. Predicted waveform for 580 μm thick PVF_2 on brass backing : 300 ns transit time.
Dashed line. Received waveform.

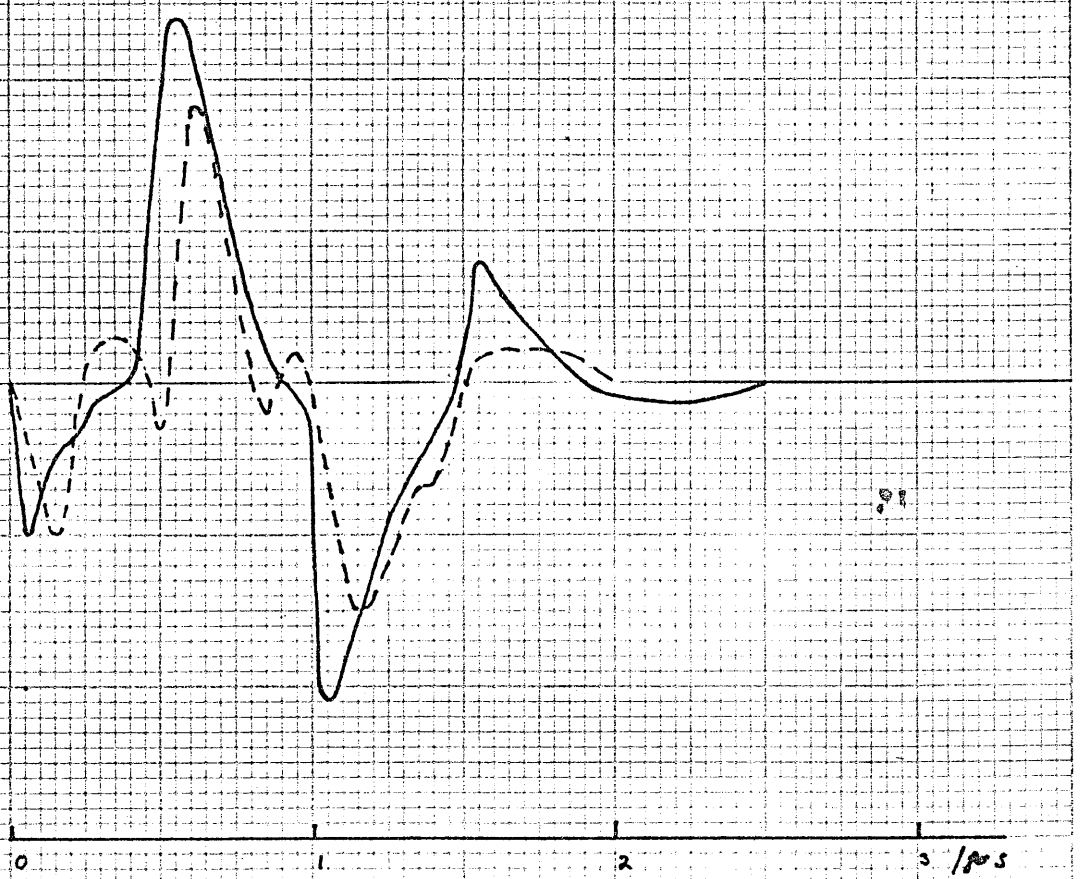

Fig. 4.37 Solid line. Predicted waveform for 580 μm thick PVF_2 on brass backing : 250 ns transit time.
Dashed line. Received waveform.

A possible explanation for the waveform not corresponding with theory is that the foil is not homogeneously polarised and that the piezoelectric properties are all concentrated on one face. This would go some way to explaining why 9 μm and 30 μm PVF_2 foil produce pulses of similar length, but then the output of the foil ought to differ significantly if the foil is inverted. Either the piezoelectric side of the foil will be separated from the backing by the thickness of the foil plus the adhesive, or it will be next to the backing separated only by the adhesive. It was already known that there was no observable difference in the output of the foil whichever way up it was on a nylon backing (Section 4.10). Two equal pieces of 25 μm PVF_2 were glued to a flat brass bar, one piece one way up and the other piece the other way up. Both pieces produced splendid ultrasonic pulses which, when received on the same transducer working in a common transmit/receive mode, were found to be as near identical as could be measured in both amplitude and timing. (Figures 4.38 and 4.39).

The initial shape of the acoustic pulse appears to be dominated by the shape of the electrical drive pulse, probably because the transit time through the film is less than the rise time of the drive pulse. The rise-time of the acoustic pulse in Figure 4.27 is about the same as the rise-time in the driving pulse in Figure 4.26, and the initial fall-times are about the same as each other.

It appears that Redwood's method of predicting the shape of acoustic pulses cannot be applied to these thin film transducers.

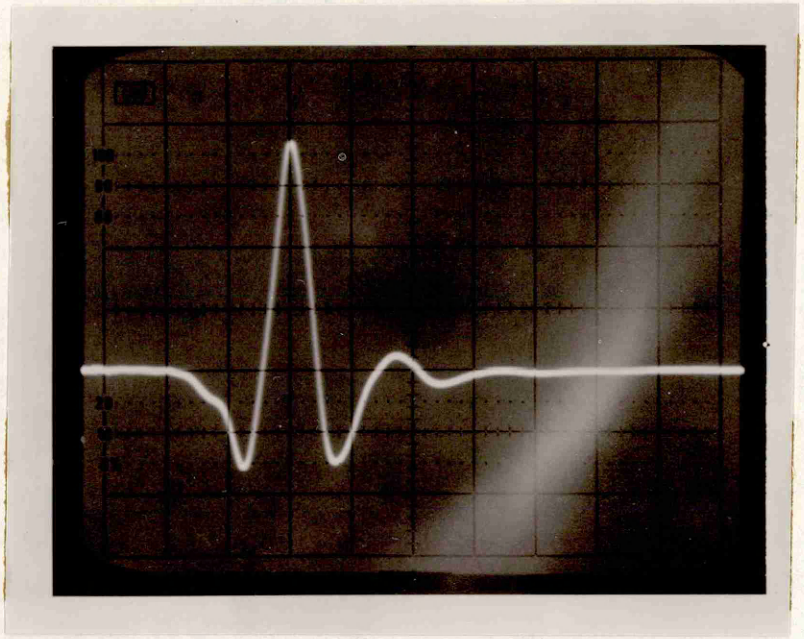

Fig. 4.38 Common mode response of 25 μm thick PVF_2 on brass backing. 100 ns per division.

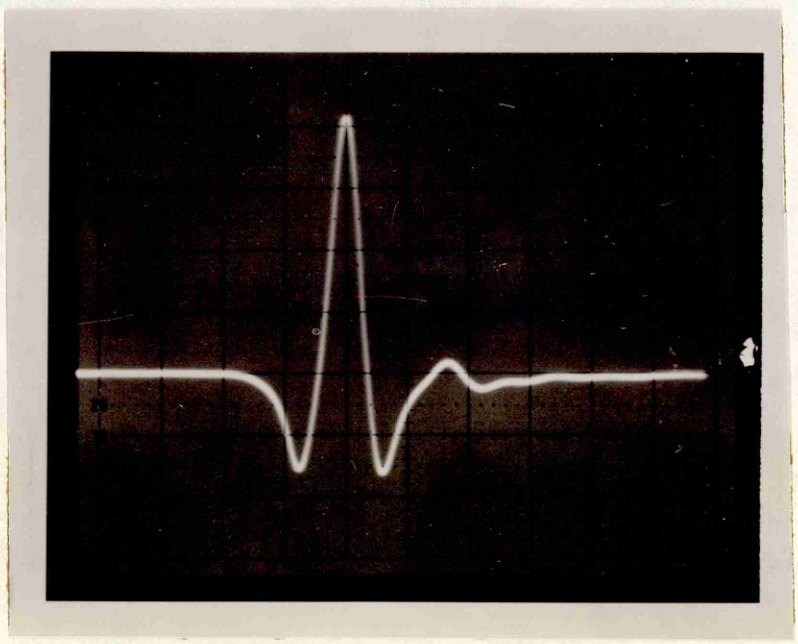

Fig. 4.39 As fig. 4.38 with PVF_2 foil inverted.

It is interesting to note that Weight (1982) remarks that if a thin element receiver is used, so that the acoustic transit time across it is much less than the duration of the incident ultrasonic pulse, then no reverberation is set up inside the transducer element. Presumably this effect operates in reverse, and explains why, in the case of 25 μm and thinner PVF_2 film, only the pulse from the face of the film is generated into the water.

Chapter 5 Design of the imaging system

5.1 Preliminary considerations

In view of the success achieved in making foil transducers based on nylon cylinders of about 50 mm diameter, it was decided to design and build an imaging system using one transmitting and four receiving transducers. A linear array holding five such transducers with equivalent spaces between would need to be about 300 mm wide, suggesting that for imaging at distances of about 200 - 300 mm, the round trip distances would be in the order of 600 mm. Pulse lengths of 100 ns or less were attainable from the transmitting foil transducers already made, and this represents a distance of 150 μm in water or one four thousandth of a likely round trip distance.

At this stage, it was not know exactly how the calculation of the round trip distances was to be achieved but the intention was to use a Rockwell AIM 65 computer working in machine code. Although such computers can be programmed to operate in base 10, their scope is then very limited. Therefore it was decided to construct the transducer array with transducer spacings that were exact multiples of 16 mm. This represents 10 in base 16, and was expected to simplify the calculation of path lengths. The AIM 65 uses the convention that the 16 digits in base 16 arithmetic are 0,1,2,3,4,5,6,7,8,9,A,B,C,D,E,F, and that all hexadecimal numbers will be preceded by a dollar sign, $. This convention will be followed here.

5.2 Field of scan

The transducers were built into a frame and fixed in a straight line at $ 50 mm spacing between cylinder centres. The total width was therefore $ 140 mm (= 320 mm).

As shown in figure 5.1, it was decided to have a rectangular scanning field with (x,y) coordinates in millimetres, such that the centre of the transmitter cylinder was at (0,0) and the centres of the four receivers were at $ (0,50), $(0,A0), $(0,F0), $(0,140). It was decided to have the target points at intervals of exactly 1 mm in the x and y directions as this would allow their x and most of their y coordinates to be represented by 1 byte. The round trip distances were to be calculated to 0.01 (Binary) mm ($\frac{1}{4}$ mm) and the results presented as a 12 bit binary number. With a scanning field of width $ 100 mm in the x direction, the maximum round trip would be in the order of $ FF0 (quarter millimetres) which constrained the range to $ 160 mm in the y direction.

Translated to denary the field of scan was to be 256 mm wide and 448 mm deep.

5.3 An imaging system without signal averaging

Figure 5.2 is a flow diagram of the imaging system as first envisaged, and is intended to show how the sequence of operations in the rectangular boxes might control the operations in the water tank and the subsequent signal processing. It was envisaged that the operations in boxes, 2,3,4,5, and 12 would be controlled by the

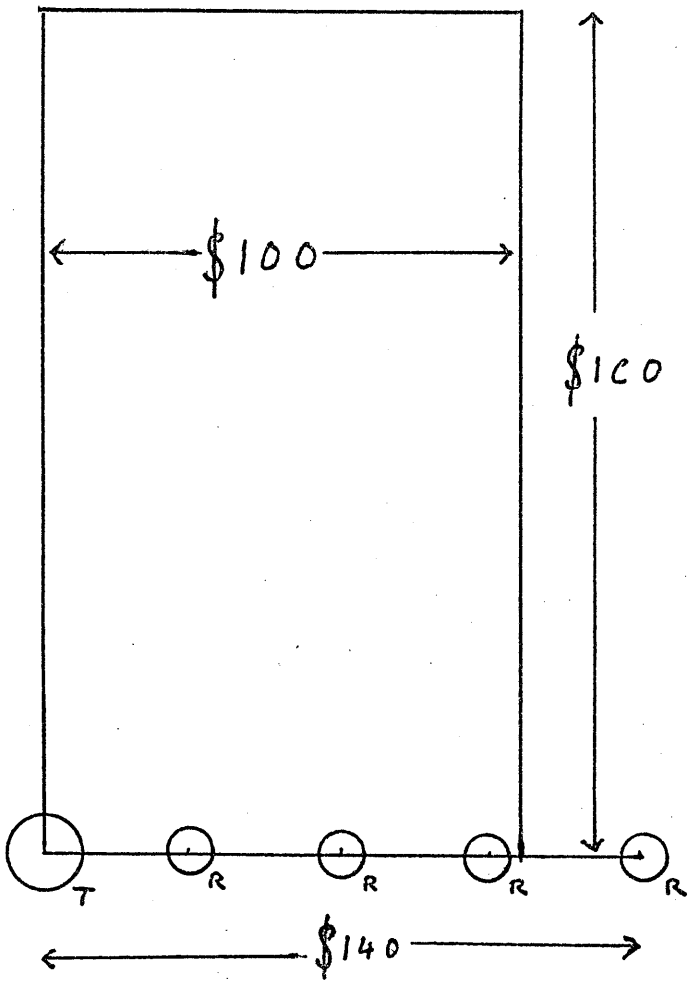

Fig. 5.1 Proposed area of scan.

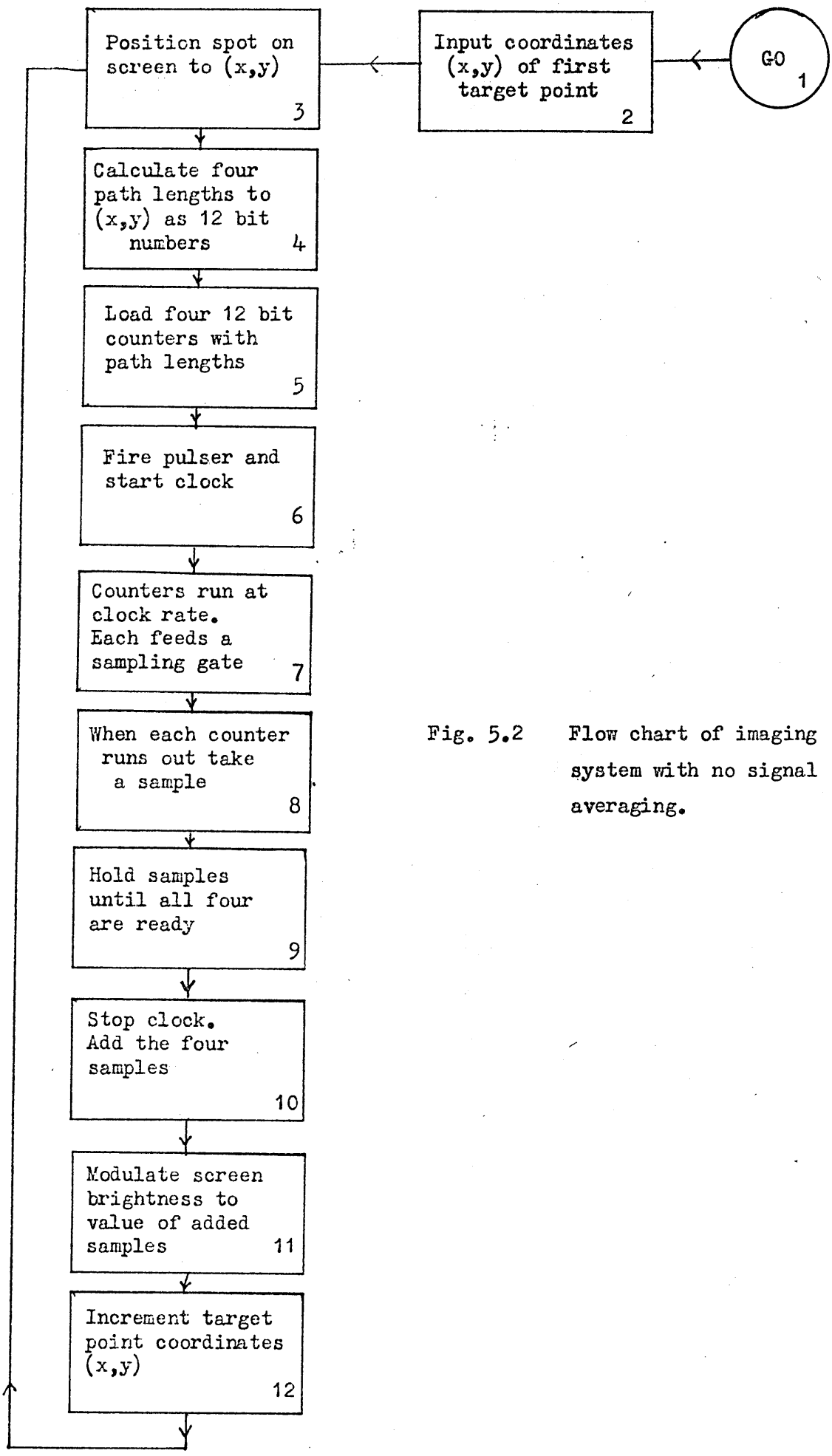

Fig. 5.2 Flow chart of imaging system with no signal averaging.

AIM computer and that operations 6,7,8,9,10 would be controlled by hard wired logic circuits.

Each count made by the counters represents $\frac{1}{4}$ mm of path length, and assuming a velocity of sound in water of 1500 ms^{-1}, the ultrasonic pulse will take 1/6 μs to cover this distance. Hence, by running the clock at 6 MHz the counters will reach zero at the same moment as the ultrasonic pulses are expected to arrive at the receivers and samples of these pulses will be taken and used to modulate the screen brightness.

This system does not allow for any signal averaging to reduce noise; each point is imaged once only and the system then moves to the next point. This system is also very wasteful of time because the hard-wired logic does nothing while the path lengths are being calculated and the computer does nothing while the ultrasonic pulses are being transmitted, received and processed.

5.4 A faster imaging system with signal averaging

The computer has a clock rate of 1 MHz and order of magnitude estimates showed that it would take several milliseconds to calculate four path lengths to 12 bit accuracy. The ultrasonic pulses would take between 300 and 700 μs to traverse the likely range of path lengths at 1500 ms^{-1}, hence it should be practical to calculate the path lengths to a target point and then to transmit and receive several ultrasonic pulses while the distance to the next target point is being calculated. This would make much better use of time and also allow signal averaging to be

performed on the sampled echoes. Figure 5.3 is a flow diagram of a system that does this.

The hard-wire loop runs at a rate determined by the time taken for the ultrasonic pulses to traverse the longest path length. The software loop is slower by a factor of ten or twenty and this allows several successive ultrasonic pulses to be transmitted and used for signal averaging while the new path lengths are being calculated.

5.5 Attenuation of the signal

This system does not allow for differences of attenuation of the ultrasonic pulses travelling different distances. An investigation of the effect of ignoring this attenuation, (which is expected to be proportional to the path lengths, section 2.2 iv) shows that there will be two main effects,

i Attenuation due to range. In Figure 5.4 an object at B will be less brightly imaged than an object at A, and calculations show that within the likely area of imaging the attenuation will be about 1 dB for every 25 mm increase in range.

ii Relative attenuation due to path length difference. In Figure 5.4 the path length for an object at D or C will be greater for receiver 4 than for receiver 1. The response from 4 will be less than from 1 for an equal signal reflected. This difference will be greatest for targets that are close to the array and off centre; as D moves towards A or C the difference will lessen.

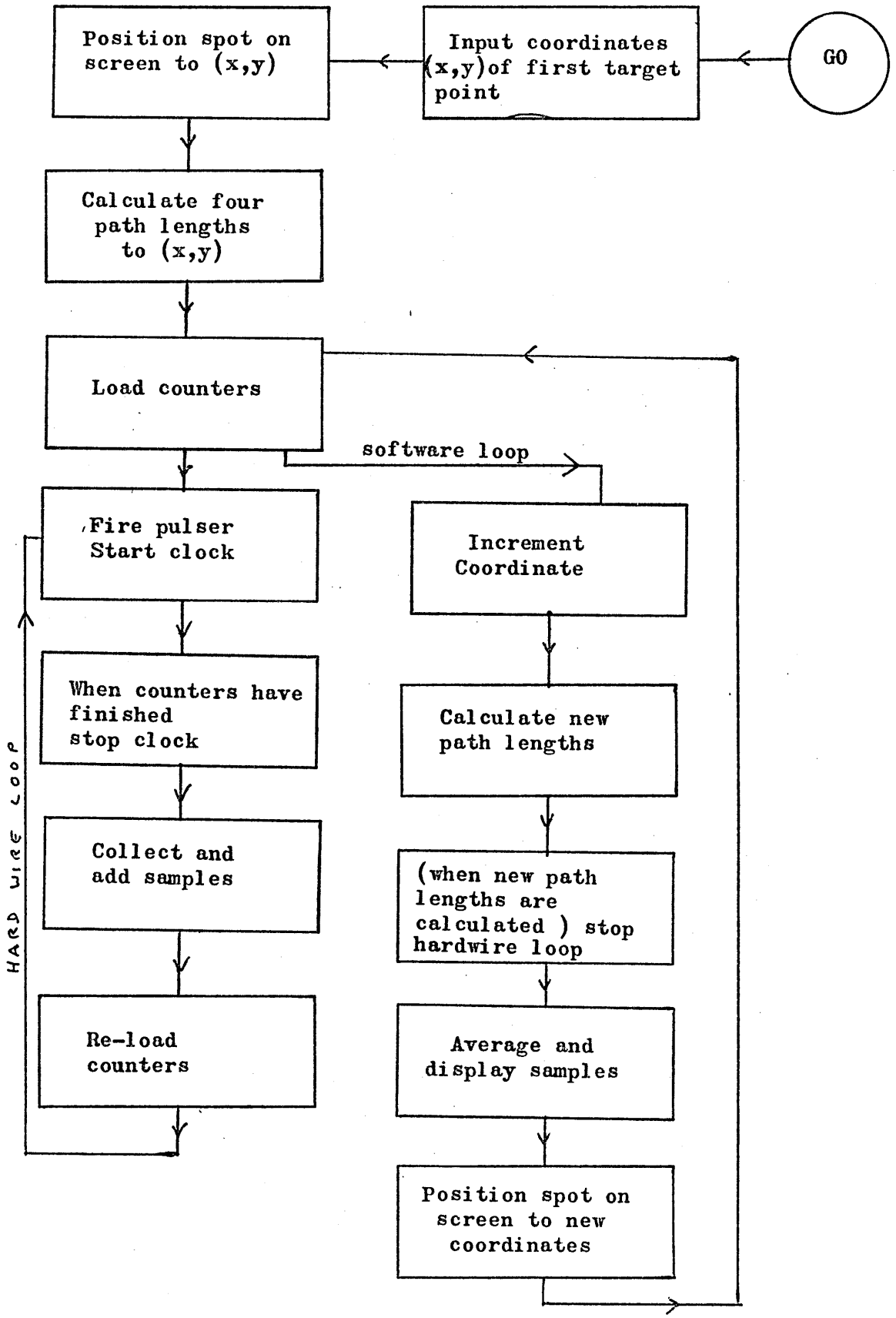

Fig. 5.3 Flow diagram of improved system.

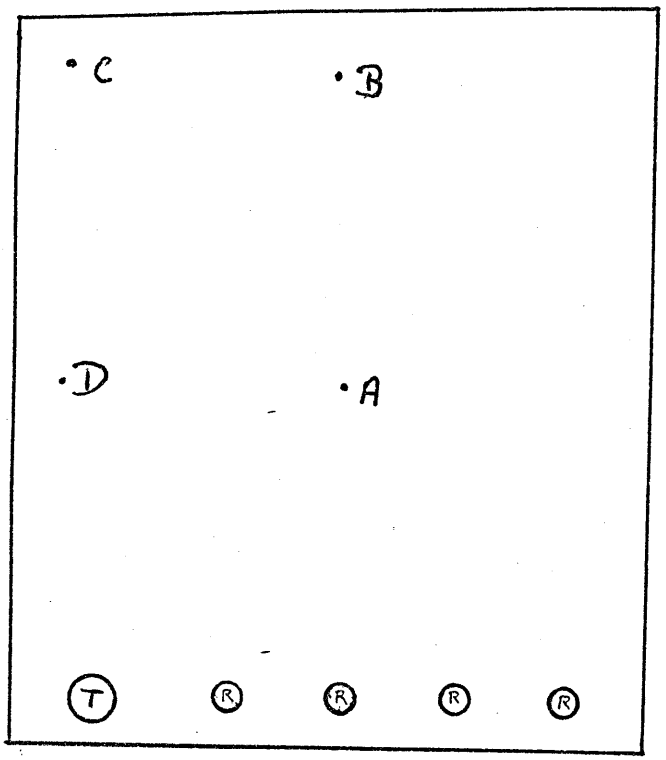

Fig.. 5.4

Target coordinates	Difference of attenuation/dB
0,100	5.6
0,150	3.9
0,200	2.8
0,250	2.2
100,100	3.0
100,150	2.6
100,200	1.8
100,250	1.1

Table 5.1

Table 5.1 shows the difference of attenuation for targets at various coordinates as received by 1 and 4. In general the effect is less than 3 dB.

It was decided that it would not be worth while incorporating devices to correct the differences in attenuation due to range or path length variation. The variation in brightness from front to back of the picture could be tolerated, and if necessary extra amplification could be applied to receivers 3 and 4 to partly compensate for their greater average path length.

5.6 The final design of the imaging system

Figure 5.5 is a simplified block diagram of the complete imaging system based on the flow diagram Figure 5.3. In this description of its operation, objects in the diagram are written with a capital letter.

The AIM 65 computer sets the address in the Digital Video Store to the first image point. (That is the pixel at the top left hand

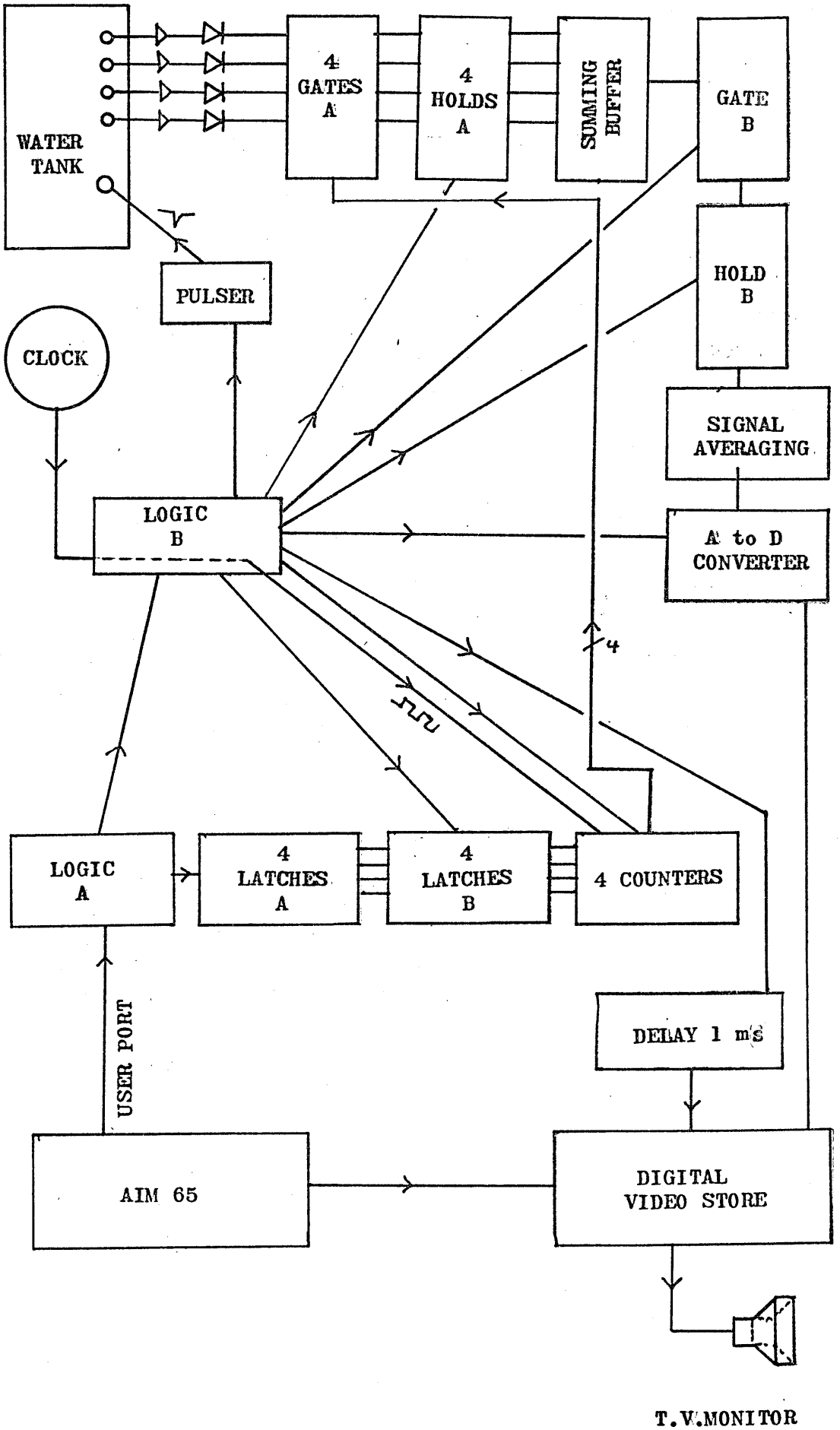

Fig. 5.5 Final design of imaging system.

corner of the display). The four path lengths, which are calculated at about 2 ms intervals one after the other, appear in turn at the User Port of the AIM 65. Each takes the form of a 12 bit number plus a two bit address. Logic A reads the address and loads the path length into the appropriate latch in Latches A. When all four path lengths have been thus loaded, Logic A informs Logic B.

Logic B:

1. Loads Latches B from Latches A.
2. Loads the Counters from Latches B.
3. Passes Clock pulses to the Counters and fires the Pulser.
4. After about 130 μs clears Holds A.

While the counters are counting down to zero, the receivers will pick up various echoes from the target. These echoes will be pulses of shape shown in Figure 5.6a which are amplified and rectified to produce a positive pulse of shape shown in Figure 5.6b. This passes to an analogue gate in Gates A.

As each counter reaches zero, it opens the appropriate analogue gate (in Gates A) for a few hundred ns and allows any pulse present during that period onto a hold capacitor in Holds A. The contents of the four hold circuits are added in the Summing Buffer, and when all four counters have reached zero and all four gates have opened and closed,

Logic B:

5. Switches off the Clock, (stopping the count).
6. Loads the Counters from Latches B.

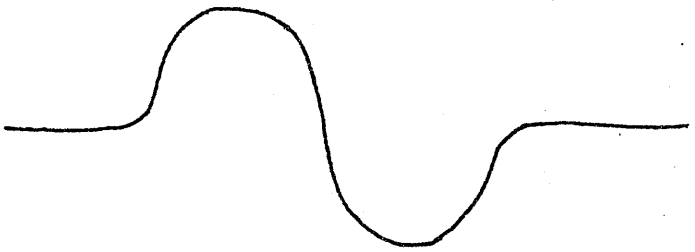

a. Shape of echo pulse

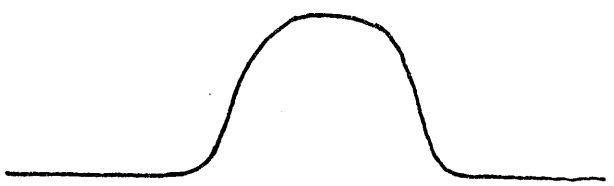

b. Shape of pulse passed to analogue gate

Figure 5.6

7. Switches on the Clock and fires the Pulser (then while the Counters are counting down)

8. Clears Hold B

9. Opens analogue Gate B and pases the sum of the four samples onto Hold B

10. After about 130 μs clears Hold A (when all counters reach zero)

11. Switches off the clock.

Logic B will continue the above sequence 6 to 11 until stopped by the computer, which, meanwhile, is calculating the path lengths for the next target point. As each path length is calculated, Logic A directs it to its appropriate latch in Latches A. Thus the system continues to focus on the target point whose path lengths are in Latches B while Latches A are filling with data for the next target point.

When the third path length has been calculated (after about 6 ms) the AIM 65 instructs Logic A to prevent Logic B from continuing its sequence after the Clock is next switched off. By this time some 10 or 20 samples will have been passed to Hold B and through the Signal Averaging circuit to the A to D Converter. Logic B waits 4 μs then sends a convert command to the A to D Converter, the output of which is put into the current address of the Digital Video Store. The video store address is then incremented after a delay of 1 ms.

When the fourth path length for the next target point has been calculated, Logic A informs Logic B which repeats its sequence with the new data.

A TV receiver continuously scans the contents of the video store and displays an image.

The digital video store was designed to have 128 x 128 pixels (section 8.7). Because of the constraints that this imposed, the field of scan was made to be either $80 mm (128 mm) wide with steps of 1 mm or $100 mm (256 mm) wide with steps of 2 mm. These options could be selected by the AIM 65 computer keyboard by keying the step size into memory location INCRM and the picture width into memory location JAMES. Similarly the depth of field of scan was limited to a maximum of $80 mm (128 mm) at the same step distance as that selected for width. The range of the top of the scan is keyed into memory location TOP, and the range of the bottom of the scan into memory location BASE.

Chapter 6 Transducers for the imaging system

6.1 Transducer construction

The transmitting transducer was made on a nylon former (Figure 6.1a) which was machined from a 25 mm radius nylon cylinder. Figure 6.1b shows the horizontal cross section through the transducer after the PVF_2 foil has been glued to the curved face and a pair of aluminium plates have been bolted to the flat surface. (The aluminium plates act as screens and are discussed in Section 6.3). Figure 6.4 shows the complete transducer. The active area of foil was 16 mm high and 20 mm long to give it a 45^{o} angle of radiation in the horizontal plane. Figure 6.2a shows the masks for the photo resist. The black areas become free of gold and chromium on their respective sides to make a central active overlap and connecting leads each end. The 2 mm wide strip along the top and bottom is to prevent the rear side of the foil from coming in contact with the water and to prevent flashover between the two faces of the foil. Figure 6.2b shows the two masks combined to give the required active area.

A BNC coaxial socket was mounted on top of the cylinder, and the rear face of the foil was connected to its centre. The front face of the foil (which comes into direct contact with the water) was connected to the outside of the BNC socket.

All the transducers were made using the method described in Section 4.10. Araldite AY103/HY991 was used to glue the PVF_2 foil to the nylon. Connections were made with R.S.Silver-Loaded Epoxy Resin, and covered with Araldite AV138/HV998.

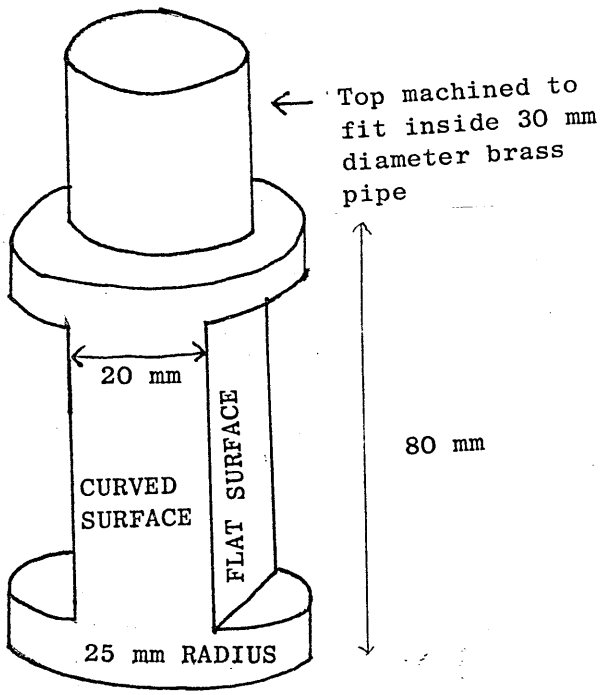

Figure 6.1a. Nylon former for transmitting transducer.

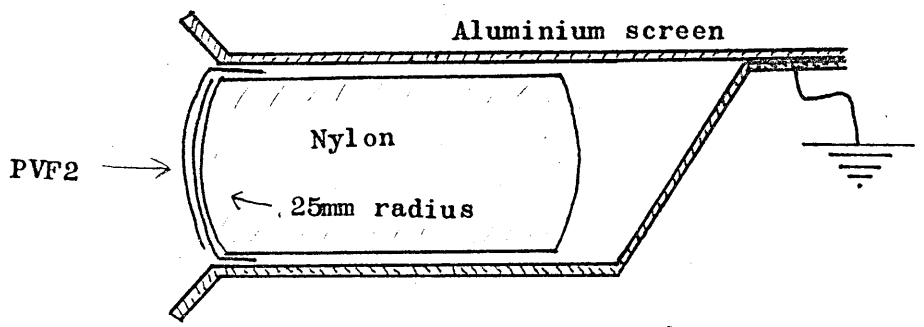

Figure 6.1b. Horizontal cross section through transmitting transducer.

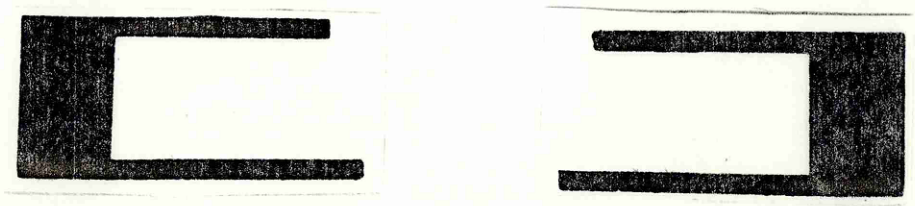

Figure 6.2a. Photographic mask for transmitting transducer foil.

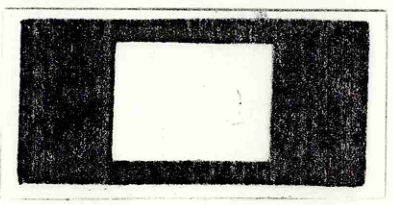

Figure 6.2b. The clear area left by combining the masks is the active transmitting area.

The receivers were made on nylon cylinders with a radius of about 16 mm. The foils were 10 mm wide and about 45 mm long in total. Their active surface covered about 130 degrees of arc when wrapped round the cylinders. Figure 6.3 shows a completed receiver.

The front surface of each foil was connected to the screen and the inner surface to the core of a 55 mm length of 50 ohm, 2.8 mm diameter coaxial cable (with a capacity of 100 pF per metre), which led to the top of the nylon cylinder where an amplifier would be put. The connections to the foils on all the transducers were made with R.S. Silver-Loaded Epoxy-Resin, and sealed over with Araldite AV138/HV998. The foils were glued with Araldite AY103/HY991. (See Section 4.10 ii).

The tops of the nylon cylinders were machined to fit tightly into 200 mm long brass tubes with an inside diameter of 30 mm, so that the tubes became an extension of the nylon cylinders. The bases of the nylon cylinders had a 2BA hole drilled and tapped at their exact centres, and these were used to bolt the cylinders to the aluminium frame at $50 mm (80 mm) intervals along a straight line on the base of the frame. (Figure 6.5). The tops of the brass tubes fitted into aluminium clamping bars with semicircular cut outs that were centred exactly above the bolt holes in the base of the frame (Figure 6.6). The transducers were thus accurately positioned and held rigidly in line. The frame and five transducers were mounted on a rigid base of aluminium 500 x 460 x 25 mm thick.

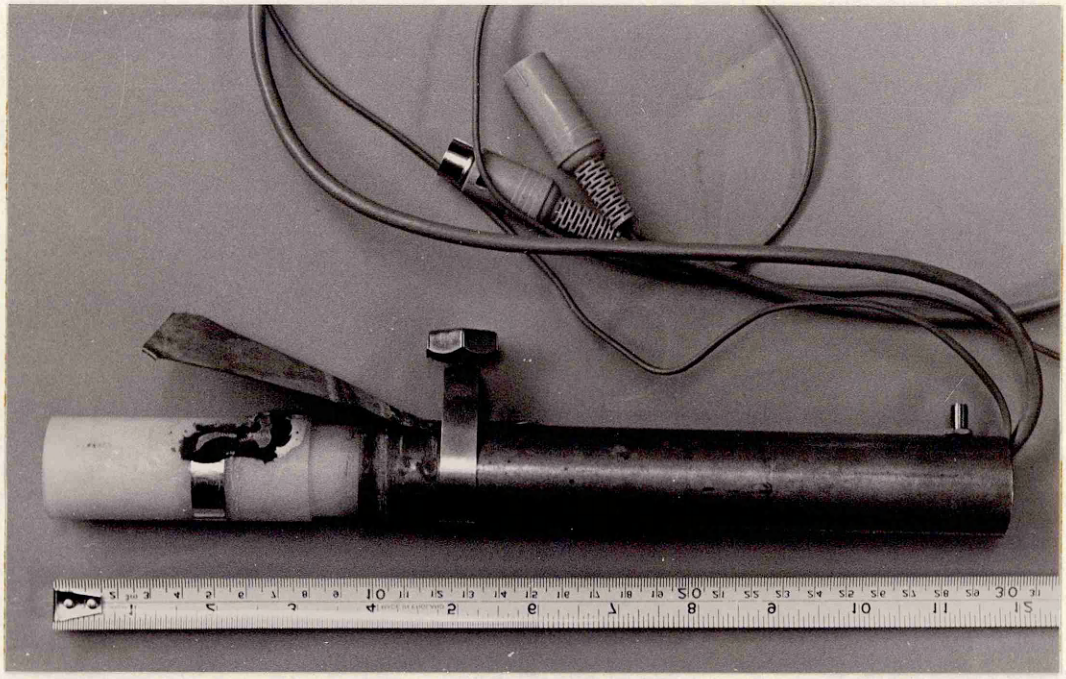

Fig. 6.3 Receiving transducer

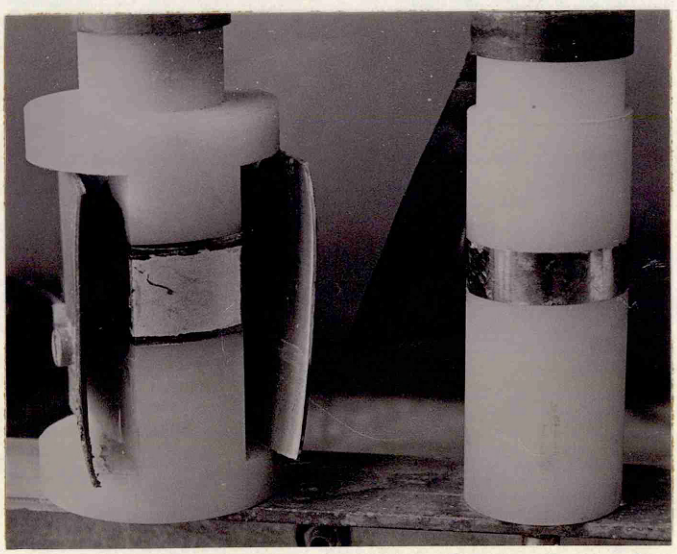

Fig. 6.4 Transmitting (left) and receiving (right) transducers.

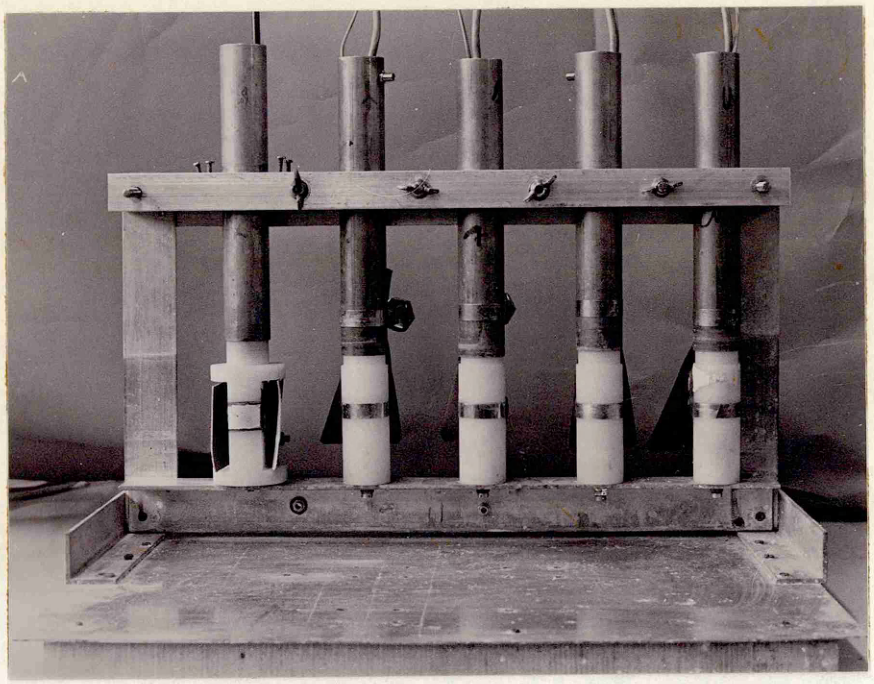

Fig. 6.5 Transducer array

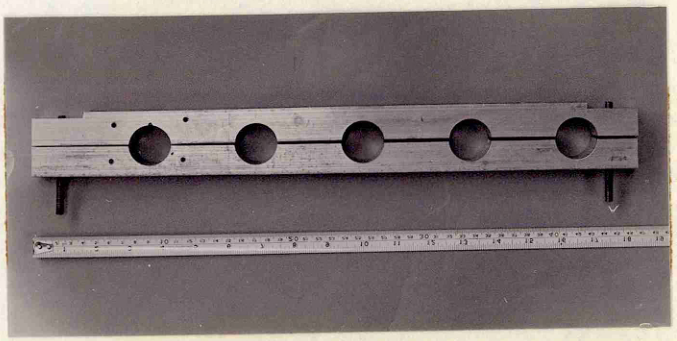

Fig. 6.6 Transducer clamping bar and scale

6.2 Transducer tests

Pulse response

The transmitting transducer was connected to the Panasonic 5052 pulser set for common mode transmit-receive. Underwater, the ultrasonic pulses transmitted by the transducer were reflected from an aluminium bar in the water and received on the same transducer. The electrical input to and output from the transducer were displayed on an oscilloscope.

Figure 6.7 shows a drive pulse across the transducer rising to -44 volts in 20 ns, and Figure 6.8 shows the loop response. The negative and positive swings are about equal and together take about 100 ns. Figures 6.9 and 6.10 show that increasing the output of the pulser to maximum gave a drive pulse rising to -160 volts in 50 ns and the response was a pulse rising to a negative maximum in 60 ns, swinging to a positive peak in a further 40 ns then falling off slowly and reaching zero after a further 400 ns.

The aluminium bar was moved so that the reflected pulse was returned to one of the receiving transducers and its output displayed on the oscilloscope. Figure 6.11 shows the response from the -44 volt drive pulse and Figure 6.12 shows the response to the -160 volt drive pulse. The latter was expected to be of most use for imaging purposes as it had considerably greater amplitude than the former. The long positive swing would be irrelevant, as the rectifier would remove it. However, it was unfortunate that the negative pulse was 100 ns wide, as this would limit the resolution of the system to a greater extent than was originally anticipated in Section 3.4, where a 20 ns pulse width was assumed.

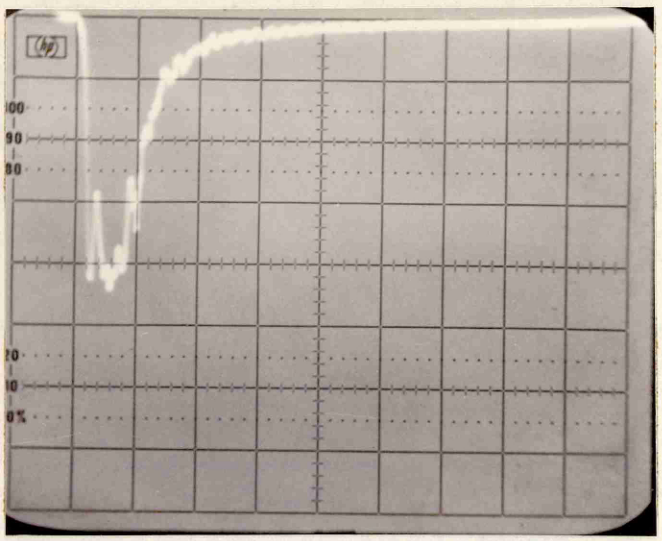

Fig. 6.7 44 volt drive pulse to transmitting transducer.
50 ns per division horizontally
10 volts per division vertically

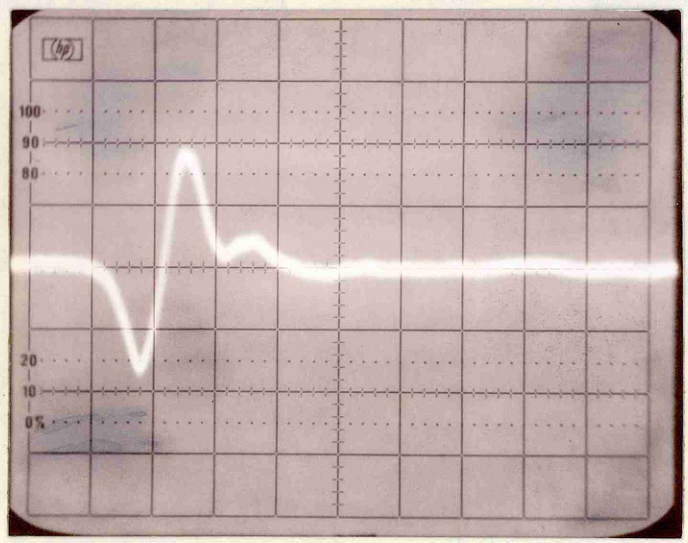

Fig. 6.8 Common mode response of transducer from drive pulse in figure 6.7
50 ns per division.

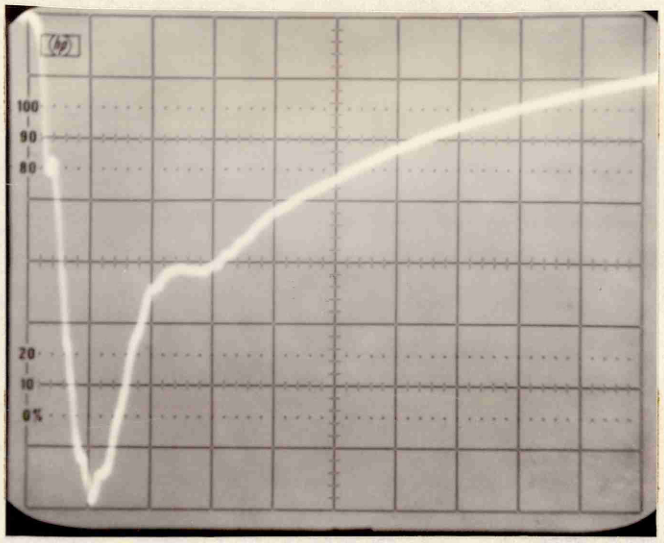

Fig. 6.9 160 volt drive pulse to transmitting transducer.
50 ns per division horizontally
20 volts per division vertically

Fig. 6.10 Common mode response of transducer from drive pulse in figure 6.9.
50 ns per division.

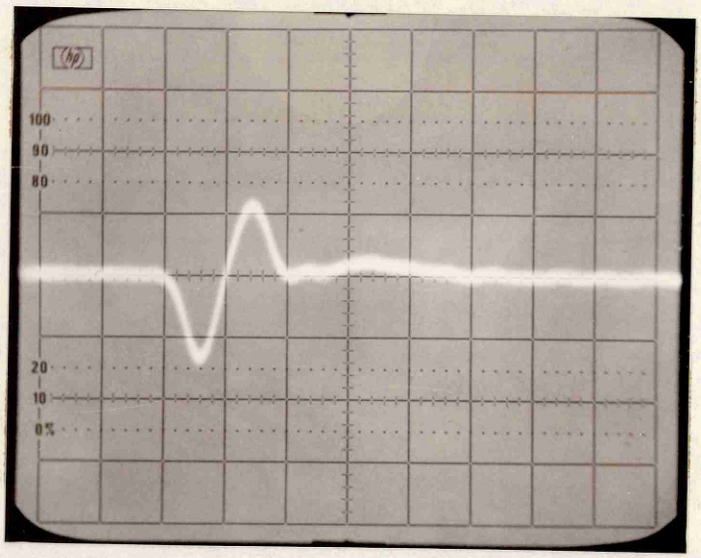

Fig. 6.11 Received pulse from drive in figure 6.7. 50 ns per division.

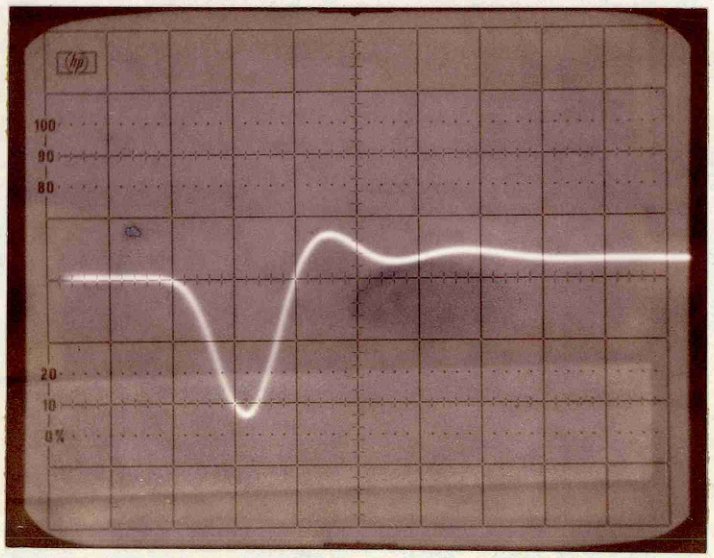

Fig. 6.12 Received pulse from drive in figure 6.9. 50 ns per division.

6.3 Transducer tests signal breakthrough

The electrical drive pulse to the transmitter broke through to the receivers, overloaded their amplifiers and produced interference in the form of a great burst of noise. This turned out to be a serious problem, because the resulting output of the receiver amplifiers (Section 8.2) was sufficiently large to break through the analogue gates (Section 8.4). A great improvement was made by fitting the transmitter with earthed aluminium plates each side of the foil. (Figures 6.1b and 6.4).

6.4 Transducer tests Frequency response

The transmitting transducer was driven by a Marconi signal generator type TF2002A5 which was modulated with a 10 µs long square pulse at 100 µs intervals. The ultrasound was received on a receiving transducer at a range of 160 mm between cylinder centres.

The peak to peak response of the receiver was measured on an oscilloscope at various frequencies and compared to the peak to peak input to the transmitter at each frequency.

The response from 0.4 to 15 MHz is shown in Figure 6.13. The greatest response is at about 6.8 MHz and the bandwidth at half power (-3 dB) is from 2.8 to 10 MHz indicating a Q of 0.94 for the system.

According to Krautkrämer (1977) the mechanical Q of a piezoelectric plate of acoustic impedance Z_o sandwiched between materials with impedances Z_1 and Z_2 can be calculated from the relation:

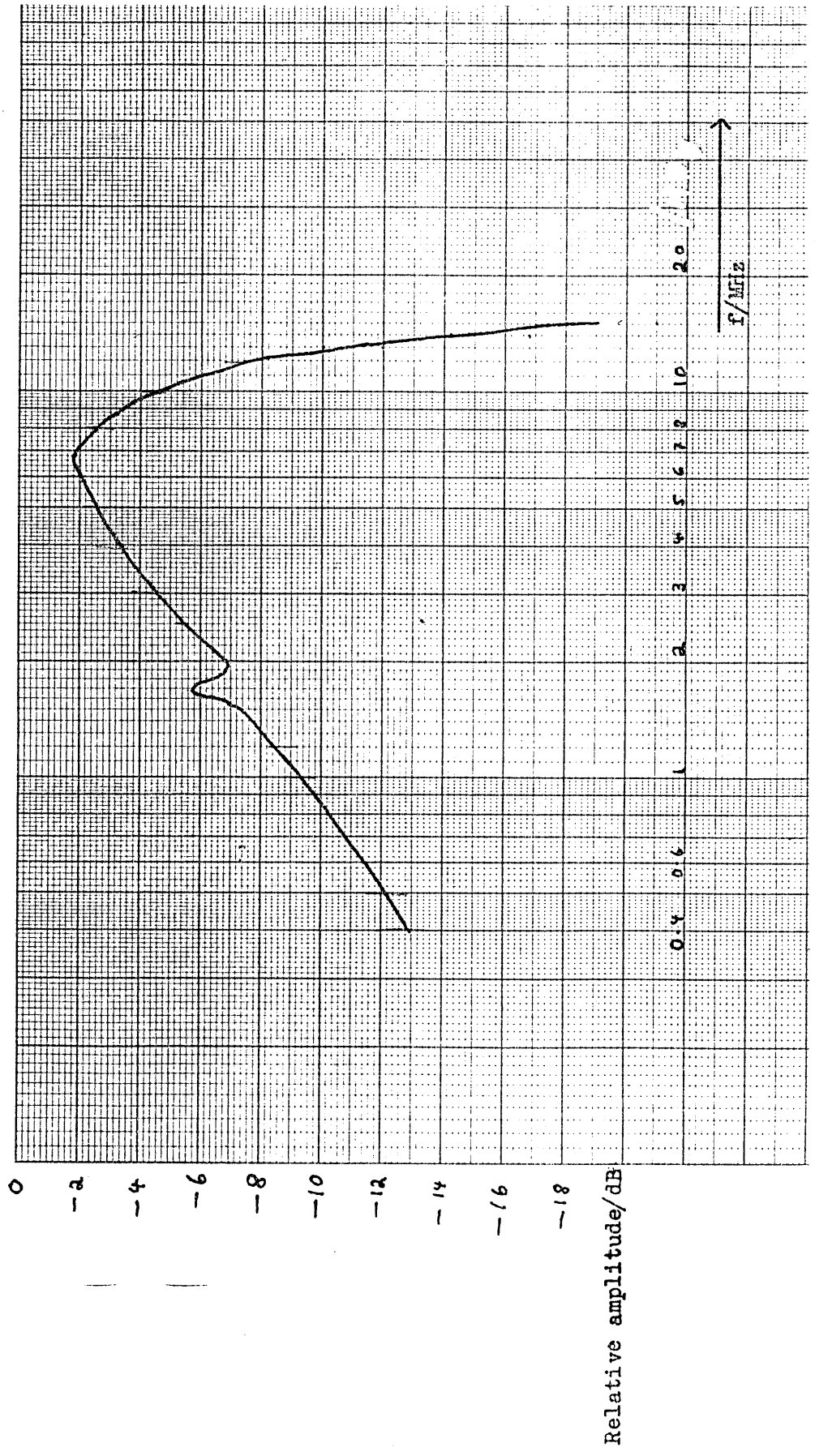

Fig. 6.13 Frequency response of the imaging system transducers.

$$Q = \pi/\ln \frac{(Z_o + Z_1)(Z_o + Z_2)}{(Z_o - Z_1)(Z_o - Z_2)}$$

(providing Z_o is greater than Z_1 and Z_2)

Putting $Q = 0.94$

$Z_1 = 1.5$ M rayl (water)

$Z_2 = 3.1$ M rayl (nylon)

then $Z_o = 3.7$ for PVF_2

This result is in the lower end of the range of values given in Table 4.2 Section 4.3.

Gooberman (1968) remarks that the frequency response of a transducer with a mechanical Q of less than 1.2 will be double peaked. It is interesting to see the little peak at 1.7 MHz, which is one quarter of the main resonant frequency.

6.5 Transducer tests Directional response

Each receiving transducer was bolted into the frame in turn and rotated around its cylinder axis while it was being insonified by the transmitting transducer. Readings of the receiver's output were taken. The response of each receiver varied by up to 3 dB at different parts of its circumference, but the averaged response of the receivers differed by only about 0.5 dB from each other. Points of low response usually corresponded with areas of the foil where the gold coating had been unintentionally removed due to accidents in etching, but there were variations in response of up to 1 dB for areas of the foils that looked perfect and identical. This suggests that the foil is not uniformly piezoelectric, but it may also

indicate that the foil was not evenly seated on its nylon former, and that, as a consequence, it was receiving more in one direction than in another in the same cylindrical plane.

The transmitting transducer behaved in a similar way, radiating over a 45^{o} angle with a variation of up to 2 dB from one part to another.

It was decided to investigate the reduction in intensity of the ultrasound with distance from the transmitter. The common-mode transmit/receive pulse-echo response of the transmitting transducer was measured for the greatest response from an aluminium target at increasing distances.

V_r is the received voltage from a pulse of ultrasound that has made a round trip of length r.

V_o is the voltage (370 mV) received at round trip path distance r_o, (which was chosen to be 108 mm). Then, if the absorption of ultrasound in the water is ignored:

$$\frac{V_r}{V_o} = \left(\frac{r}{r_o}\right)^n \quad \text{for some n}$$

The value of n depends on the mode of spreading of the ultrasound. If the spreading is cylindrical, $n = -\frac{1}{2}$ and, if the spreading is spherical $n = -1$

$$\ln \frac{V_r}{V_o} = n \ln \frac{r}{r_o}$$

Figure 6.14 is a plot of $\ln \frac{V_r}{V_o}$ against $\ln \frac{r}{r_o}$, and corresponding values of r are put on a scale along the top.

The foil has a flat direction along the axis of the cylinder and this is 16 mm wide. That would give it a near field distance of about $\frac{16^2}{4\lambda}$ where λ is the wave length of the ultrasound. If the frequency is taken as 7 MHz then λ = 214 μm and the near field due to this flat portion would be expected to extend to about 300 mm. The graph in Figure 6.14 has a slope of about $-\frac{1}{2}$ for the lower values of r where spreading is cylindrical in the near field and it steepens to about -1 at about 300 mm, indicating spherical spreading in the far field. The graph goes steeper than -1 because of the absorption of the ultrasound in the water.

Any method of correcting for attenuation over different path lengths would have to take the graph in Figure 6.14 into account. The spreading appears to be mainly cylindrical for path lengths of less than 120 mm and mainly spherical for path lengths over 300 mm.

6.6 Transducer tests Schlieren visualisation

Figure 4.18, Section 4.11, shows the Schlieren visualisation of the ultrasonic wave front from the transmitting transducer, and Figure 4.20 shows the wave front from a receiving transducer used as a transmitter.

Figures 4.22 and 4.23 show the damaged receiving transducer. Both receiving and transmitting transducers were damaged beyond repair by the high voltage used in the Schlieren system. New ones had to be made.

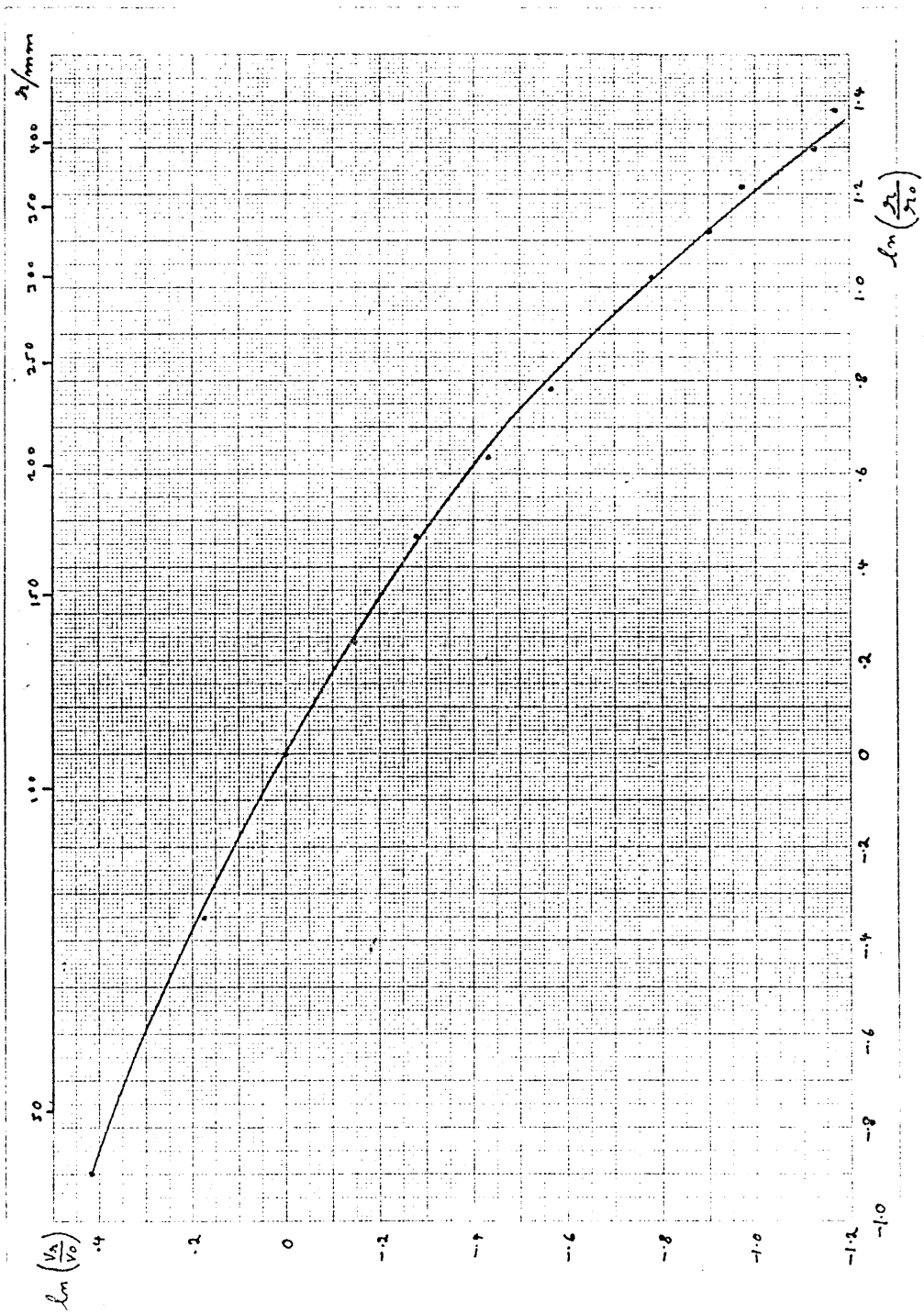

Figure 6.14.

Relative attenuation against normalised distance

Chapter 7 Computation for the imaging system

7.1 Methods of calculating the path lengths

It was decided to use the AIM 65 computer to calculate the path lengths. The problem to be solved is shown in diagram 7.1. A transmitter with radius t is at (0,0) and the receivers with radius r are at (a,0) (2a,0) etc. The path lengths are:

i. $(x^2 + y^2)^{\frac{1}{2}} + \{(x - a)^2 + y^2\}^{\frac{1}{2}} - (r + t)$

ii. $(x^2 + y^2)^{\frac{1}{2}} + \{(x - 2a)^2 + y^2\}^{\frac{1}{2}} - (r + t)$

etc.

Alternative approaches to these calculations were considered:

i. Calculate the four path distance for each point (x,y) every time they are required. This will take several milliseconds of computer time for each point (x,y).

ii. Calculate all the path distances for all values of (x,y) in the scanning field and put them into a look-up table before imaging starts. During imaging the computer would extract the values of the four path lengths for each point (x,y) from the look-up table by indexed addressing. This would take about 75 μs per point (x,y) but would require about 600 kilobytes of memory for the look-up table if one were to involve the complete field of scan. A picture of 100 x 100 pixels would require at least 60 K bytes of memory (and that with only four receivers).

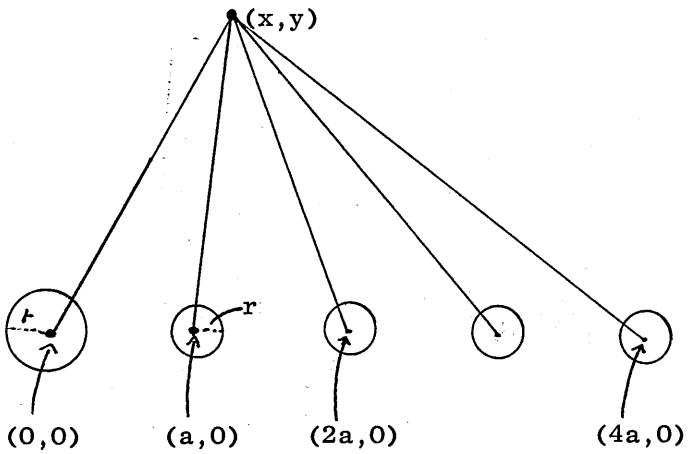

Fig. 7.1 Plan diagram of transducer array.

As only 4 K bytes of random access memory were available, the second alternative was rejected, and it was decided to calculate each path length when it was required.

However, in a developed system, the use of a look-up table should be seriously considered.

Although the obvious approach to calculating the path lengths is to use Pythagoras's theorem this has the disadvantage of requiring squares and square roots. Apart from the problem of devising a program to calculate square roots quickly, a 12 bit result implies that 24 bit numbers must be handled during the calculation.

Three other possible methods were investigated;

iii. Scanning will normally be done by holding y constant and incrementing x until each line is scanned. With y constant, the path to any receiver will form a triangle of constant area for any value of x. By calculating and storing the area of each triangle for each value of y, it is possible to find the length of the perimeter of the triangle for each value of x. Deducting the transmitter-receiver distance gives the path length.

iv. Each target point (x,y) is at the intersection of a set of ellipses centered on the transmitting and each of the receiving transducers (section 3.4). The path length is 2a in the ellipse equation $\frac{x^2}{a^2} + \frac{y^2}{b^2} = 1$.

v. If the eccentricity of the ellipse is e, $e^2 = \frac{a^2 - b^2}{a^2}$

Then the path length is the transmitter-receiver spacing divided by e.

In fact although these methods appear favourable to begin with, they all give rise to quadratic equations. Using Pythagoras's theorem, one has to find five separate square roots if four receivers and one transmitter are used. Using one of the other methods, one has to find at least four square roots for the quadratic equations, and the gain in time through doing one less square root would be very small, and would probably be offset by other factors.

7.2 Calculation of square roots

It was decided to use the Pythgoras method in spite of the problems that might arise from 24-bit numbers and square roots, and therefore it was necessary to devise a method of producing square roots in machine code software.

Methods considered were:

i. Use Newton's successive approximation formula:

$$U_k = \tfrac{1}{2} \left(U_{k-1} + \frac{a}{U_{k-1}}\right)$$

where U_{k-1} is the previous and U_k the present estimate for $\sqrt{a}$. This requires long division to get a/U_{k-1}. Dividing a 24 bit number by a 16 bit number would require 24 loops of about 75 clock cycles making about 1800 clock cycles. Another 90 would probably be needed to cope with the adding and halving operations making a total of almost 2000. Using a starting value of $U_{k-1} = 1000$, up

to five iterations will be required for a 24 bit number making a total time of 10 milliseconds for one square root.

ii. Take the logarithm, halve it, take the antilogarithm. The quickest way of calculating the logarithm of a number is probably to use a Newton-Raffson approximation method. By the time one had found the antilogarithm as well, this would take at least twice as long as method i.

iii. Square root by odd number subtraction. This works because the square root of an integer is equal to the number of successively higher odd numbers that can be subtracted from it. Scanlon (1980) gives a machine code program to do this for a 16 bit number. He says that the program is "not particularly fast". The time taken depends on the number of subtractions that can be made, hence it is roughly proportional to the square root obtained. Scanlon's program takes 2.45 ms to calculate $\sqrt{1000}$ and 9.56 ms for \$ $\sqrt{FF00}$. Even if a 24 bit number could be square rooted on a program of the same length, it would take 150 ms to find \$ $\sqrt{FE0000}$.

iv. Square root by division into paired digits. This method depends on the expansion of $(a + b + c.....)^2$ being $a^2 + b^2 + c^2.... + 2(ab + bc + ac ....)$, that is the sum of all the terms squared plus two times the sum of all the pair multiples. As this method does not seem to be generally known, instructions are now given to find the square root of a denary number as an example.

Take $\sqrt{1032.3369}$. Divide the digits into pairs either side of the decimal point, as 10 / 32. / 33 / 69. Subtract the largest possible perfect square from the first pair, in this case 9. 10 - 9 = 1; pretend you are doing long division and bring down the next pair. You now have the number 132. $\sqrt{9}$ = 3 goes on the top line as shown below. Double this, 6 begins the next calculation. Estimate x when sixty plus x goes x times into 132. x = 2.

Subtract, bring down next pair, double top line. Next x = 1. Finally 6423 goes 3 times. x = 3. If it did not you would bring down 2 zeros and carry on. It gets more and more difficult for obvious reasons. However $\sqrt{1032.3369}$ = 32.13.

```
    3  2   1  3
 3)10 32. 33 69
    9
 62) 1 32
    1 24
641)    8 33
        6 41
6423)1 92 69
     1 92 69
```

Although this method is very tedious in denary arithmetic, it is very simple in binary. The first largest perfect square can only be 1, and x can only be 1 or 0. Doubling the top line is achieved by moving it one place to the left. No division is needed, only a comparison to find whether a top line digit should be 0 or 1, followed by a subtraction in the latter case. In a computer, the pairs of binary digits can be pushed onto the stack, pair by pair. By pushing the least significant pair first and the most significant

pair last, the pairs can be pulled off the stack in the correct order. As will be shown in section 7.3, a square root program based on this system will require up to 1700 clock cycles to find the square root of a number of up to 24 bits. Consequently, the time taken should not exceed 1.7 ms, and this method was chosen as being the fastest.

7.3 The square root algorithm

Figure 7.2 shows an algorithm to produce square roots from a binary number. A 24 bit number is mentioned but, in principle, this algorithm will cope with a number of any length if the bit pairing is arranged appropriately. The numbers pushed onto the stack will be of the form of six zeros followed by 00, 01, 10 or 11. The number $F0 (four ones followed by four zeros) is quite distinct from any of these and is used as an end marker to show when the stack is empty. X, Y, Z and R are used as variables. The first number off the stack becomes X; further numbers from the stack are Z. R will be the result, Y represents the divisor: X is then the dividend. Leading pairs of zeros are removed by the first loop, and a zero result is made by the branch at "X = $F0?".

The process continues to the square root procedure which follows one of two loops depending on whether Y is greater than X or not. After a maximum of 12 loops the result R is produced. The square root program based on this algorithm is shown in Appendix 2 and takes between 1350 and 1700 clock cycles to process a 24 bit number of which the last four bits are zeros. The time difference depends on which loop predominates.

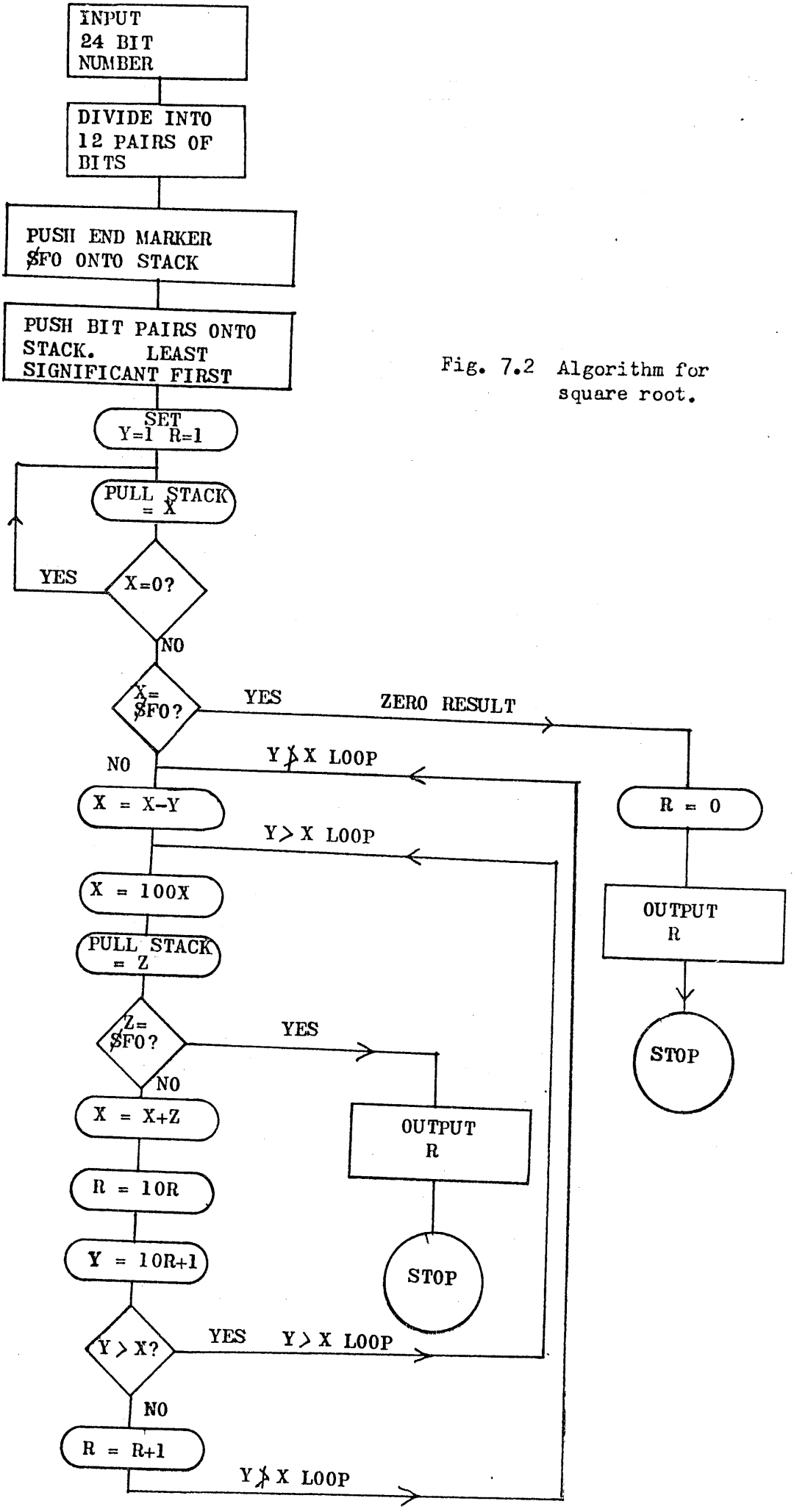

Fig. 7.2 Algorithm for square root.

In a practical test on the AIM 65, six 24-bit numbers taken at random took between 1.45 and 1.71 ms, four 20-bit numbers took between 1.22 and 1.42 ms and a 17-bit number took 1.09 ms. These results are an order of magnitude better than Newton's method and two orders of magnitude better than the odd number subtraction method.

7.4 The remainder of the program

It was necessary to devise methods for adding, subtracting and multiplying numbers of up to 3 bytes, and the individual programs for doing this are modified versions of those given by Zaks (1978) and Leventhal (1979).

At this stage it was decided to modify the design so that the maximum range to be imaged would be $FF (255) mm instead of $1CØ (448) mm. This has the advantage of allowing the range to be held on one byte of memory and obviates the need to square a two-byte number, saving time and memory space. Figure 7.3 is the algorithm for finding the path length. d represents the target point distance along the y axis and n the distance along the x axis, both in millimetres. The number of bytes of memory taken up by each item is shown, and the symbols in brackets refer to the labels in the assembler language program. The effect of pushing two pairs of zeros onto the stack (box 8) is to multiply the hypotenuse length by binary 100 or denary 4, thus giving a result in quarter millimetres. The first column of the algorithm finds the outgoing distance. The second column is the algorithm for finding the return distance.

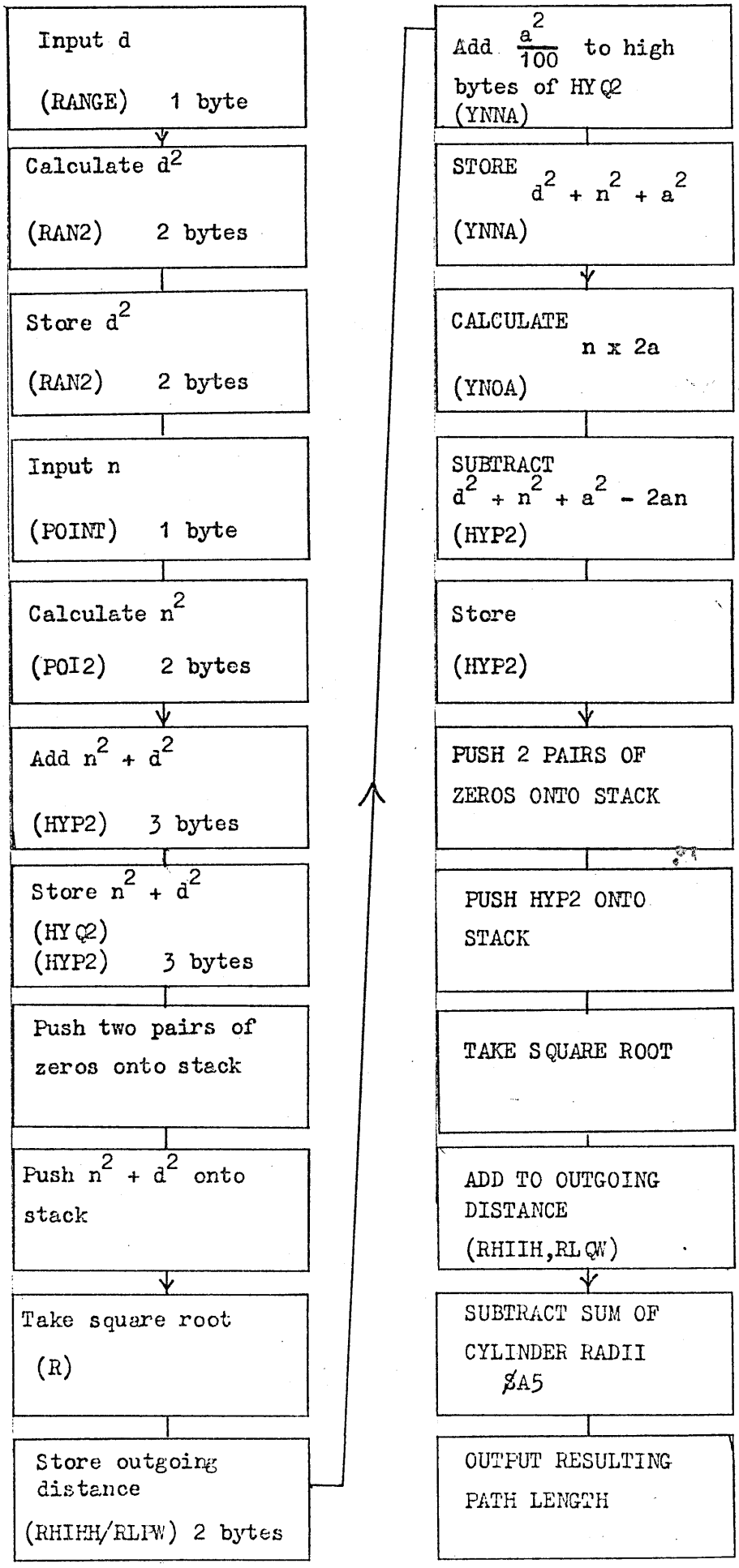

Fig. 7.3 Procedure for calculating the path length.

The distance is $\{(n - a)^2 + y^2\}^{\frac{1}{2}}$, and a complication arises from the term (n - a), as this can be negative. To get round the problem of squaring a negative number, note that $(n - a)^2 + y^2$ expands to $n^2 + y^2 + a^2 - 2a$. The sum of the first three terms must always exceed 2a (because the result is a positive number) and $n^2 + y^2$ has already been calculated and stored as HYQ2.

The values of a^2 and 2a are constants for a particular receiver and can be inserted into the program as numbers. The actual hexadecimal numbers are:

Receiver	a^2	2a
1	1900	A0
2	6400	140
3	E100	1E0
4	19000	280

The terminating zeros result from the transducers being spaced at exact multiples of $10 mm. There is no need to store zeros, so the numbers put into the program are (in hexadecimal):

Receiver	a^2/$100	2a or 2a/$10
1	19	A0
2	64	14
3	E1	1E
4	0190	28

The values of a^2/$100 are added to the higher bytes of HYQ2 to give $a^2 + n^2 + y^2$ (YNNA), then 2a is multiplied by n to give 2an (YNOA). In the case of receivers 2, 3 and 4, this is all done in subroutine SRETN.

After the square root is taken the outgoing distance is added, and the sum of the radii of the transmitting and receiving transducers is subtracted. In fact this is $A6 (quarter mm) but as the square root program calculates to the nearest whole number down, and two such roots are added, the overall result calculated is usually one quarter mm. less than the true value. For this reason $A5 mm are subtracted, not $A6.

7.5 The complete program

The full program (KOKO7) is shown in assembly language in Appendices 1 and 2 as printed out by the AIM 65 from its editor. Explanations of each part have been typed in afterwards. The program is long (647 bytes), because there are only two subroutines. This is a deliberate compromise between taking up memory space and taking up running time. The program has very few comments, and these are brief. This is also deliberate, partly to save memory but mainly because the AIM 65 is so constructed that if a line in the editor exceeds 20 characters in length, then the first twenty will be deleted on the display.

The main program runs from $0D00 to $0E89 and the first eleven instructions initialise the system. The final twenty seven instructions arrange for incrementing the target point in a rectangular

raster of predetermined size. The square root subroutine (SBQRT) runs from $0B00 to $0BA8, and the other subroutine (SRETN) from $0BC0 to $0C16.

The path lengths are fed to the user port on the AIM, the eight lowest bits on $A001 and the four highest on $A000. (Against these appear the comments "1st, 2nd etc. OUTLO/OUTHI"). Output A000 also has the numbers $00, $40, $80 and $C0 added as codes to steer the path lengths to the appropriate latches. (Section 8.1).

The AIM 65 sends a strobe in the form of a positive going 1 µs pulse to user port pin CB2 at the same time as the four highest bits and the latch address codes are fed to user port pins A000. This tells the peripheral electronics that the data on the user port is now valid and to load the appropriate latch.

The program takes about 3,4 ms to compute the first path length, then the other three path lengths are computed after 5.1, 6.8 and 8.5 ms respectively. These figures vary by 250 µs either way depending on the data.

Chapter 8 Electronics for the imaging system

8.1 Overall description

Figure 8.1 shows the overall circuit diagram for the imaging system, and Figure 8.2 is a flow diagram of the system. The software loop is on the left of Figure 8.2 and the electronic and acoustical loop is on the right. Strobe 4 starts the latter loop by setting D flip flop 2, concurrently monostable 2 allows 3 μs delay for the loading of counters before firing the pulser and starting the count down. While the counters are counting down, the analogue holds 1 - 4 are cleared. After all the analogue gates have opened and closed, the clock is stopped and analogue hold 5 is cleared and then filled with the sum of all four received signals. Normally the cycle will then repeat in order to transmit the maximum number of pulses during the 6 ms available for signal averaging. However, at short imaging ranges, there may be some problem with the echoes of the previous pulse not dying away before the new echo arrives, so monostable 3 has been introduced to give a minimum delay between pulses that can be set from 100 to 400 μs.

After about 6 ms, the computer will have loaded 3 sets of new data into the data latches and strobe 3 sets D flip flop 1. This can happen at any moment so the electronic and acoustical loop carries on until it has finished its present cycle. The analogue signals are averaged by a low pass filter and then converted to digital form and stored in the appropriate address in the digital video store. The digital store address is then incremented and after a delay of about 1 ms, the computer will send strobe 4 to repeat the complete process for the next image point.

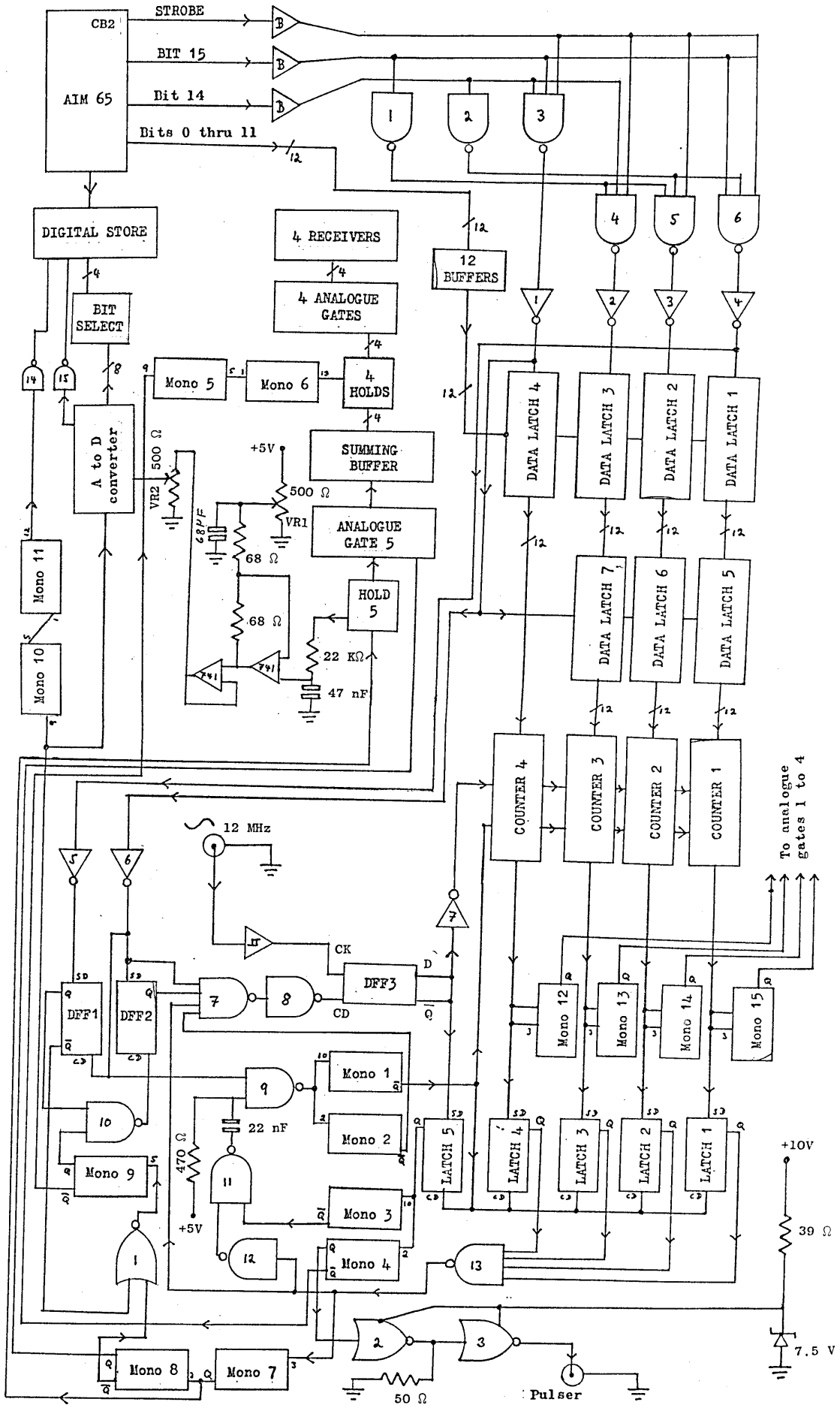
CB2
STROBE
BIT 15
Bit 14
Bits 0 thru 11
AIM 65
DIGITAL STORE
BIT SELECT
A to D converter
4 RECEIVERS
4 ANALOGUE GATES
12 BUFFERS
Mono 5
Mono 6
4 HOLDS
SUMMING BUFFER
ANALOGUE GATE 5
HOLD 5
Mono 11
Mono 10
VR2
500 Ω
VR1
500 Ω
68 pF
68 Ω
68 Ω
741
741
22 KΩ
47 nF
+5V
DATA LATCH 4
DATA LATCH 3
DATA LATCH 2
DATA LATCH 1
DATA LATCH 7
DATA LATCH 6
DATA LATCH 5
COUNTER 4
COUNTER 3
COUNTER 2
COUNTER 1
To analogue gates 1 to 4
12 MHz
CK
D
CD
DFF3
DFF1
DFF2
Mono 12
Mono 13
Mono 14
Mono 15
Mono 1
Mono 2
Mono 3
Mono 4
Mono 9
22 nF
470 Ω
+5V
LATCH 5
LATCH 4
LATCH 3
LATCH 2
LATCH 1
+10V
39 Ω
7.5 V
Mono 8
Mono 7
50 Ω
Pulser

Fig. 8.1

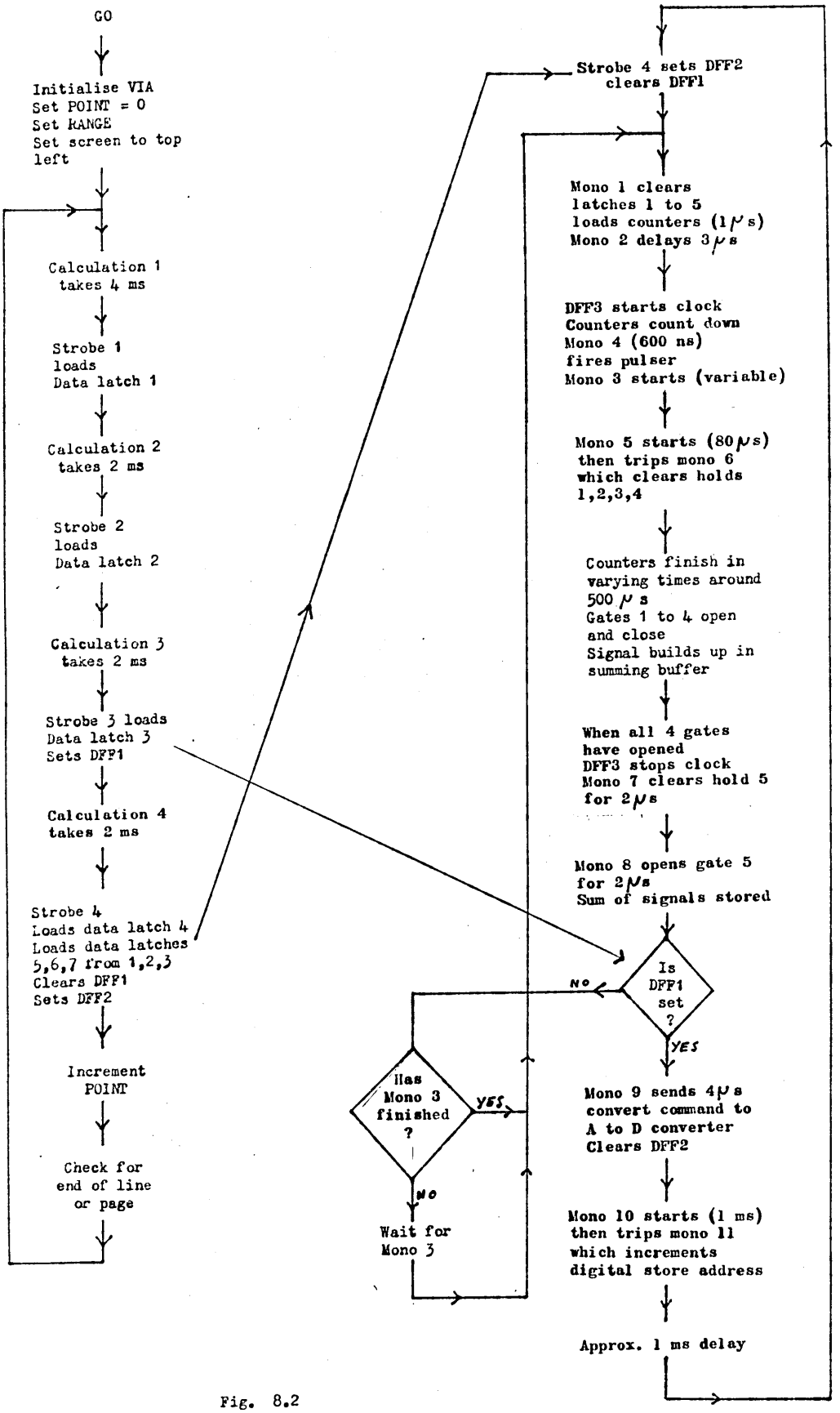
GO
Initialise VIA
Set POINT = 0
Set RANGE
Set screen to top left
Calculation 1 takes 4 ms
Strobe 1 loads Data latch 1
Calculation 2 takes 2 ms
Strobe 2 loads Data latch 2
Calculation 3 takes 2 ms
Strobe 3 loads Data latch 3 Sets DFF1
Calculation 4 takes 2 ms
Strobe 4 Loads data latch 4 Loads data latches 5,6,7 from 1,2,3 Clears DFF1 Sets DFF2
Increment POINT
Check for end of line or page
Strobe 4 sets DFF2 clears DFF1
Mono 1 clears latches 1 to 5 loads counters (1μs) Mono 2 delays 3μs
DFF3 starts clock Counters count down Mono 4 (600 ns) fires pulser Mono 3 starts (variable)
Mono 5 starts (80μs) then trips mono 6 which clears holds 1,2,3,4
Counters finish in varying times around 500μs Gates 1 to 4 open and close Signal builds up in summing buffer
When all 4 gates have opened DFF3 stops clock Mono 7 clears hold 5 for 2μs
Mono 8 opens gate 5 for 2μs Sum of signals stored
Is DFF1 set ?
NO
YES
Has Mono 3 finished ?
YES
NO
Wait for Mono 3
Mono 9 sends 4μs convert command to A to D converter Clears DFF2
Mono 10 starts (1 ms) then trips mono 11 which increments digital store address
Approx. 1 ms delay

Fig. 8.2

Figure 8.1 gives more detail. Before imaging starts, a special program is run through the AIM 65 to set up the video store. Then the selected values of the ranges of the top and bottom of the picture and its width (see section 5.6) are keyed into the AIM 65. Upon keying "G RETURN" the AIM 65 starts to calculate the path lengths. As each path length is calculated, it is sent via the buffers to the 12 bit data latches 1 - 4. As mentioned in section 7.5, the numbers 0, $40, $80 and $C0 are added to the data for latches 1, 2, 3 and 4 respectively. This has the effect of putting the numbers 00, 01, 10 or 11 onto bits 14 and 15 of the userport A000. The strobe pulse and bits 14 and 15 go via buffers (marked B) to NAND gates 1 - 6, which together with inverters 1 - 4 use the particular combination of zeros and ones to enable the appropriate data latch to load. Strobe 4, as well as loading data latch 4, also loads data latches 5, 6 and 7 from data latches 1, 2 and 3, sets D flip flop 2 and triggers monostables 1 and 2 (which are on one 74123 chip) via NAND gate 9. Monostable 2 creates a 3 µs delay while monostable 1 loads the 12 bit counters from the data latches and clears latches 1 - 5. (These latches are on one 74118 chip). The strobe pulse also holds D flip flop 3 cleared (via NAND gates 7 and 8), while the 3 µ sec delay is being set up by monostable 2.

6 MHz clock pulses are obtained from a 12 MHz signal generator via a Schmitt trigger and D flip flop 3 which has its D input connected to its $\overline{Q}$ output. This divides the 12 MHz clock rate by two, and can be stopped by holding CD at 0. After 3 µs, $\overline{Q}$ of monostable 3 returns to 1, thus setting D flip flop 3 via NAND

gates 7 and 8. The first falling edge of the clock pulse sets latch 5 and (via inverter 7) starts the count down. Latch 5 trips monostables 3 and 4 and thus fires the pulser via NOR gates 2 and 3. These are line drivers type 74128. The pulser has an input impedance of about 50 Ω and is connected to the output of NOR gate 3. The 50 Ω resistor to earth from NOR gate 2 is to ensure a constant current drain while switching.

Monostable 5 is also tripped and delays 80 μs before tripping monostable 6 for 5 μs to clear the holds 1 - 4. The reason for this delay is that the analogue gates are not perfect, and leak a certain amount of charge to the holds. Therefore the holds are cleared as late as practical as at any normal imaging distance no signal will be returned in less than 100 μs. (Monos 3, 4 and 5, 6 are type 74123). Meanwhile, counters 1 - 4 will reach 0 in varying times, and upon doing so, send pulses to trigger monostables 12 - 15 and set latches 1 - 4. Monostables 12 - 15 (type 74121) open analogue gates 1 - 4 for the selected sampling time and transfer the sampled analogue signals to the hold circuits, whence they are added in the summing buffer. When latches 1 - 4 have all been set, NAND gate 13 triggers monostables 1 and 2 via NAND gates 12, 11 and 9 (providing monostable 3 has finished. If not, monostable 3 will trigger them when it finishes). The cycle repeats with the counters being loaded with same data as before, and latches 1 - 5 cleared.

Meanwhile NAND gate 13 also trips monostable 7 (type 74121) to clear hold 5 for 2 μs. Then monostable 8 (type 74121) opens analogue gate 5 for 2 μs, and the summed signal is stored in hold 5. As

the cycle repeats a succession of values of signal is stored in hold 5 and is averaged by the low pass filter consisting of the 22 KΩ and the 47 nF capacitor. This has a time constant of about 1 ms. The analogue gate produces a small standing voltage and this is balanced out by the 500 Ω potentiometer (VR1) and the two 68 Ω resistors. The averaged signal is taken via the 741 operational amplifiers and a second 500 Ω potentiometer (VR2) to the input of an A to D converter type RS427 fitted with a 270 kHz clock. The cycle repeats until D flip flop 1 is set by strobe 3, whereupon the tripping of monostable 8 causes D flip flop 2 to clear via NOR gate 1, monostable 9 and NAND gate 10. The clock is disabled until DFF_2 is reset. Mono 9 (type 74121) sends a 4 μs convert command to the A to D converter. The conversion takes between 30 and 40 μs. The A to D converter signals that the digital data are valid by a pulse through NAND gate 15 to the digital store. (NAND 15 is a buffer type 7437). The A to D converter has an 8 bit output but the digital video store has only a 4 bit input. Using a 4 pole 5 way rotary switch, one can select those four of the eight bits which are expected to be the most significant and direct them to the digital store. Monostable 9 also triggers monostable 10 which delays 1 ms before tripping monostable 11 to increment the digital store address via NAND gate 14 (a buffer type 7437). Monostables 9 and 10 are both on a 74123 chip.

8.2 Receiver amplifiers

Each receiver is fitted with an amplifier mounted on top of the nylon cylinder and enclosed in the brass tube. Figure 8.3a shows two receivers and the transmitter with the brass tubes removed.

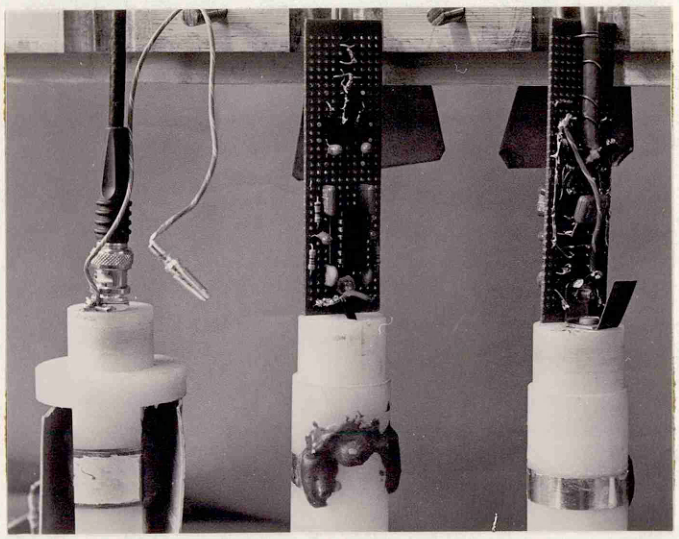

Fig. 8.3a Two receivers and transmitter with brass tubes removed to show receiver amplifiers and direct connection to transmitter.

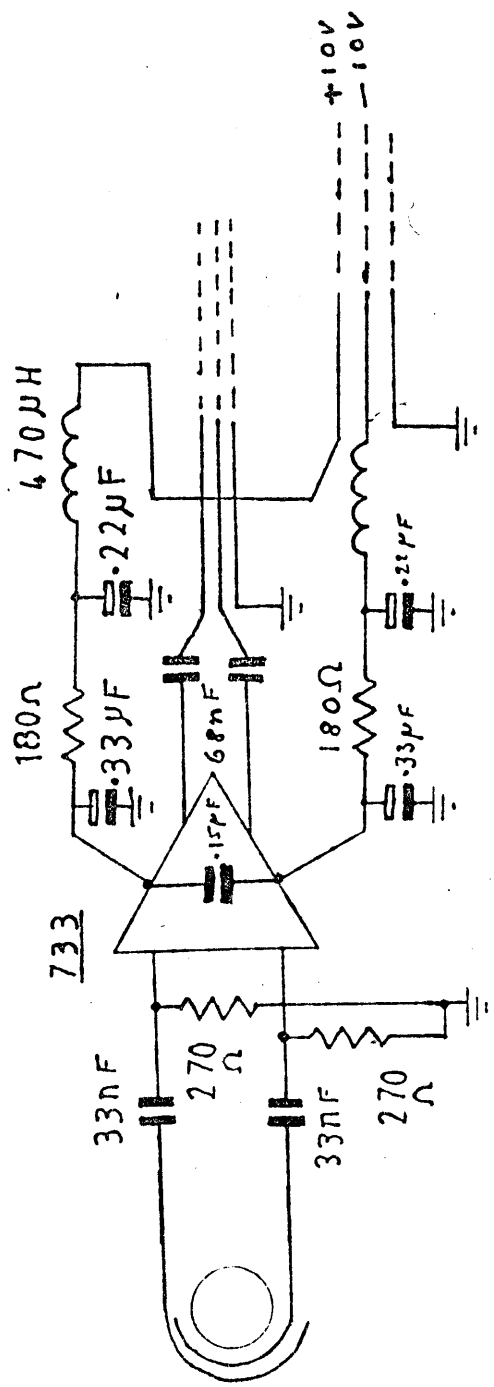

Fig. 8.3 Receiver amplifier.

The receiver amplifiers are made on pin board and bolted to the top of the nylon cylinder.

Figure 8.3 is the circuit of the receiver amplifier. A short length of coaxial cable (section 6.1) connects the PVF_2 to the differential inputs of a 733 amplifier via two 33 nF capacitors. The capacitors are necessary to prevent the formation of a d.c. path from the foil to earth. This prevents electrolytic action on the foil surface and avoids biasing the amplifier (section 4.6).

The 733 amplifier can be set at voltage gains of 10, 100, and 300 by connecting various pins. For the purpose of imaging it was set at 100. Plus and minus 10 volt rails had to be brought to the amplifier by way of a metre or so of cable, and although this was screened there was a considerable amount of electrical pickup. This was kept to a minimum with the filter consisting of the 470 μH inductors and the 220 nF capacitors. It was found necessary to use a differential amplifier with differential outputs fed into a twin screened cable type RS 367 - 527 leading to a second amplifier with differential input. This was mainly because there was a great deal of radio interference at just over 10 MHz in the laboratory, and any other method (such as earthing the outside of the PVF_2 foil) caused a great deal of unwanted pickup. The twin screened cable was found to have a characteristic impedance of about 50 Ω and the frequency response of the cable with a 50 ohm load was level up to 40 MHz and only 1.2 dB down at 72 MHz.

With a voltage gain of 100 the amplifier was found to be rather

unstable, and it proved necessary to earth every unused pin on the 733 and every metal fixing bracket. It was necessary to earth the amplifier to its covering brass tube using the shortest possible lead. This was achieved by bolting a piece of springy phosphor bronze strip to the amplifier mounting bracket so that the strip pressed against the inside of the brass cylinder when it was pushed over the top. Further to that, it was found necessary to connect the brass tubes directly to the water in the tank by clamping phosphor bronze strips to the outsides of the tubes and letting the ends of the strips hang in the water. A disadvantage of the 733 as an amplifier is the large offset voltage it produces at its output. The 68 nF capacitors are needed to block this. Figure 8.3a shows two of the receiver amplifiers mounted on top of the receivers.

8.3 Further amplification

The twin screened lead from each receiver amplifier goes to a second 733 also set with a gain of 100. Filters consisting of a 5 Ω resistor and a 1.5 nF capacitor have a 3 dB frequency of about 21 MHz and remove most of the radio interference picked up in the leads. Figure 8.4 shows the circuit. The BSX88 transistor acts as a rectifier and emitter follower to drive the analogue gate. A pulse received by the receiver usually has the appearance of Figure 8.9 and the 10 kΩ potentiometer is set so that the output of the emitter has the appearance of Figure 8.10. The 20 Ω potentiometer in the collector circuit was originally put in to limit the output of the emitter follower to about 1 volt (see section 8.4). However, it was also found to be useful in restricting the dynamic range of the system when studying images from low intensity echoes. The frequency

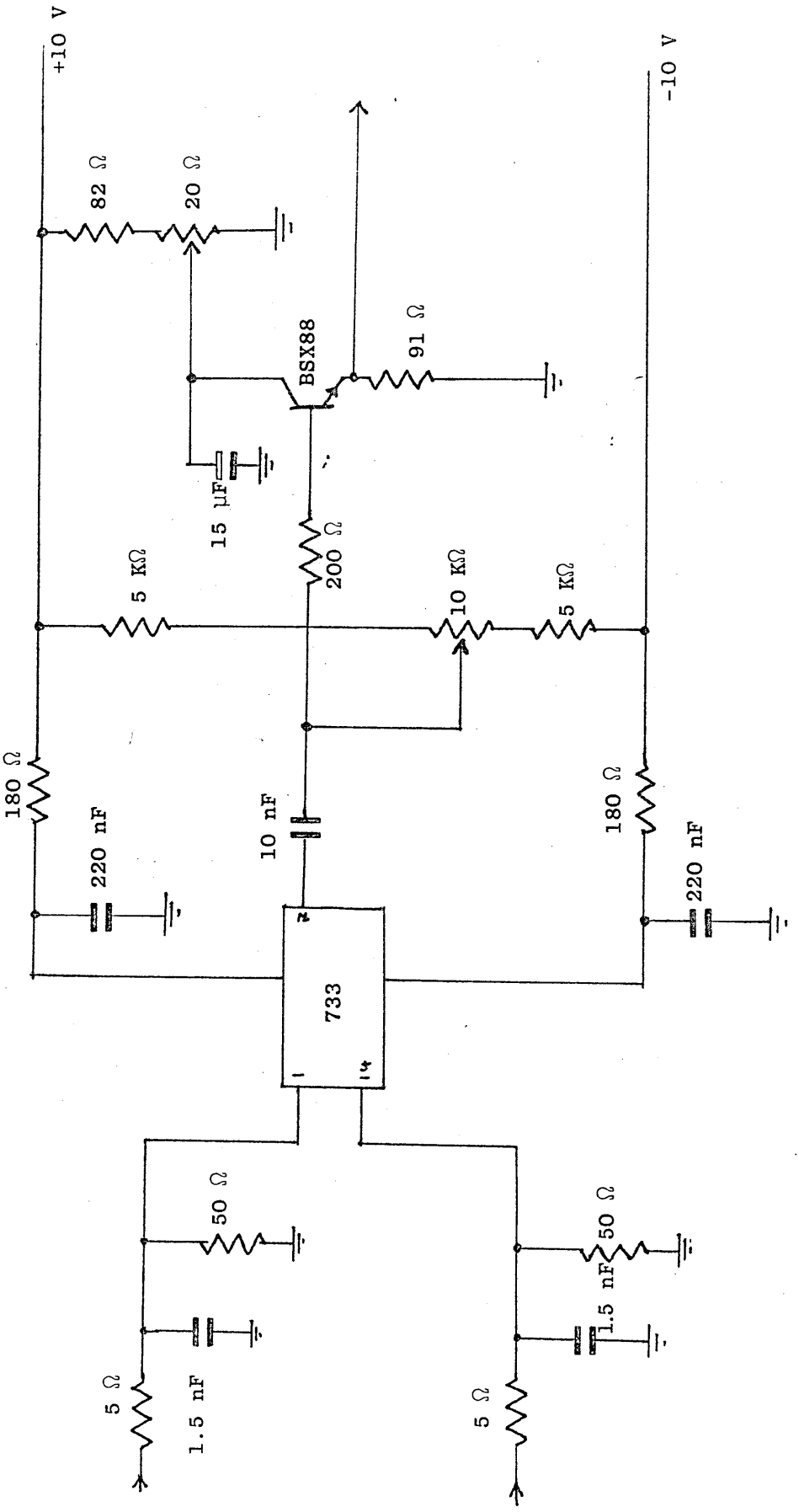

Fig. 8.4 Amplifier and emitter follower.

response of two amplifiers together is flat between 0.4 and 10 MHz. The voltage gain of the four sets of amplifiers differed by up to 0.5 dB. This was regarded as being acceptable.

8.4 Analogue gate

The circuit used is shown in Figure 8.5. Considerable problems were experienced in finding a suitable circuit for an analogue gate. There did not appear to be anything available commercially that gave a gate time of less than several microseconds. Circuits were devised that gave a gate time in the order of 100 ns but which left the analogue signal of about 0.5 volts on top of a 5 volt pedestal. The circuit used was developed by P. Garner of the Department of Electronics, Open University for a different purpose and has been adapted for the imaging system. It has the advantages of producing a pedestal-free output with a gate time down to 100 ns or less. It has the disadvantages of not accepting inputs of less than about 0.1 volt, while inputs of greater than about 1 volt will break through the closed gate. For this reason the input voltage has to be limited by the 20 Ω potentiometer in Figure 8.4. The analogue gate also has an inherent fault of leaking a small charge onto the hold capacitor. This is shown in the bottom trace of the top left hand picture of Figure 8.8 which shows the effect on the output of the gate of clearing the hold capacitor every 600 μs. The vertical scale is 0.3 volts/cm.

The positive going gate pulse is applied to a 7404 inverter that has its rails connected to - 5 V and earth. The resulting negative going pluse passes through the transformer primary and drives the

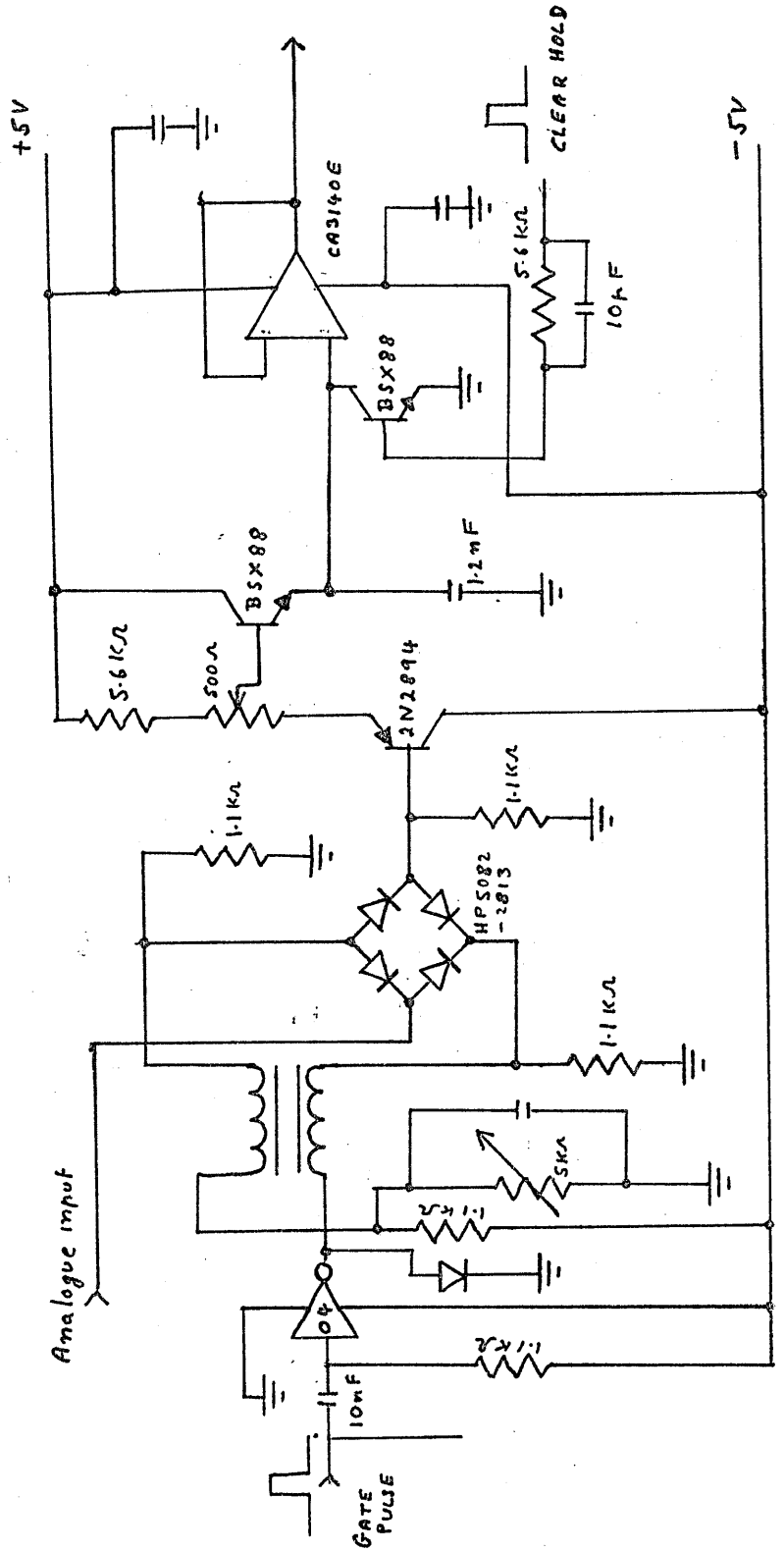

Fig. 8.5 Analogue gate.

bottom corner of the diode bridge negative (Figure 8.5). The transformer has a turns ratio of 1 to 1 and is connected so that the top corner of the diode bridge is driven positive at the same time as the bottom corner is driven negative, thus turning all the diodes on. The analogue signal that passes through the gate is held in the 1.2 nF capacitor. This can be cleared by a positive pulse on to the base of the second BSX88 transistor.

8.5 Summing buffer

The circuit is shown in Figure 8.6. The outputs of analogue gates 1 - 4 are added and divided in the ratio 680/1500 = 0.45. This is to avoid overloading analogue gate 5. The analogue gates produce an offset voltage output of about + 0.5 V. The 500 Ω potentiometer is set to balance this out.

8.6 Testing the electronics

The result of testing the amplifiers was reported in section 8.3. The frequency response is flat between 0.4 and 20 MHz, and the gain differs by a maximum of 0.5 dB from one amplifier to another.

A special program was written for the AIM 65 in BASIC to simulate the effect of the real machine languages program and to test the hardwired logic circuits and the analogue gates. The program (KOE12) is listed in Figure 8.7. It allows the operator to load the data latches with a set of predetermined numbers. The numbers can simulate any time delay or path length, but it was found convenient to be able to select delays of 300, 400, 500 and 600 microseconds, or a delay corresponding to 512 mm of path length in water, or for

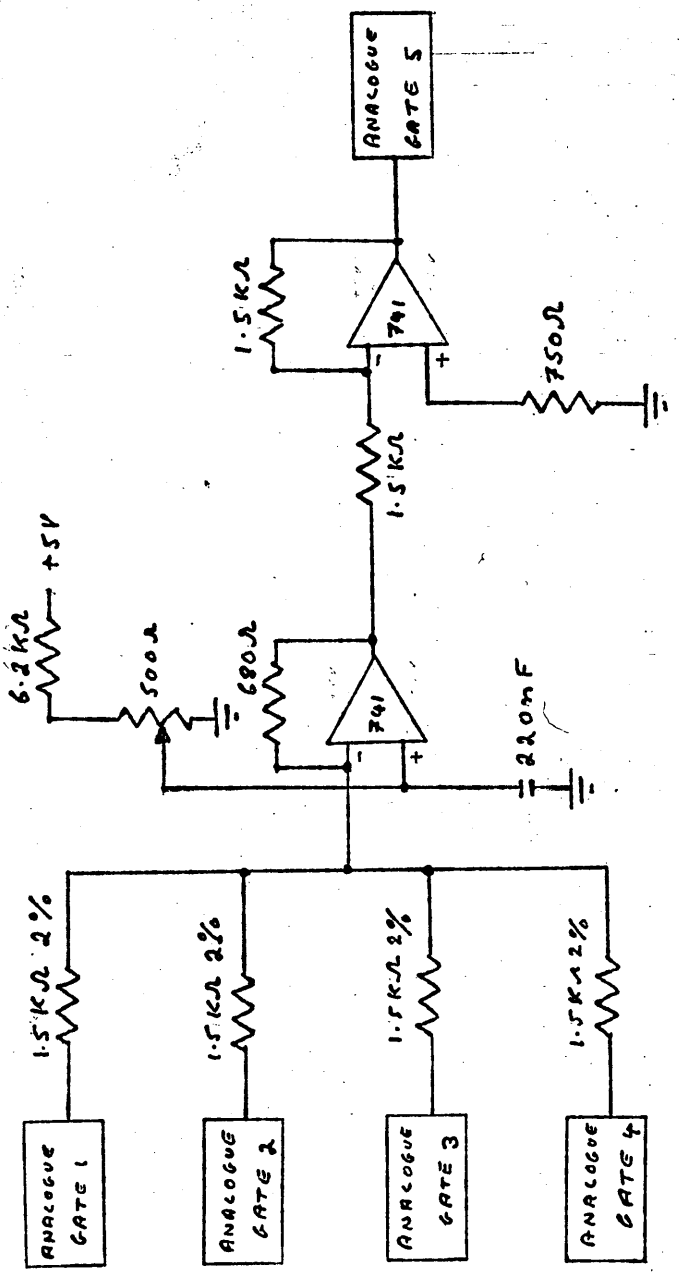

Fig. 8.6 Summing buffer.

```
 10 B=40960
 20 A=40961
 40 POKE40972,160
 50 POKE40962,255:PO
KE40963,255
 60 PRINT"?0FOR SET
NUMBERS,?2FOR600COUN
TS,4FOR600/601/602/6
03COUNTS"
 61 PRINT"?0THER NUM
ER FOR OWN COUNTS""
 62 PRINT"?6 FOR 512
MM PATH"
 63 PRINT"8 FOR 300,
00 MUSEC DE MUSEC DE
LAYS"
 65 INPUTX
 70 IFX=0THEN500
 75 IFX=8THEN900
 80 IFX=2THEN600
 90 IFX=4THEN700
 95 IFX=6THEN800
 100 INPUTD,E
 110 INPUTF,G
 120 INPUTH,I
 130 INPUTJ,K
 200 F=F+64
 210 H=H+128
 220 J=J+192
 230 POKEA,E:POKEB,D
 270 POKEA,G:POKEB,F
 310 POKEA,I:POKEB,H
 350 POKEA,K:POKEB,J
 390 GOTO230
 500 D=5:E=85:F=10:G
=170:H=9:I=153:J=6:K
=102
 505 PRINT"SET NUMBE
RS"
 510 GOTO200
 600 D=2:F=2:H=2:J=2
 601 E=88:G=88:I=88
 602 K=88
 605 PRINT"600 COUNT
S"
 610 GOTO200
 700 D=2:F=2:H=2:J=2
 701 E=88:G=89
 702 I=90:K=91
 705 PRINT"600INCREM
ENT"
 710 GOTO200
 800 D=8:E=0:F=8:G=0
:H=8:I=0:J=8:K=0
 805 PRINT"512MM PAT
H"
 810 GOTO200
 900 D=7:F=9
 901 H=11:J=14
 902 E=8:G=96
 903 I=184:K=16
 910 PRINT" 300,400,
500,600 MSD"

 920 GOTO200
```

Fig. 8.7 Test program KOE 12

counts of 600, 601, 602 and 603. The BASIC program runs at a speed which repeatedly injects the same selected numbers into the data latches at about 12 ms intervals. This is slightly slower than the real program operates. The operation of the hardwired logic can be checked using this program and an oscilloscope.

The performance of the analogue gates was checked using the BASIC program and three pulse generators were arranged to simulate four received signals. The pulse generators gave a succession of 1 μ sec long pulses at intervals of 300, 400, 500 and 600 μs after being triggered by the BASIC program. The pulses were fed via potentiometers to all four of the receiver inputs and the BASIC program was set to open the analogue gates at 300, 400, 500 and 600 μs after triggering the pulse generators. The gates should therefore open at the same moment that a pulse arrives at the analogue input.

Figure 8.8 shows the oscilloscope trace when set at 200 μs per cm. The lower trace shows the output of the summing buffer and the upper trace (a straight line) shows the resulting input voltage to the A to D converter. As stated earlier (section 8.4) the analogue gate has an inherent fault of leaking a small charge onto the hold-capacitor. In Figure 8.8, the input to the A to D converter has been zeroed for zero signal input to the receivers by adjusting VR1 on Figure 8.1. This allows the maximum of the leaked charge to be regarded as zero volts. It can be seen that the top trace rises through the same distance as the peak value of the bottom trace showing that the circuit is working correctly and linearly.

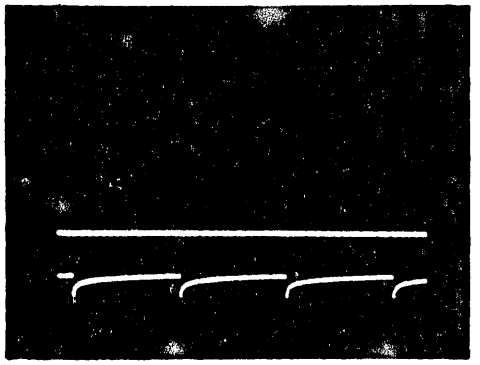

All inputs zero.

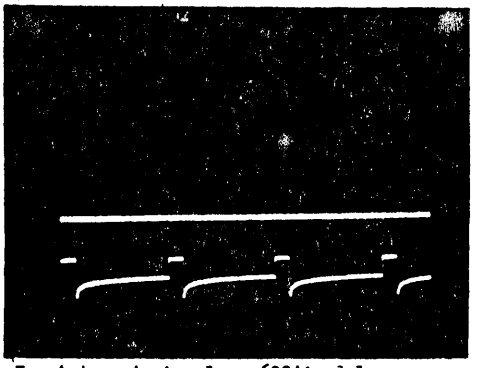

Input to gate 4 only. 600μs delay.

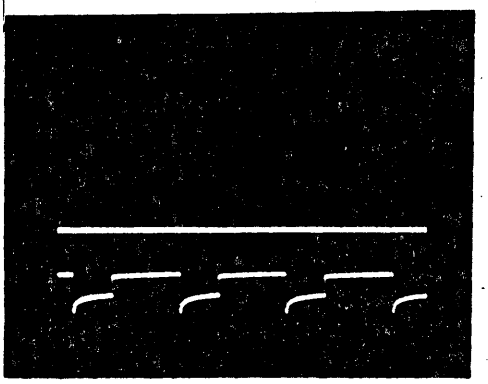

Input to gate 1 only. 300μs delay.

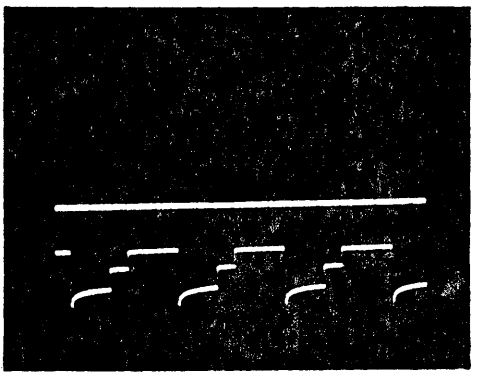

Inputs to gates 1 and 2.

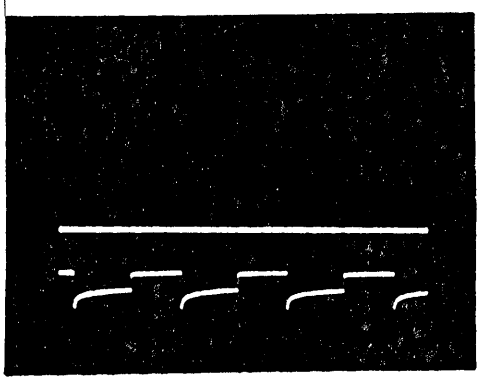

Input to gate 2 only. 400μs delay.

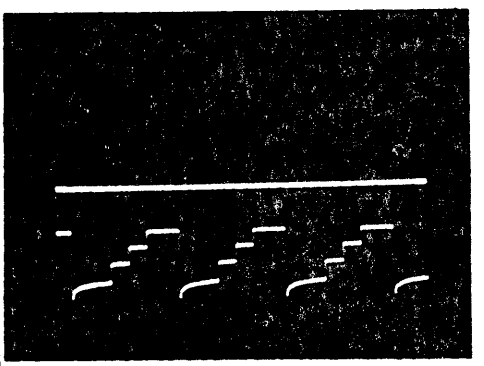

Inputs to gates 1, 2 and 3.

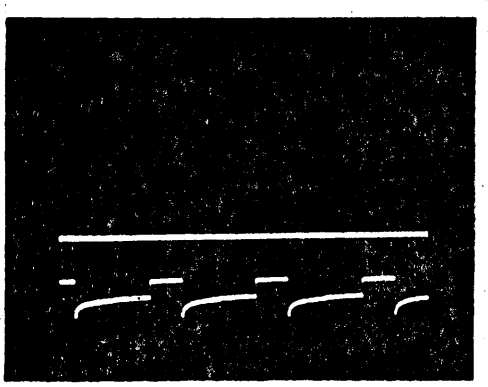

Input to gate 3 only. 500μs delay.

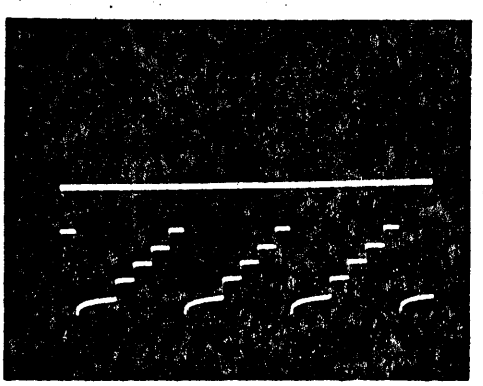

Inputs to gates 1, 2, 3 and 4.

Fig. 8.8.

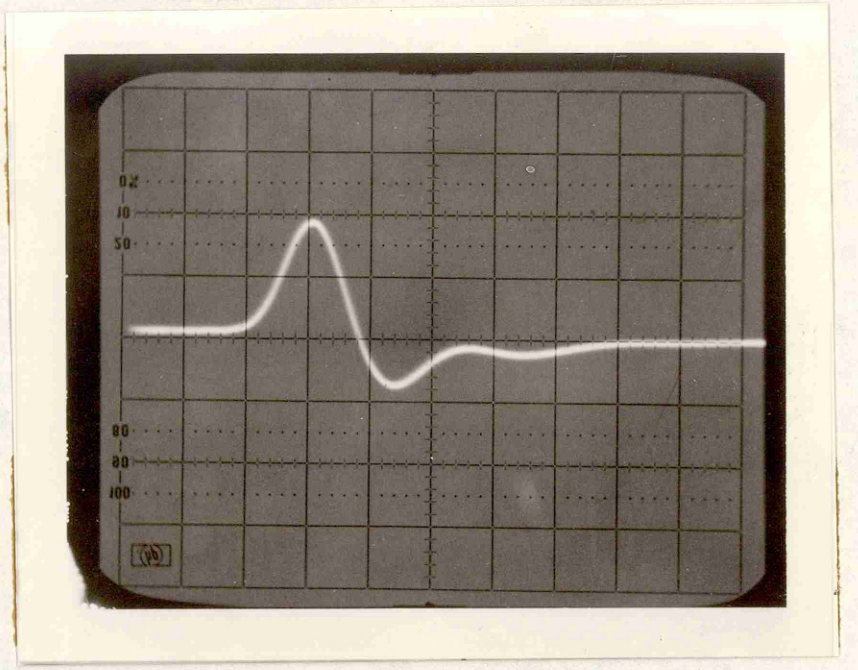

Fig. 8.9 Typical pulse received by receiving transducer. 50 ns per division.

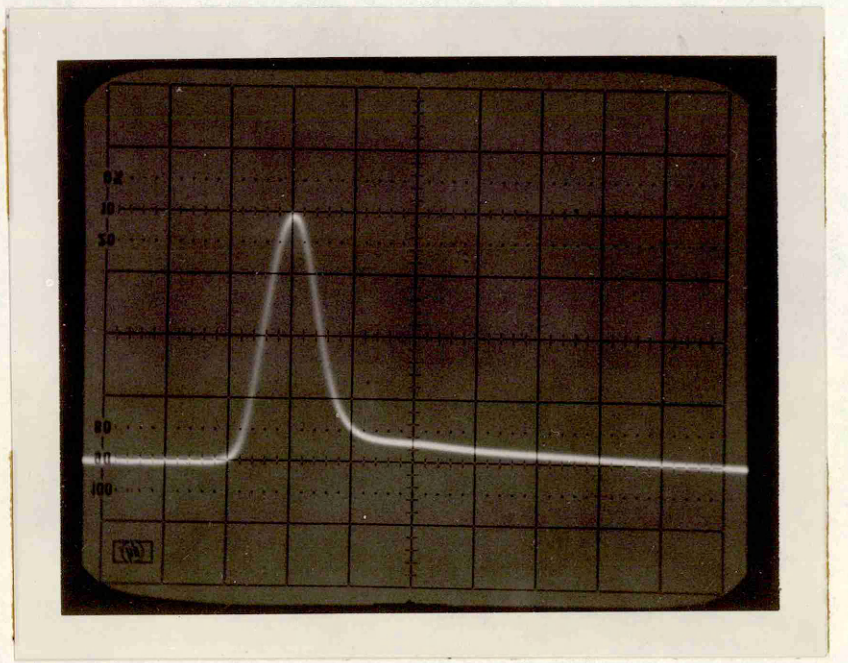

Fig. 8.10 Typical pulse from emitter follower, applied to analogue gate. 50 ns per division.

8.7 The digital video store

The ideal video store would have had a capacity of 256 x 256 pixels. With 256 pixels taking up two thirds of a scan line of 64μs the memory would have to be accessed at $\frac{256}{\frac{2}{3} \times 64}$ = 6 MHz. In fact, the dynamic RAMS intended for the memory could not be accessed at much more than 1.5 MHz, and consequently it would have been necessary to interleave four banks of memory to allow access at 6 MHz. This would have required 256 K of 4-bit RAM and funds were not available for this. A compromise of 128 x 128 pixels was decided upon. This required 32 K of 4-bit RAM as two memory banks had to be interleaved. However it also allowed one to write and store two separate pictures.

The specification of the store was:

1. It must be able to be continuously scanned by a television monitor of standard 625 lines.

2. It must give a picture on the monitor of 128 x 128 pixels.

3. Each pixel is to be square and span four scan lines.

4. The picture is to have 16 grey levels set by a 4-bit digital input.

5. It must be able to write new data at a rate of at least 200 Hz. The data will be presented asynchronously and at irregular intervals of between 6 and 10 ms.

6. It will be desirable to be able to write and store two separate pictures and display either.

7. It must be possible to add one picture to another and display the average pixel brightness. This would allow for the simulation of eight receivers while only using four. See section 9.2.

A digital store to this specification was designed and built by P. D. Wilson of the Electronics Discipline, Open University. It is filed by the Electronics Discipline, under drawing number FT 568. 21/10/1980.

Chapter 9 The imaging system in operation

9.1 First results

As was envisaged earlier (Chapter 3), the images consist of sets of elliptical arcs intersecting on the target. It was found that the dynamic range of the system was insufficient to cope with the range of signal intensities that were reflected back to the receivers. The specular reflections from one point on the surface of a metal target were so much stronger than any other echoes that they dominated the image. A point on a flat metal bar tended to give a strong reflection to one receiver and no discernable reflection at all to the other three, each of which would receive strongly from a different point on the bar. It was found that vertical metal cylinders gave the clearest images as they reflected at about the same intensity over an angle to all the receivers. However, all that was imaged was a very small piece of the front face of the cylinder. This meant in turn that with the analogue gates set at less than 400 ns (giving a range resolution of about 0.3 mm) and sampling at 1 mm intervals, these point reflections might only be picked up by one or two of the analogue gates. For this reason the gates were usually opened for 1.3 μs.

Figures 9.1 and 9.2 are typical of the images that were obtained of the front face of a 51 mm diameter steel cylinder. If the brightness control on the monitor is turned down, the arcs disappear and a bright point image is left. Figure 9.3 shows the image of two 19 mm diameter brass cylinders. More than one target of this nature can only be imaged in certain configurations because the near cylinder may block one or more of the paths of the ultrasound reflected from the far cylinder.

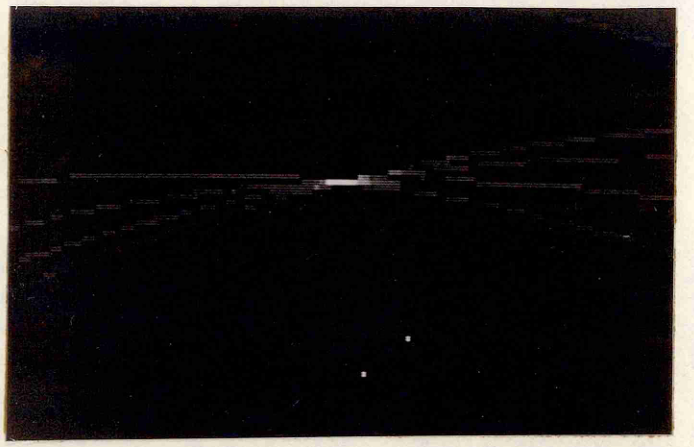

Fig. 9.1 Image of steel cylinder

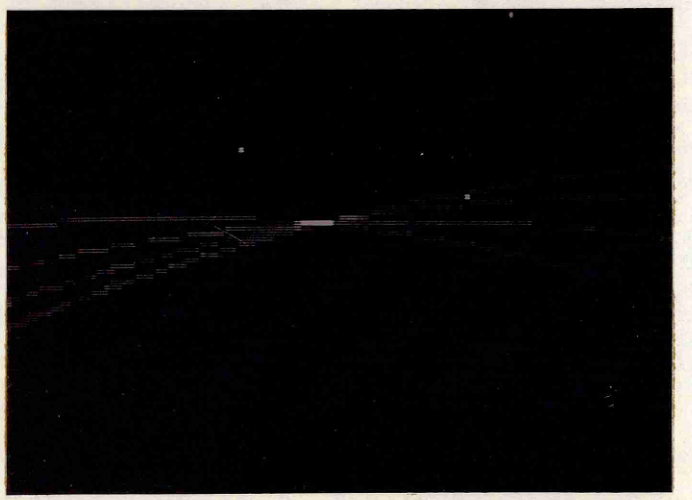

Fig. 9.2 Image of steel cylinder

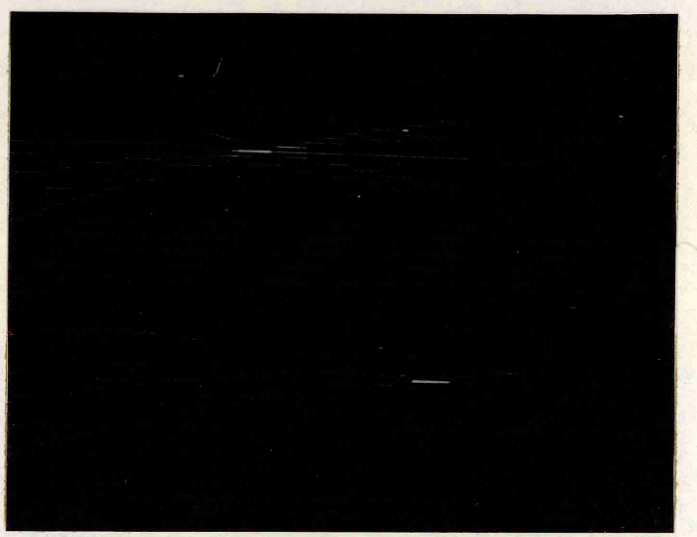

Fig. 9.3 Image of two brass cylinders

In Section 3.5, it was predicted that the horizontal resolution would be poor in comparison with the range resolution. All the images confirm this prediction. Figure 9.8 shows the improvement in resolution obtained by restricting the gate width to 500 ns.

9.2 Simulation of eight receivers

It soon became clear that the performance of the system was severely limited by having only four receivers. It was decided to simulate a system with eight receivers by making an image with four receivers, moving the receivers to new positions, making another image and averaging it with the first image. The design of the video store allowed this (Section 8.7).

Moving four receivers to new positions was difficult. It was much easier to move the transmitter and the target, so that their relative positions remained the same, and this had the same effect as moving the four receivers the opposite way.

It was decided to put the transmitting transducer near the centre of the array with two receivers either side. The first picture was to be taken with the transmitter at +$50 (80 mm), and the four receivers at - $40, 0, + $80 and + $SCO. (-64, 0, 128 and 192 mm). The transmitter and target were then moved $20 mm (32 mm) to the left. The target was regarded as being at the same coordinate for both pictures hence the transmitter was still at $50 but the receivers were now at -$20, + $20, + $AO and + $EO (-32, 32, 160 and 224 mm). These distances were all chosen in the light of experience to give simple numbers for the computer programs. Two new programs were written,

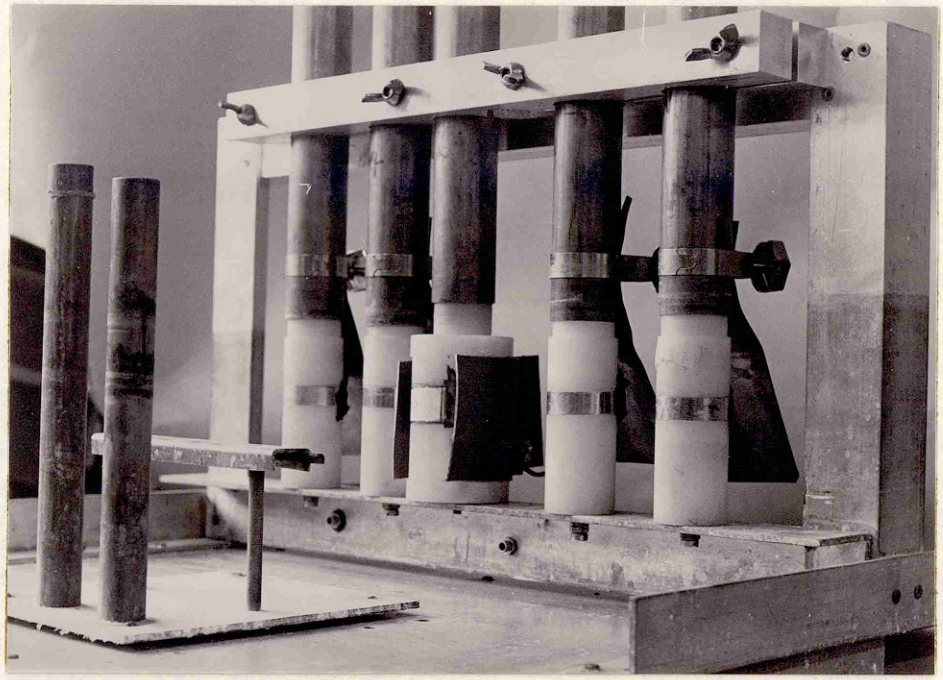

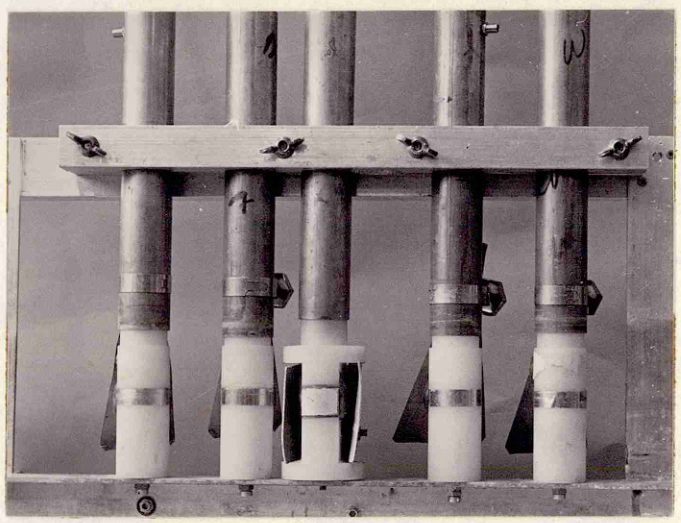

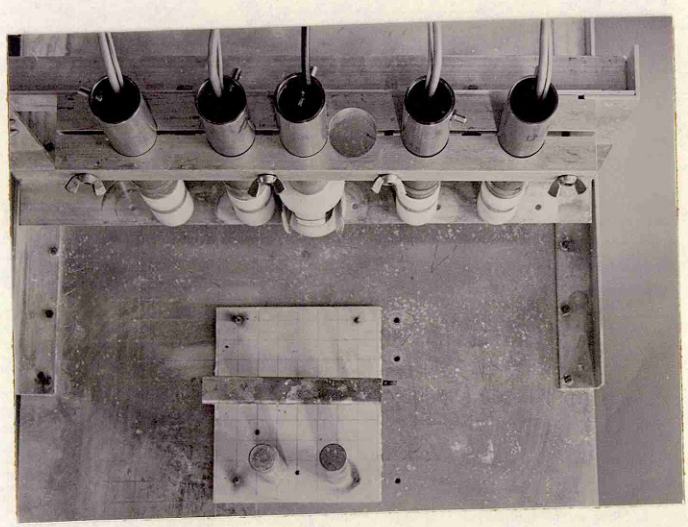

Fig. 9.4 Various views of the array and target used to simulate eight receivers.

one for each position of the transmitter and target. These are essentially the same as the original program for the transmitter at one end but with different constants written in to allow for different transducer spacings.

Figure 9.4 shows various views of the array with the transmitter on the left of centre. The target, consisting of two vertical brass cylinders is also on the left hand position. The cylinders are bolted to a movable base plate which fits into locating holes and can be moved exactly 32 mm to the right to fit into other locating holes. The transmitting transducer can be moved exactly 32 mm to the right by undoing the wing nuts and moving it to the empty hole in the clamping bar. The wing nuts are then replaced and tightened. The table on the base plate can be used to carry other targets which must be securely clamped to it.

Figure 9.5 shows the image obtained of one cylinder using four receivers. Figure 9.6 shows the image after simulating eight receivers. The screen brightness has been turned up to show the arcs. If the brightness is turned down, the appearance is as in Figure 9.7.

Figure 9.8 shows the effect of turning the gate opening time down to 500 ns. The arcs become discontinuous. In this particular case, all eight arcs appear to be present, but with a point reflector this does not always happen. In the case of the 500 ns gated image, it is interesting to see that the horizontal resolution is perhaps twice as good as for the 1.3 μs gated images.

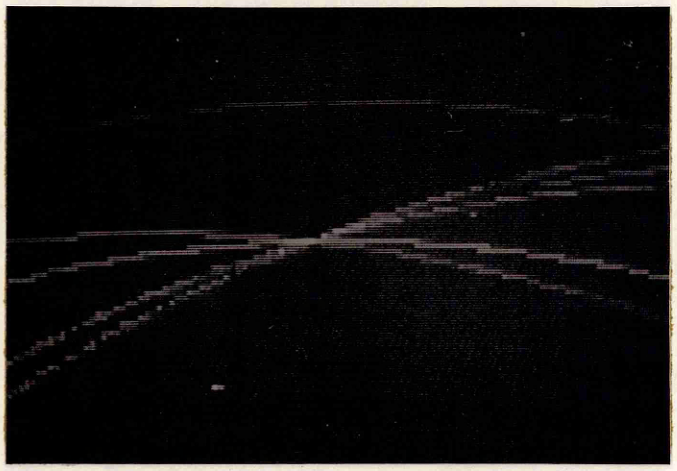

Fig. 9.5 Image of brass cylinder with four receivers.

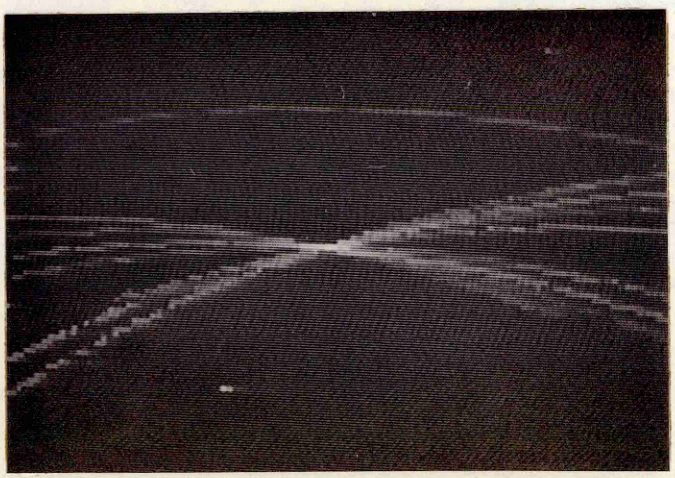

Fig. 9.6 Image of brass cylinder with simulation of eight receivers.

Fig. 9.7 Image of brass cylinder using simulated eight receivers and with reduced brightness

Fig. 9.8 Image as in figure 9.6 with gate length reduced to 500 ns.

Using two cylinder targets side by side, as in Figure 9.4 creates ambiguities as predicted in Section 3.5. Figure 9.9 shows the effect of using four receivers and Figure 9.10 shows the improvement using the simulated eight receivers. The image brightness remains the same but the single arcs almost disappear and the ambiguities are much reduced in intensity.

Fig. 9.9 Image of two brass cylinders using four receivers.

Fig. 9.10 Image of two brass cylinders using simulated eight receivers.

Chapter 10 Discussion and conclusions

10.1 Resume of advantages of the time delay system

In Chapter 2, various advantages of the time delay system of ultrasonic imaging were postulated. Now that a working system has been demonstrated, it is worth examining how far these ideas hold.

i. "The system does not need to be phase sensitive which should reduce circuit complexity."

A phased array requires a variable phase delay for each of several transmitting units and a variable phase delay for each receiving unit (Section 1.10). In the time delay system that has been built, the single transmitter needs no delay and the receivers need one time delay each. Increasing the number of receivers in the time delay system would increase the number of address lines required and thus increase the complexity of the circuit presently comprising NAND gates 1 to 6 in Figure 8.1. The AIM 65 computer has a 16 bit user port and under the present arrangements, 12 of these are needed for data leaving 4 for addressing data latches. Hence it could cope with a maximum of 16 sets of data for 16 receivers. If more than 16 receivers are required, some different method of addressing the data latches will be required. Otherwise, providing the calculation of path lengths can be done at a reasonably high rate, the present system could cope with any number of receivers with the following extra electronics.

A total of n receivers would require 2 n -1 12-bit data latches, n 12-bit counters, n + 1 latches, n monostables and n + 1 analogue

gates. In Figure 8.1, NAND gate 13 would require n inputs, Otherwise the circuits mainly involving NAND gates 7 to 13, NOR gates 1, 2 and 3, D Flip flops 1, 2 and 3 and monostables 1 to 11 could cope with any number of receivers. In these respects the circuitry of a time delay imaging system should be much simpler than a phased array.

ii. "It is expected that the calculation of a time delay would be easier than a phase delay."

The calculation of a time delay to 12 bit accuracy is simple and straight forward, but it does take a comparatively long time to calculate each path length inturn using the AIM 65. An improvement in speed could be made by storing and re-using the square of the range which will remain constant during the whole of one scan line. The squares of the successive lateral distances can be calculated by adding 2n + 1 to the square of the n^{th} distance to get the square of the $n + 1^{th}$ distance. However, the majority of the time is taken up by the calculation of square roots, and an improvement in the speed of calculating the squares can only produce an overall speed gain of about 10%.

Furthermore, a system which re-uses data calculated for a previous path length makes it difficult, if not impossible, to introduce random test numbers into the system to check the calculation. For this reason, the squares of numbers were individually calculated in this development system.

iii. "Because there is no need to correlate phase, the ultrasonic pulse lengths can be much shorter than those used in phased array systems. This will improve range resolution."

It has been demonstrated that pulses of one cycle can be generated and used to produce an image. The pulses have a half cycle of 100 ns length which represents a distance resolution of 150 nm in water. This is only one fifth as good as the resolution hoped for in Chapter 3. However, the data in Figures 3.4 and 3.5 is still valid if the numbers are taken to be the number of resolvable points in a 5 mm interval. Even so, the range resolution is in the order of 100 nm in water. In steel or aluminium, the range resolution would be in the order of 400 nm.

iv. "Ideally a pulse of one cycle can be used. There will be no interference effects and no side lobes to create ambiguities."

Various targets were imaged at different parts of the field of scan, and at no time did any spurious image appear that could have been generated by a side lobe. A single point target in any position always gave one set of arcs that crossed on the equivalent point of the viewing screen. Two or more targets gave sets of arcs that intersected in other places giving rise to low and high level ambiguities as foreseen in Section 3.5. Increasing the number of receivers increased the number of ambiguities but reduced their overall intensity. The ambiguities that arise in a time delay system because arcs cross in places where there is no target can be compared with the ambiguities in a phased array arising from

side lobes. In both cases, the strength of the ambiguities is reduced by increasing the number of transducer elements in the array.

v. "The device could operate in the near field of the array."

In fact the device that was constructed operates best when the target is close to the array. The range resolution improves slightly with increasing target range, but the lateral resolution becomes steadily worse. In the far field of the array, the best achievable lateral resolution will be limited to the width of the array. Furthermore, the greater the distance of the target, the more accurately distances will have to be calculated.

10.2 Transducer array design

Two designs of transducer array were tested. One had the transmitting transducer at one end of the array and the other near the centre When the latter system was tried out, it was noticed that the arcs appeared to cross each other at a greater angle. Compare Figures 9.1 and 9.2, where the transmitter was at one end, with Figure 9.5, where the transmitter was near the centre of the array. This suggests that there might be some improvement in lateral resolution if the transmitter is in the centre.

Because of practical problems in their manufacture, both arrays are much bigger than anything envisaged for use in a practical application. For the image in Figure 9.1, the array was 320 mm wide and the distance between transducer centres was 80 mm. For Figure 9.5,

the array was 256 mm wide and the distance between centres of pairs of neighbouring receivers was 64 mm. The two middle receivers were 128 mm apart. For Figure 9.6, the simulated array was 288 mm wide and the distance between neighbouring receiver centres was 32 mm. The two middle receivers were 96 mm apart.

It can be seen that the arcs get closer together as the distance between the receiving transducers is reduced. This will increase the areas each side of the target point that are subject to low and high ambiguity, because arcs which are more nearly concentric will take more distance to become clearly separate from each other. Fortunately, the excellent range resolution of the system allows the arcs to be separated in a very short lateral distance. This is most noticeable in Figure 9.8, where the gate length is reduced to 500 ns.

10.3 Electronics

The receiver amplifiers could probably be improved upon. The type 733 is a convenient I.C. and it is useful to be able to vary the voltage gain so easily. However, it produces a high offset output voltage which has to be blocked by capacitors. The final versions of the amplifier in Figure 8.4 and the analogue gates were built with printed circuits on a ground plane. This method of construction might improve the stability of the receiver amplifiers. A new circuit using transistors instead of the type 733 might also improve signal-to-noise ratio.

The analogue gate is not ideal. Although it produces a pedestal-free output and can operate down to 100 ns or less, it has an effective range 0.1 to 1.0 volts, and the received signals do not necessarily come within this range. Strong signals have to be limited and weak signals do not get through. A new sample and hold circuit, SHM - 7, has recently come on to the market. This has a 40 ns acquisition time and can cope with inputs up to plus or minus 5 volts. It seems likely that it would be ideal for the imaging system, but it costs £94 in 1982.

The four-bit video store has insufficient dynamic range. Although a range of sixteen grey levels just about covers the range of a television display, it was apparent that the dynamic range of the signals that were being picked up was much greater. Experience has shown that for development work, it is not necessary to have a scanning area with depth equal to the width. An eight-bit video store giving 128 pixels wide by 64 pixels deep would be more useful than the four-bit store giving 128 x 128 pixels.

10.4 Design, operation and effectiveness of PVF_2 foil transducers for time delay imaging

PVF_2 foil has the unique advantage that it is flexible and can be wrapped around a cylinder to make a transducer which can send and receive over a plane angle under water. Furthermore, it has the advantage of being highly damped and thus producing a very short pulse of one cycle. In general, pulses of 100 ns or less were obtained using 25 μm thick film. This is vital for the imaging system and the single wavefront is well shown in the Schlieren

images in Figures 4.18, 4.19 and 4.20. Figures 4.20 and 4.21 demonstrate that edge waves, if they exist at all, are of very low intensity when compared with the output from a ceramic transducer. Because the film is thin, a high electric field can easily be developed across it, and because its specific acoustic impedance is approximately 3.5 Mrayl it makes a relatively good acoustic match with water. It compares favourably with a barium titanate plate transducer when used as an underwater transducer (see Section 4.5). The nylon backing makes a very good acoustic match, because the specific acoustic impedance of nylon is approximately 3.0 Mrayl, and is acoustically well damped so that no unwanted echoes are generated inside it.

The aluminium coating supplied with some makes of PVF_2 foil is unsatisfactory, mainly because of its poor adhesion to the foil and its susceptibility to corrosion. Gold coated foil should be used, either with the gold sputtered directly on to the foil or with a layer of gold evaporated over a layer of cromium in a two stage process. This avoids both of these major problems and several other minor problems. (Sections 4.7 and 4.9).

The literature concerning the piezo-electric properties of PVF_2 film is not unanimous in its conclusions, but it seems likely that the best results will be obtained with uniaxially stretched PVF_2 poled at least 100 MV m^{-1} (section 4.4).

10.5 Conclusions

It has been demonstrated that images of point reflectors under

water can be obtained with a time delay system using four receivers, and that a considerable improvement in the reduction of background noise and ambiguity can be expected when using eight receivers. The inference is that the image quality will improve even more with a greater number of receivers.

The limited dynamic range of the system caused by the video store which had only four bits, prevented the observation of images from targets other than specular reflectors.

Furthermore, it proved impossible to obtain images from inside target objects in the water. This was to be expected because of the refraction of ultrasound passing into the target from the water. Images inside solids might be most easily obtained by attaching the transducers directly to the solid body. If the inside of a solid body is to be imaged under water a more sophisticated computer program will be needed to compensate for the refraction effects. (Section 3.6).

Chapter 11 Future work

11.1 Computer simulation

Eight receivers have been simulated in a practical system, and the next step is to simulate the effect of a larger number of receivers and target points using a computer. Various arrangements of transducer layout and spacing together with different target points can be set up on a computer, the corresponding arcs calculated and put into a video store. The final result can be studied on a television receiver and recorded. The effect of varying the number and position of receiving transducers can be studied and the corresponding effects on the suppression of ambiguities noted.

11.2 Reduction of ambiguities by sectioning the transmitting transducer

The present arrangement of insonifying the whole field of scan irrespective of the position of the target point being investigated means that the arcs through each image target point extend across the complete width of the screen. This in turn means that almost any two target points in the field of scan can mutually interfere to produce ambiguities. In Figure 11.1, target points at P_1 and P_2 produce low level ambiguities at the points marked A_1 and A_2, although P_1 and P_2 are in completely different areas from A_2. It should be possible to cut out this type of ambiguity by sectioning the transmitting transducer into a curved switched array. (Figure 11.2). By synchronising each section with the lateral coordinate of the point being investigated, the arcs, through a given image point, would only appear in the area of the screen around that image point insonified by that section (Figure 11.3). Thus no ambiguities

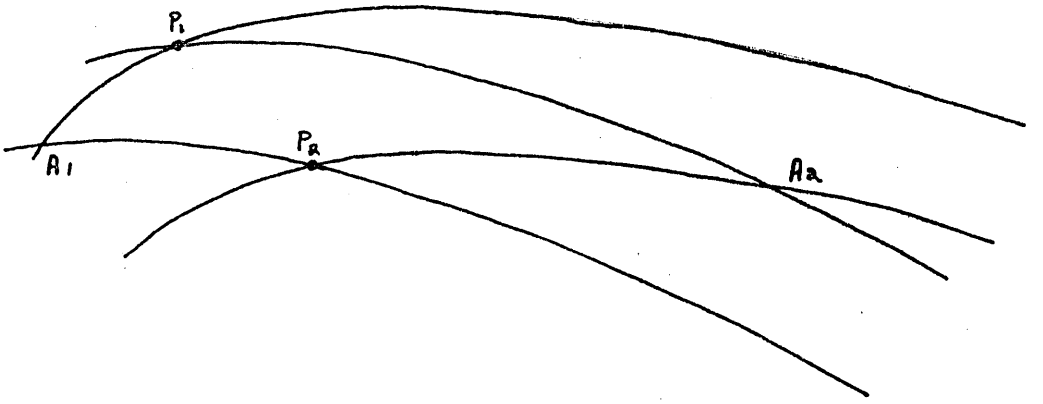

Fig. 11.1 Ambiguities arising from arcs spreading across the whole screen.

Fig. 11.2 Sectioned curved transmitting transducer. (Cross section)

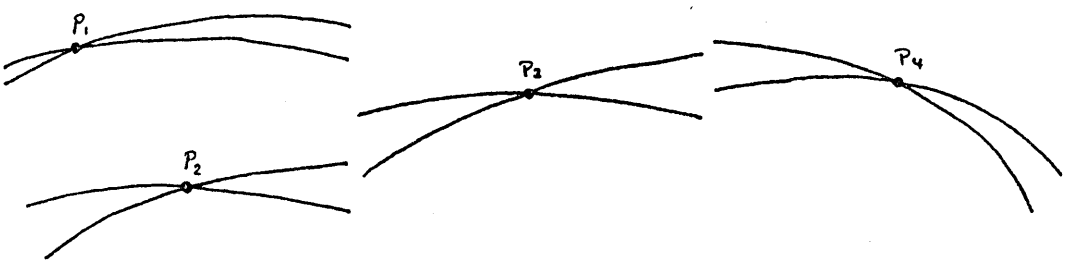

Fig. 11.3 Arcs arising from four target points when transmitting transducer is in three sections.

could be created between target points in different sections. The principle could be extended to the C scan situation by sectioning a dome shaped transmitting transducer horizontally and vertically and synchronising each section with both the horizontal and vertical coordinates of the point being investigated.

A sectioned transmitting transducer was constructed, but broke down before experiments on reducing the number of ambiguities could be conducted. (Section 4.10, Figure 4.13 and Section 4.11).

PVF_2 transducers are now made commercially and the manufacturers will have expertise on avoiding breakdown. Consultations with manufacturers are advised.

11.3 Image repetition rate

With the present method of computing the path length by microprocessor, the frame rate for a picture of 128 x 128 pixels is a little over two minutes. If the computing time can be reduced by the use of hard-wired circuitry, so that it is no longer the limiting factor, then the frame rate will be limited by the velocity of sound, the path length and the number of samples required for signal averaging. The present system is larger than is envisaged for a practical system, which might have an array 100 mm wide and hence a path length of up to 300 mm. In water, this would take up to 200 μs, so that five samples for signal averaging would take 1 ms. The frame rate would then be about 16 seconds. In steel or aluminium, the sound velocity is about 6000 ms^{-1} which brings the path time down to 50 μs. The frame rate with five samples would

be four seconds. A system producing an almost immediate but noisy picture in, say, one second followed by a later picture with noise suppressed after about ten seconds might be the ideal practical solution.

11.4 Imaging in metal

In Section 3.6, it was pointed out that a metal object under water would be difficult to image because of refraction at the water-metal boundary. This problem could be overcome by attaching an array of transducers directly to the metal specimen to be imaged. (In the Sonoscan system (Sections 1.12 and 10.4), the transducer is directly coupled to the specimen). PVF_2 is not a good acoustic match to metal, especially not to steel with its high acoustic impedance. If sufficient acoustic energy could be transmitted into and received from a steel specimen in direct contact with PVF_2, the good ranging resolution of the pulses generated by PVF_2 would be a great advantage. It is suggested that a flat belt of PVF_2 could be made into a flexible array and wrapped around the specimen to be imaged. A computer program designed to suit the shape of the test piece would allow it to be imaged internally.

11.5 A suggestion for a circular array

A conventional transducer acts as a piston source and produces a plane "direct wave" which propagates in the geometrical beam region, and a diffracted edge wave which propagates in all directions from the edge of the piston. See Figure 11.4 and the Schlieren pictures in Figure 4.21 (Weight 1978). Weight (1982) has shown that if a thin annular transducer is used it will produce waves equivalent to

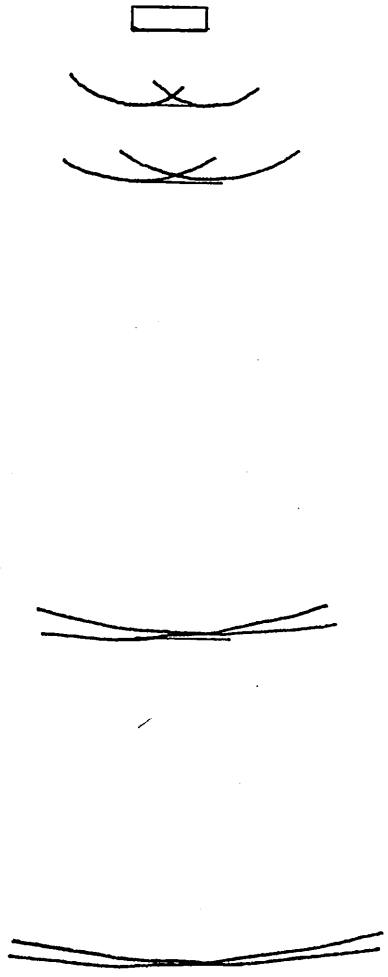

Figure 11.4

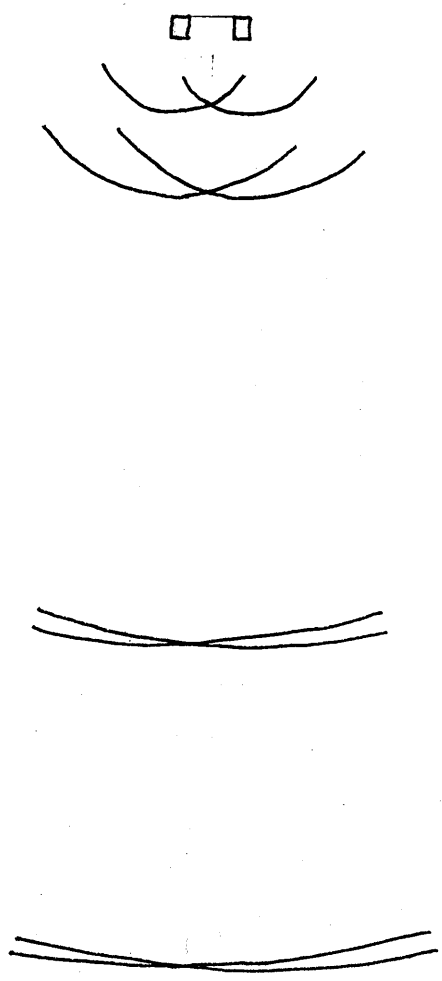

Figure 11.5

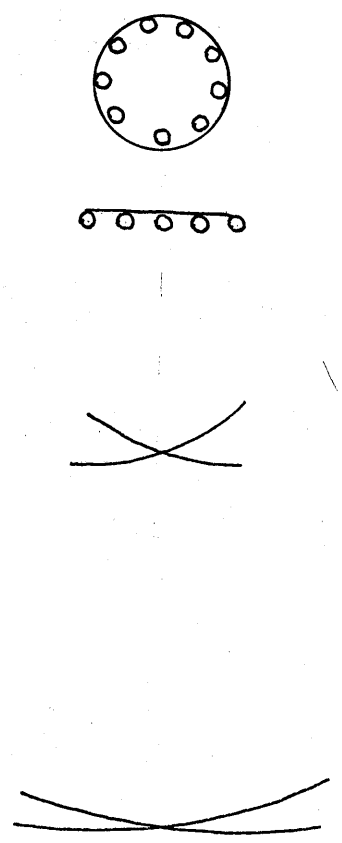

Figure 11.6

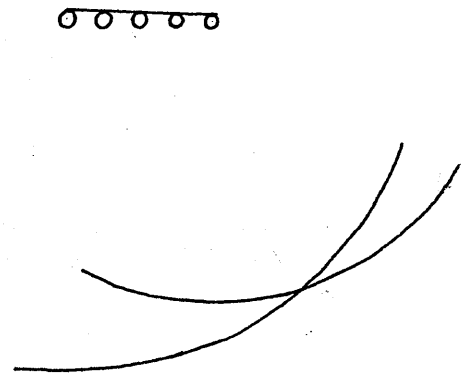

Figure 11.7

Edge waves and circular array

edge waves which can be focussed along the axis of the annulus to give very good range and lateral resolution as in Figure 11.5. Weight's annular transducer might be approximated by an annular array of separate transducers (Figure 11.6). Suppose each transducer was a dome of PVF_2, acting as a transmitter and receiver, and each fired in phase when transmitting, then the array should produce short "edge" pulses which would focus along the axis of the array with good lateral resolution as well as range. By introducing time delays into the system, the annular array of transducers could be used in a time delay C scan imaging system which would have good range and lateral resolution (Figure 11.7).

It seems probable therefore that for C scanning, it would be best to have the transducers in a circle which has its plane parallel to the plane of the C scan (Figure 11.6). Weight reports that his annular transducer, which could be regarded as an infinite number of separate sources arranged in a circle, produces no side lobes when used with a short pulse. A computer simulation should show how many individual transducers are needed in a circular array to reduce ambiguities to an acceptable level.

Appendix 1

Program for the imaging system with the transmitting transducer at one end of the array.

KOKO7 EDITOR FILE

HELEN=$9C00		Video store start address
INCRM=$60		Picture increment
BASE=$61		Picture near range limit
TOP=$62		Picture far range limit
JAMES=$63		Picture width
RANGE=$40		2 registers for range co-ordinate.
RANN=$41		
RAN2L=$43		Square of range co-ordinate. H & L
RAN2H=$42		
POI2L=$47		Square of horizontal co-ordinate. H & L
POI2H=$46		
HYP2J=$48		Squares of distances. H & L
HYP2H=$49		
HYP2L=$4A		HYP2 series are same as PAIR series
HYQ2J=00		HYQ2 series are squares of outgoing
HYQ2H=01		distances only.
HYQ2L=02		
RLOW=$51		
RHIGH=$50		Registers for R, X, Y. Low and
XLOW=$53		High bytes.
XHIGH=$52		(Variables used in square root
YLOW=$55		procedures)
YHIGH=$54		
YNNAJ=03		
YNNAH=04		Registers used in squaring
YNOAJ=05		return distances. J, H & L
YNOAH=06		
YNOAL=07		
RHIAH=$10		Outgoing distances.
RLPW=$11		Low & High bytes.
RHITH=$12		
RLQW=$13	1	
RHIJH=$14	2	Registers for total distances
RLRW=$15		
RHIKH=$16		
RLSW=$17	3	Low & High bytes
RHILH=$18		
RLTW=$19	4	
PAIRA=$4A		
PAIRB=$49		Same as HYP series (Square root
PAIRC=$48		subroutine operates on these)
POINT=$44		2 registers for horizontal
POINN=$45		co-ordinate
ASQRE=$09		
ASQRD=$0A		Stores for a^2 and 2a in subroutine
TWOA=$0B		SRETN

The letters, L, H and J on the end of a label indicate Low, High and Highest byte respectively.

```
*=$0D00                  Start of main program
LDY JAMES                Sets picture width
LDA #$FF
STA $A002
STA $A003                Sets VIA registers
LDA #$A0;PULSE OUT
STA $A00C;PCR
LDA #00
STA POINT
LDA TOP                  Initialises picture with
STA RANGE                first point and first line
STA HELEN                Initialises TV scan at top left
GO LDA RANGE             Main program loop starts
STA RANN
KERTA LDA #00
STA RAN2L;INIT RES
LDX #08
SOLMU LSR RANGE ;
BCC NOADD
CLC                      Squares range co-ordinate
ADC RANN;A=A+RANN
NOADD ROR A
ROR RAN2L
DEX
BNE SOLMU
STA RAN2H
LDA POINT
STA POINN
KERTB LDA #00
STA POI2L
LDX #08
SOLMV LSR POINT
BCC NOADE                Squares horizontal co-ordinate
CLC
ADC POINN
NOADE ROR A
ROR POI2L
DEX
BNE SOLMV
STA POI2H
CLC
LDA RAN2L
ADC POI2L                Adds squares and stores (as
STA HYP2L                square on hypotenuse of outgoing
STA HYQ2L                distance) in HYP2 series
LDA RAN2H
ADC POI2H
STA HYP2H
STA HYQ2H
LDA #00
ADC #00
STA HYP2J
STA HYQ2J
JSR SBQRT                Calls square root subroutine
```

```
LDA RHIGH
STA RHIHH
LDA RLOW                    Stores outgoing distances
STA RLPW
```

```
CLC
LDA HYQ2H                   Adds ∅ 1900 to square of outgoing
ADC #$19                    distance
STA YNNAH                   Stores in YNNA series
LDA #00
ADC HYQ2J
STA YNNAJ
```

```
LDA POINN
STA POINT
LDA #00
STA YNOAL
LDX #08
SOLMA LSR POINT             Multiplies POINT by ∅A0
BCC NOADA                   Stores in YNOA series
CLC
ADC #$A0
NOADA ROR A
ROR YNOAL
DEX
BNE SOLMA
STA YNOAH
```

```
SEC
LDA HYQ2L                   Subtracts YNOA from YNNA
SBC YNOAL
STA HYP2L
LDA YNNAH
SBC YNOAH
STA HYP2H
LDA YNNAJ
SBC #00
STA HYP2J
JSR SBQRT                   Calls square root subroutine
```

```
CLC
LDA RLOW
ADC RLPW                    Adds outgoing distance to return
STA RLQW                    distance for receiver 1.
LDA RHIGH
ADC RHIHH
STA RHIIH
```

```
SEC                         Subtracts sum of cylinder radii and
LDA RLQW                    outputs first result to VIA with 0
SBC #$A5                    as latch address
STA $A001;1ST OUT LO
LDA RHIIH
SBC #00
STA $A000;1ST OUT HI
```

```
LDA #$64;2ND ASQRD
STA ASQRD
LDA #00                     Sets a^2 = ∅64 and 2a = ∅14 for
STA ASQRE;HI ASQD=00         subroutine
LDA #$14;2ND 2A             SRETN
STA TWOA
JSR SRETN
```

```
CLC
LDA RLOW
ADC RLPW
STA RLRW
LDA RHIGH
ADC RHIHH
STA RHIJH
```

Adds outgoing distance to return distance for receiver 2

```
SEC
LDA RLRW
SBC #$A5
STA $A001;2ND OUT LO
LDA RHIJH
SBC #00
STA RHIJH;2ND OUT HI
CLC
ADC #$40
STA $A000
```

Subtracts sum of cylinder radii and outputs second result to VIA with ∅4 as latch address

```
LDA #$E1;3RD ASQRD
STA ASQRD
LDA #$1E;3RD 2A
STA TWOA
JSR SRETN
```

Sets a^2 = ∅EI

2a = ∅IE

for subroutine SRETN

```
CLC
LDA RLOW
ADC RLPW
STA RLSW
LDA RHIGH
ADC RHIHH
STA RHIKH
```

Adds outgoing distance to return distance for receiver 3

```
SEC
LDA RLSW
SBC #$A5
STA $A001;3RD OUT LO
LDA  RHIKH
SBC #00
STA RHIKH;3RD OUT HI
CLC
ADC #$80
STA $A000
```

Subtracts sum of cylinder radii and outputs third result to VIA with ∅8 as latch address

```
LDA #$90;4TH ASQRD
STA ASQRD
LDA #$01;ASQRD HI=01
STA ASQRE
LDA #$28;4TH 2A
STA TWOA
JSR SRETN
```

Sets a^2 = ∅90

and 2a = ∅IE

for subroutine SRETN

```
CLC
LDA RLOW
ADC RLPW
STA RLTW
LDA RHIGH
ADC RHIHH
STA RHILH
```
Adds outgoing distance to return distance for receiver 4

```
SEC
LDA RLTW
SBC #$A5
STA $A001;4TH OUT LO
LDA RHILH
SBC #00
STA RHILH;4TH OUT HI
CLC
ADC #$C0
STA $A000
```
Subtracts sum of cylinder radii and outputs fourth result to VIA with ØC as latch address

```
LDA RANN
STA RANGE
LDX INCRM
LDA POINN
STA POINT
THIS INC POINT
DEX
BNE THIS
```
Reloads range
Reloads horizontal co-ordinate and increments it by value in INCRM

```
CMP POINT
BCS RANDO
CPY POINT
BCC KIM
```
Checks for end of raster line

```
JMP GO
```
Loops back to program start

```
KIM LDA #00
STA POINT
RANDO LDX INCRM
TIINA DEC RANGE
DEX
BNE TIINA
```
Decrements range for start of new line

```
LDA BASE
CMP RANGE
BCS POHJA
```
Checks minimum range not passed

```
JMP GO
```
Loops back to program start

```
POHJA LDA TOP
STA RANGE
STA HELEN
JMP GO
```
Returns range to maximum
Reinitialises scan in video store
Loops back to program start

```
*=$0BC0
SRETN CLC
LDA HYQ2H
ADC ASQRD
STA YNNAH
LDA ASQRE
ADC HYQ2J
STA YNNAJ
```

a^2 added to 3rd and 2nd bytes of square of outgoing distance Result stored in YNNA series

```
LDA POINN
STA POINT
LDA #00
STA YNOAL
STA YNOAJ
LDX #08
SOLMB LSR POINT
BCC NOADB
CLC
ADC TWOA
NOADB ROR A
ROR YNOAL
DEX
BNE SOLMB
STA YNOAH
```

Multiplies horizontal co-ordinate by 2a

Result stored in YNOA series

```
ASL YNOAL
ROL YNOAH
ROL YNOAJ
ASL YNOAL
ROL YNOAH
ROL YNOAJ
ASL YNOAL
ROL YNOAH
ROL YNOAJ
ASL YNOAL
ROL YNOAH
ROL YNOAJ
```

Multiplies value now in YNOA series by $10

```
SEC
LDA HYQ2L
SBC YNOAL
STA HYP2L
LDA YNNAH
SBC YNOAH
STA HYP2H
LDA YNNAJ
SBC YNOAJ
STA HYP2J
```

Subtracts YNOA from YNNA

```
JSR SBQRT
```

Calls square root subroutine

```
RTS
```

Returns to main program

Appendix 2

The square root subroutine.

```
*=$0B00                 Square root subroutine
SBQRT LDA #$F0
PHA                     Pushes end marker and final
LDA #00
PHA                     zeros on to stack
PHA
LDX #04
LOOPA LDA #00
CLC
ROR PAIRA
ADC #00                 Pushes stack with 4 pairs of
LSR PAIRA
BCC STACA               bits from least significant byte
TENA ORA #02
STACA PHA
DEX
BNE LOOPA
LDX #04
LOOPB LDA #00
CLC
ROR PAIRB
ADC #00                 Pushes stack with 4 pairs of
LSR PAIRB               bits from middle byte
BCC STACB
TENB ORA #02
STACB PHA
DEX
BNE LOOPB
LDX #02
LOOPC LDA #00
CLC
ROR PAIRC
ADC #00                 Pushes stack with 2 pairs of
LSR PAIRC               bits from most significant byte
BCC STACC
TENC ORA #02
STACC PHA
DEX
BNE LOOPC
LDA #01
STA YLOW
STA RLOW                Sets registers to start
LDA #00
STA YHIGH               square root procedure
STA RHIGH
STA XHIGH
```

```
FIRST PLA ;FIRST PAI
R                          Pulls first pair and
CMP #00
BEQ FIRST ;DELLEAD0        deletes leading zeros
CMP #$F0
BEQ ZERO                   Checks number not zero
STA XLOW
EIOLE SEC ;X=X-Y           Start of square root
LDA XLOW
SBC YLOW                   procedure
STA XLOW
LDA XHIGH
SBC YHIGH
STA XHIGH
KYLLA ASL XLOW
ROL XHIGH
ASL XLOW
ROL XHIGH ; X=100X
PLA   ;NEXT PAIR
CMP #$F0                   Pulls next pair
BEQ LOPPU
CLC                        (Branches to LOPPU if finished)
ADC XLOW                   Continues square root program
STA XLOW
LDA #00                    branching back to KYLLA or
ADC XHIGH ;PAIRADD         EIOLE and pulls subsequent
STA XHIGH
ASL RLOW                   pairs until end marker
ROL RHIGH;R=10R            ØF0 causes branch to LOPPU
LDA RLOW
ASL A ; R=10R
ROL YHIGH ; YHCARRY
ADC #01
STA YLOW; NEW Y
CLC
LDA XHIGH
CMP YHIGH
BCC KYLLA ;Y>X
BNE AC
LDA XLOW
CMP YLOW
BCC KYLLA
AC CLC
INC RLOW ;R=R+1
BNE EIOLE
INC RHIGH
JMP EIOLE
ZERO LDA #00
STA RLOW                   If result zero then R = 0
LOPPU RTS
```

REFERENCES

Ahmed, Mahfuz, (1979) Holography and its application to acoustic imaging. Proc. IEEE, Vol. 67, No. 4. April 1979. pp.481, 482.

Aldridge, E.E., (1972) Ultrasonic Holography and Nondestructive Testing. Materials Research and Standards. Vol. 12, No. 12. Dec. 1972. pp. 13-22.

Alquie, C., Lewiner, J., and Friedman, C. (1976) Piezoelectric electret transducer for ultrasonic generation and detection up to microwave frequencies. Applied Physics Letters, Vo. 29, No. 2. pp.69-71. July 1976.

Bachman, M.A., Gordon, W.L., Koenig, J.L., Lando, J.B. (1979), An infrared study of phase-III poly(vinylidene fluoride), J.Appl.Phys. 50(10) pp. 6106-6211. Oct 1979.

Bacon, D.R., (1982), Characteristics of a pvdf Membrane Hydrophone for Use in the Range 1-100 MHz. IEEE Transactions on Sonics and Ultrasonics, Vol. SU-29, no. 1. pp.18-25. January 1982.

Beaver, W.L., Maginness, M.G., Plummer, J.D. and Meindl, J.D. (1975). Ultrasonic Imaging using two-dimensional Transducer Arrays. Proc. Cardiovascular Imaging and Image Process Theory and Practice for meeting at Stanford Univ. 1975, Jul 10-17. Vol. 72, pp.17-23. 1975.

Blitz, Jack. (1967) Fundamentals of Ultrasonics. Second Edition, London Butterworths 1967.

Blitz, Jack. (1971) Ultrasonics: Methods and Applications. London Butterworths 1971.

Brendon, B.B., (1975). History and present status of liquid surface acoustical holography. J. Acoust. Soc, Am., Vol. 58, No. 5, pp.951-955. Nov. 1975.

Brown, P. and Galloway, R. (1976) Recent developments in underwater imaging using the ultrasonic image converter tube. Ultrasonics. Vol. 14 No.6. pp.273-277. Nov. 1976.

Bui, L., Shaw, H.J., and Zitelli, L.T. (1976). Experimental broadband ultrasonic transducers using PVF_2 piezoelectric film. Electronics Letters. Vol.12, No.16, pp.393 and 394. 5th Aug. 1976.

Bui, L., Shaw, H.J., and Zitelli, L.T. (1977). Study of Acoustic Wave Resonance in Piezoelectric PVF_2 film. IEEE Transactions on sonics and ultrasonics, Vol. SU-24, No. 5, pp.331-336. Sept. 1977.

Burkard, H., Pfister, G. (1974). Reversible pyroelectricity and inverse piezoelectricity in polyvinylidene fluoride. J. Applied Physics, Vol.45., No.8. pp.3360-3364. August 1974.

Crecraft, D.I., Davies, C.J.S. (1981). A time delay ultrasonic imaging system using PVF_2 trasnducers. Ultrasonics International 81 Conference proceedings. I.P.C. Science and Tehcnology Press Ltd. pp. 302-306.

Crecraft, D.I., Davies, C.J.S.,Hall, K.G. (1982). Visualisation of ultrasonic waves launched by PVF_2 piezofilm transducers. Electronics letters. Vol. 18, No.1, pp. 16 & 17. 1982.

Doyle, P.A., (1977). Acoustical absorption in Bragg diffraction imaging. J. Phys. D: Appl.Phys., Vol. 10, pp.655-664. 1977.

Fukada, E., and Furukawa, T. (1981). Piezoelectricity and ferroelectricity in polyvinylidene fluoride. Ultrasonics, January 1981.

Gooberman, G.L. (1968). Ultrasonics Theory and Application. English Universities Press. London 1968.

Hanstead, P.D. (1977). Sonoscan: A real-time ultrasonic imaging technique. Proc. of Ultrasonic International Conference. I.P.C. Science and Technology Press.

Hanstead, P.D. (1981). Proceedings of the Royal Society London A.374. pp. 491-502 (1981).

Harrold, S.O. (1969). Solid state ultrasonic camera. Ultrasonics April 1969.

Harrold, S.O. (1974). Solid state ultrasonic imaging. Ph.D. thesis University of Warwick. August 1974.

Hayman, A.J. (1979). Schlieren visualisation of focused ultrasonic images. Ph.D. Thesis. The City University, London 1977.

Havlice, J.F. and Taenzer, J.C. (1979). Medical Ultrasonic Imaging: An Overview of Principles and Instrumentation. Proc. IEEE Vol.67 No.4 pp620-638. April 1979.

Hill, C.R. (1976). Ultrasonic Imaging. J.Phys.E.(G.B.) Vol.9 No.3 pp153-163. March 1976.

Jones, H.W. (1977). An Experimental Study of Sokolov Image Converter Tubes. Acustica. Vol.37 No.1 pp1-10. 1977.

Kawai, H. (1969). The Piezoelectricity of Poly (vinylidene Fluroide). Japan. J. Appl.Phys.8. pp975-976. May 1969.

Kepler, R.G. and Anderson, R.A. (1978). Piezoelectricity and pyroelectricity in polyvinylidene fluoride. J.Appl.Phys 49 (8) pp4490-4494. August 1978.

Krautkramer, J. and H. (1977). Ultrasonic testing of materials. Springer-Verlag. 1977. Berlin.

Latour, M. (1980). Importance des processus d'injection dans la formation de l'effet piezoelectrique du poly(fluorure de vinylidene). J. Physique. Lettres 41. pp35-38. Janvier 1980.

Leung, W.P. and Yung, K.K. (1979). Internal losses in polyvinylidene fluoride (PVF_2) ultrasonic transducers. J.Appl. Phys. 50 (12) pp8031-8033. December 1979.

Leventhal, D.A. (1979). 6502 Assembly language programming. Osborne (McGraw-Hill. Berkeley, California). 1979.

Maginness, M.G. Plummer, H.D. and Meindl, J.D. (1974). An Acoustic Image Sensor using a transmit-receive array. Proc. Acoustical Holography. Vol.5 pp619-631.

Micheron, F. and Lemonon, C. (1978). Moulded piezoelectric transducers using polar polymers. J. Acoust. Soc.Am. 64 (6) pp 1720-1721. December 1978.

Melen, R.D., Macovski, A. and Meindl, J.D. (1979). Application of Integrated Electronics to Ultrasonic Medical Instruments. Proc. IEEE Vol.67 No.9. pp 1274-1286. Sep 1979.

Murayama, N., Nakamura, K., Obara, H. and Segawa, M. (1976). The strong piezoelectricity in polyvinylidene fluoride (PVDF). Ultrasonics. pp 15-33. January 1976.

Murayama, N. (1975). Persistent Polarization in Poly (vinylidene Fluoride). I.Surface Charges and Piezoelectricity of Poly(vinylidene Fluoride) Thermoelectrets. Journal of Polymer Science. Vol.13 pp 929-946. 1975.

Newman, B.A., Yoon, C.H., Pae, K.D. and Scheinbeim, J.I. (1979). Piezoelectric activity and field-induced crystal structure transitions in poled poly(vinylidene Fluoride) films. J.Appl.Phys. 50 (10). pp 6095-6100. Oct 1979.

Ohigashi, H. (1976). Electromechanical properties of polarized polyvinylidene fluoride films as studied by the piezoelectric resonance method. J.Appl.Phys. Vol.47. No.3. pp 949-955. March 1976.

Oshiki, M. and Fukada, E. (1976) Piezoelectric Effect in Stretched and Polarized Polyvinylidene Fluoride Film. Japanese Journal of Applied Physics. Vol.15. No.1. pp 43-52. January 1976.

Penttinen, A. and Luukkala, M. (1977). A high resolution ultrasonic microscope. Ultrasonics. pp 205-210. Sept.1977.

Pennwalt Corporation. Undated. Leaflet "Kynar". Produced by Pennwalt Limited, Doman Road, Camberley, Surrey, England. Tel. Camberley 63383. Ext. 98.

Plummer, J.D., Swartz, R.G., Maginness, M.G., Beaudouin, J.R. and Meindl, J.D. (1978). IEEE Transactions on Sonics and Ultrasonics, Vol. SU25. No.5. pp 273-280. Sept. 1978.

Quate, C.F., Atalar, A. and Wickramasinghe, H.K. (1979). Acoustic Microscopy with Mechanical Scanning - A Review Proc. of the IEEE. Vol.67. No.8. pp 1092-1114. August 1979.

Redwood, M. (1963). A study of waveforms in the generation and detection of short ultrasonic pulses. Applied Materials Research. April 1963. pp 76-84.

Scanlon, L.J. (1980). 6502 Software design. Howard W. Sams and Co. Inc. Indianopolis 1980.

Scheinbeim, J.I., Chung, K.T., Pae, K.D. and Newman, B.A. (1979). The dependence of the piezoelectric response of poly(vinylidene fluoride) on phase-1 volume fraction. J.Appl.Phys. 50 (10) pp 6101-6105. Oct. 1979.

Sessler, G.M. (1-81). Piezoelectricity in polyvinylidene fluoride. J.Acoust.Soc.Am. 70 (6) pp 1596-1608. Dec. 1981.

Sussner, H. (1979). The Piezoelectric polymer PVF_2 and its applications. 1979 Ultrasonics Symposium. pp 491-498.

Sussner, H. and Dransfeld, K. (1978). Importance of the Metal-Polymer Interface for the Piezoelectricity of Polyvinylidene fluoride. Journal of Polymer Science: Polymer Physics Edition Vol.16. pp 529-543. 1978.

Swartz, R.G. and Plummer, J.D. (1980). On the Generation of High-Frequency Acoustic Energy with Polyvinylidene Fluoride. IEEE Transactions on Sonics and Ultrasonics, Vol.SU-27. No.6. pp 295-303. November 1980.

Swartz, R.G. and Plummer, J.D. (1980). Monolithic Silicon-PVF_2 Piezoelectric arrays for ultrasonic imaging. Acoustical Imaging. Vol.8. A.Meterell Ed. New York Plenum 1980. pp 69-95.

Szilard, J. and Hanstead, P.D. (1982). New Imaging Techniques. Ultrasonic Testing Edited by J. Szilard. John Wiley and Sons Ltd. Chichester 1982.

Tamura, M., Hagiwara, S. Matsumoto, S. and Ono, N. (1977). Some aspects of piezoelectricity and pyroelectricity in uniaxially stretched poly(vinylidene fluoride). Journal of Applied Physics, Vol.48. No.2., pp 513-521. Feb. 1977.

Wade, G. (1975). Acoustic Imaging with Holography and Lenses. IEEE Transactions on Sonics and Ultrasonics. Vol.SU-22, No.6. pp 385-394. November 1975.

Wang, T.T. (1979). Piezoelectricity in β-phase poly(vinylidene fluoride) having a "single-crystal" orientation. J.Appl.Phys. 50 (10). p 6091-6094. Oct. 1979.

Weight, J.P. and Hayman, A.J. (1978). Observations of the Propagation of Very Short Ultrasonic Pulses and their Reflection by Small Targets. J.Acoust.Soc.Am. 63. pp 396-404. 1978.

Weight, J.P. (1982). The propagation and reception of wide-band ultrasonic pulses. Ph.D. thesis. The City University. April 1982.

Woodward, B. (1977). The Suitability of Polyvinylidene Fluoride as an Underwater Transducer Material. Acoustica (Germany). Vol.38. No.4. pp 264-268. Oct. 1977.

Zaks, R. (1978). Programming the 6502. Sybex. Paris. 1978.